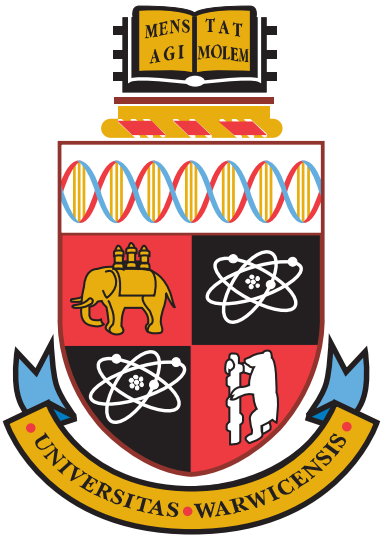

On the nature of γ-ray burst hosting galaxies

by

Karl Mikael Svensson

Thesis

Submitted to the University of Warwick

for the degree of

Doctor of Philosophy

Physics

January 2011

THE UNIVERSITY OF WARWICK

"En god [fysikers] första egenskaper;
förakt för sanningen och en djup respekt för det sannolika."
– Fritiof Nilsson Piraten

Contents

List of Tables

List of Figures

Acknowledgements

I am greatly thankful to The University of Warwick, and to the Vice Chancellor for funding me for the duration PhD course. The Department of Physics, and in particular the Astronomy and Astrophysics group have been of great inspiration, help and support. I am very grateful to all the staff here for invaluable help. I am greatly thankful to my supervisor, Dr. Andrew Levan, for his guidance, teachings and help shaping this thesis into being, and to Professor Tom Marsh for leading the Astronomy group, and as my secondary supervisor. Many people have contributed with discussions and ideas, and amongst them I am especially thankful to Professor Nial Tanvir at Leicester University for his help, ideas and thorough attention to both papers this thesis is based on. Last but not least, I owe thanks to all of my family – to my dear Mother, Father and Sister for all the support you have given me, and to my darling Louella, *Mahal kita!*

Declarations

Following is a declaration of the extent of original work, of collaborations and of submitted and/or published work contained in the thesis titled "On the nature of γ-ray burst hosting galaxies".

This thesis is an original work, and has not been submitted in part or full to any other University for any qualification. Major contributions to all work contained in this thesis is made by the author. Collaborations are specified below.

Chapter 1 is an introduction the subjects that are served as the main course of this thesis. It does not contain any original work unless specifically mentioned. All due credits are cited within.

Chapter 2 is based on the paper Svensson et al. (2010), published in *the Monthly Notices of the Royal Astronomical Society* (MNRAS). Collaborators for this work are: Andrew J. Levan, Nial R. Tanvir, Andrew S. Fruchter and Louis-Gregory Strolger. The main contribution to the original work is produced by author of this thesis. Non original work contained within this chapter, or data not produced by this collaboration is cited therein.

Collaborators for Chapter 3 are Andrew J. Levan and Nial R. Tanvir. The main contribution to the original work is produced by author of this thesis. Non original work contained within this chapter, or data not produced by this collaboration is cited therein.

Chapter 4 is based on the paper Svensson et al. (2011), submitted to MNRAS, Collaborators for this work are: Andrew J. Levan, Nial R. Tanvir, Daniel A. Perley, Michal J. Michałowski, Kim L. Page, Joshua S. Bloom, Brad Cenko, Jens Hjorth, Pall Jakobsson, Darach Watson, and Peter J. Wheatley. The main contribution to the original work is produced by author of this thesis.

Abstract

Long γ-ray bursts (GRBs) are uniquely powerful explosions at cosmological distances. As they mark the deaths of massive stars, they act as beacons of star formation and point out faint galaxies in the distant universe. Thus, they allow us to probe the conditions and the evolution of galaxy formation and metal enrichment throughout the universe. However promising as these prospects are, they need rely on a firm foundation based on the understanding of how the formation of gamma-ray bursts depend on the galactic environments. That is, do GRBs trace all star formation, or are they biased to metal poor and low mass hosts? Here I will explore the host galaxies of these events in order to understand how they relate to the properties of their galaxy populations. Like gamma ray bursts, core-collapse supernovae (CCSN) are the "grand-finale" of the life of massive stars. Providing a census of all massive star formation, they are an ideal control group to compare GRB hosts with at low redshifts. I employ this method to compare restframe properties of the host populations, concluding that GRB hosts are in comparison to CCSN hosts drawn from a compact, low mass and irregular galaxy population. This suggests an inherent bias amongst GRB progenitors, and that they prefer low metallicity environments. Furthermore, the GRB locations on their hosts have higher surface luminosities than for CCSNe, suggesting that GRB progenitors are more massive and short lived than those of CCSNe. Although the low redshift sample only appear to trace star formation in sub-luminous irregular galaxies, I will also show that this need not be strictly true everywhere: I will study the luminosity-metallicity and mass-metallicity relations of GRB hosts up to $z \sim 6$, and show that at high redshift where the universal metallicity is lower than in the present day universe, GRB hosts appear to follow the metallicity relations of that era. While GRBs might be biased tracers of star formation in the local universe, this suggests that above $z \gtrsim 3$, the universal metal enrichment is low enough that GRBs trace all star formation. Even at intermediate redshift, I will show that not all GRB hosts are blue and sub-luminous. The host of the dark burst GRB 080207 is extremely red, massive and with high inferred dust and gas content. I will discuss how the difficulties of obtaining accurate positions for highly extinguished bursts may have adversely affected host samples and follow-up strategies, and show that the increasing number of well studied dark burst suggest that many of them are massive and dust rich. This implies that, even at lower redshifts, a complete census of *all* GRBs may trace a higher fraction of star formation then inferred by only optically bright bursts.

Abbreviations

ACIS	-	AXAF CCD Imaging Spectrometer
ACS	-	Advanced Camera for Surveys
AGN	-	Active Galactic Nucleus
AXAF	-	Advanced X-ray Astrophysics Facility [Chandra X-Ray Observatory]
BAT	-	Burst Alert Telescope
BATSE	-	Burst Alert and Transient Source Explorer
BCD	-	Basic Calibrated Data
BSG	-	Blue Supergiant
CC-SN	-	Core-Collapse Supernova
CGRO	-	Compton Gamma Ray Observatory
EXIST	-	Energetic X-ray Imaging Survey Telescope
ERO	-	Extremely Red Object
fIR	-	far Infrared
FORS2	-	FOcal Reducer and low dispersion Spectrograph 2
GMOS	-	Gemini Multi-Object Spectrograph
GOODS	-	Great Observatories Origins Survey
GRB	-	Gamma Ray Burst
GROND	-	Gamma-Ray Burst Optical and Near-Infrared Detector
HST	-	Hubble Space Telescope
IMF	-	Initial Mass Function
IR	-	InfraRed
IRAC	-	InfraRed Array Camera
JCMT	-	James Clark Maxwell Telescope
JWST	-	James Webb Space Telescope
LMC	-	Large Magellanic Cloud
LRIS	-	Low Resolution Imaging Spectrograph
NICMOS	-	Near Infrared Camera and Multi-Object Spectrometer
nIR	-	near Infrared
NIRI	-	Near InfraRed Imager and spectrometer
MIPS	-	Multiband Imaging Photometer for Spitzer

PANS	-	Probing Acceleration Now with Supernovae
PC	-	Photon Counting
QSO	-	Quasi-Stellar Object
RSG	-	Red Supergiant
SDSS	-	Sloan Digital Sky Survey
SCUBA2	-	Sub-millimetre Common User Bolometer Array 2
SED	-	Spectral Energy Distribution
SFR	-	Star Formation Rate
SN	-	Supernova
TKRS	-	Team Keck Treasury Redshift Survey
ULIRG	-	Ultraluminous Infrared Galaxy
USNO	-	United States Naval Observatory
UV	-	Ultraviolet
UVOT	-	UltraViolet/Optical Telescope
VLT	-	Very Large Telescope
WFC3	-	Wide-Field camera 3
WFPC2	-	Wide-Field Planetary Camera 2
WT	-	Window Timing
XRT	-	X-Ray Telescope

Chapter 1

Introduction

In the Aristotelian paradigm of cosmology the Universe consisted of the heavens and the Earth. The heavenly bodies, the Sun, Moon and the planets revolved in spheres around Earth and they were perfect. Hence, the celestial world was immutable and never changed – change only occurred in the earthly domain. Thus transient phenomena on the night sky, perhaps most notably the comets, must inherently be earthly and atmospheric events that occur within the distance of the Moon.

Such remained the view of the Universe for hundreds of years. Perhaps the very beginning of modern astronomy began with Tycho Brahe, later to become astronomer royal at the Danish court. Tycho would be one of the first astronomers to realise the importance of measurements, that is the ability to make consistent and accurate measurements, and how to use their statistics – something taking for granted today. Although Tycho's later career would see him construct the largest astronomical devices of his time, allowing precise measurements of angles – the discovery we credit him for mostly today, occurred in 1572, when Tycho would notice that the new light in the sky did not move in relation to the fixed stars. This lack of apparent parallax meant that the newcomer was distant, and not an atmospheric event, but was located at least beyond the Moon and the planets. He

called it "The new star" – "De nova stella" (Brahe, 1573). To us, it's better known as SN 1572. By this discovery, Tycho disproved the ancient universe of Aristotle, and what is more important, he did so with the same scientific method of observation and inference as used in modern science. The centuries following would bring even greater understanding of the universe we live in, and just like Tycho, we understand the crucial role of observations. Though where Tycho only had the aid of his bare eyes, optical telescopes would soon come to revolutionise astronomy, and until today, when we can observe the sky in almost any wavelength from gamma-rays to radio, from the ground or from space. Although science has made enormous progress the last centuries, there still remain questions about the universe that we do not understand. Observing transients, much like Tycho did with SN 1572, has proved to be an invaluable tool to modern astronomy. From Cepheid variable stars we first understood the scale of the universe outside our own galaxy by being able to make distance measurements to neighbouring galaxies (Hubble and Humason, 1931) and from type Ia supernovae as standard candles we have learnt the shape of the universe (see e.g. Filippenko and Riess, 2000, for a review). By virtue of their their great luminosities, supernovae have long interested astronomers. The different types of supernovae can tell us different things about the universe, from providing cosmic standard candles to pointing out regions of active star formation.

While supernovae (SNe) have a rich and long history of observations dating back almost two thousand years, gamma-ray bursts were not discovered until the 1960s. By this time the space age had enabled the development of semiconductor detectors and satellite borne observatories in Earth orbit. Although they are newcomers in the cosmic zoo, they have already provided a wealth of scientific results from both theory and observation. In this thesis I aim to study the host environments of gamma-ray bursts. I will begin with giving a brief introduction to a few subjects in modern astronomy, necessary in order to appreciate the context of the

following chapters. In the following section, I will describe the evolution of the massive stars that are the progenitors of both long GRBs and supernovae. Following this I will carry on to the stages immediately after the gravitational core-collapse at the end of the massive stars life cycle, that produce either a SN or a GRB. I will study their observational imprints and the physics behinds these events. I will motivate the study of their host galaxies by discussing how GRBs, owing to their unique properties, are an exciting prospect for exploring the high redshift universe. Chapters 2, 3 and 4 present the main objective of the thesis, new and original research and results by the author. Chapter 5 is a conclusion and summary of the thesis and the main results presented within, as well as a brief summary of the future of direction of the field.

1.1 Evolution of massive stars

Star formation is the process where clouds of gas and molecular dust fragment and collapse until the central temperature of the proto-stars reaches a temperature high enough to start hydrogen burning. The fragmentation process results in a powerlaw distribution $\xi(M_\star)$ of the masses $M_\star$ of the newly formed stars, the initial mass function (IMF)

$$\xi(M_\star) \propto \left(\frac{M_\star}{M_\odot}\right)^{-\alpha}, \tag{1.1}$$

where $\xi(M_\star)$ gives the fraction of total stellar mass at $M_\star$. The slope α of the IMF is typically ~ 1.35 (Salpeter, 1955) - such that massive stars are rare, and low mass stars are numerous. The evolutionary path of a star (e.g. as illustrated in Figure 1.1 by the core density and temperature), and its endpoint, depends crucially on its initial mass. Hence it is convenient to define low mass stars as those that after the main sequence (MS) and giant phase become white dwarfs. Consequently, high mass stars are those that end their lives in core collapse events, often giving

rise to luminous explosions like SNe and GRBs.

Main sequence life time scales broadly as $\tau_{MS} \approx M_{\star}^{-2}$ as a result of the increased rate of nuclear burning required to balance the gravity of more massive stars (e.g. Prialnik, 2000). The defining feature of the main sequence is hydrogen fusion into helium in the core, achieved in the simplest case by the proton–proton (p–p) chain. Although the p–p chain is effective at relatively low temperatures, the energy production rate q scales with temperature T as $q_{p-p} \propto T^4$, which is a significantly lower temperature dependence than that of the carbon, oxygen, nitrogen (CNO) cycle (e.g. von Weizscker, 1938; Bethe, 1939) [1], which scales as $q_{CNO} \propto T^{16}$. Even at intermediate masses, $M_{\star} \gtrsim 1.3 M_{\odot}$, the energy production on the main sequence will be dominated by the CNO cycle.

The high luminosities of massive stars effectively support radiatively driven stellar winds that can drive mass loss rates $\dot{M_{\star}} \sim 10^{-6} M_{\odot} yr^{-1}$ (Markova et al., 2004). As the mass loss depends on the opacity of the stellar atmosphere, it scales broadly with metal abundance, Z, as $\dot{M} \propto \sqrt{Z}$ (e.g. Kudritzki and Puls, 2000; Crowther et al., 2002). For massive stars, this suggests that the mass loss timescale is comparable to the MS lifetime. Hence, very massive stars can loose a significant fraction of their hydrogen envelopes before they explode.

Stellar winds are also significant in their interactions with rotating stars. By carrying away angular momentum they slow the rotation of the star, an effect that is magnified in the presence of a magnetic field where the wind is locked with the co-rotating stellar magnetic field. As the wind moves further out, conservation of angular momentum leads to further decreased rotation. As we will return to later, the rotation of the star when it reaches the end of its life cycle can have significant

[1] For completeness, we note that the CNO cycle is actually a *bi-cycle*. The primary cycle begins with ${}^{12}_{6}C + {}^{1}_{1}H \rightarrow {}^{13}_{7}N + \gamma$ and concludes with ${}^{15}_{7}N + {}^{1}_{1}H \rightarrow {}^{12}_{6}C + {}^{4}_{2}He$, i.e. converts hydrogen to helium without changing the abundance or isotope ratio of the C, N, and O catalysts. The other possible cycle that begins with ${}^{14}_{7}N + {}^{1}_{1}H \rightarrow {}^{15}_{8}O + \gamma$ and ends with ${}^{17}_{8}O + {}^{1}_{1}H \rightarrow {}^{14}_{7}C + {}^{4}_{2}He$ is less probable than the main cycle above.

consequences for how the dying star explodes.

After the core is depleted of hydrogen, energy production in the core is halted and as a result the core contract under gravity to maintain hydrostatic equilibrium until temperature reaches the limit of helium burning, $T \sim 10^8 K$. Hydrogen burning now continues in a shell surrounding the core, while in the core itself, the triple-alpha process fuses helium into carbon and oxygen. Successive core/shell nuclear burning stages continue until the core consists of ^{56}Fe at which point no more energy can be released by fusion into heavier elements, ^{56}Fe has the highest binding energy per nucleon of all elements. As the stellar core is turned into iron ashes, it is surrounded by an "onion" layer structure of increasingly lighter elements separated by nuclear burning fronts and a hydrogen envelope at the outermost.

A core devoid of any source of pressure to balance the inward force of gravity cannot remain in hydrostatic equilibrium, hence a gravitational collapse begins. As the core density increases, the free electron gas soon becomes degenerate, and the core mass reaches the Chandrasekhar limit. Since the electron degeneracy pressure isn't enough to halt the collapse it continues until heavy nuclei start to capture free electrons, e.g.

$$ {}^{N}_{A}X + e^{-} \rightarrow {}^{N}_{A-1}Y + \nu_e. \tag{1.2} $$

The loss of electrons decreases the core pressure and allows the collapse to accelerate further while the core temperature increases to $T \sim 10^9$ K. At this temperature thermal photons are energetic enough to start photo-disintegration of iron nuclei,

$$ {}^{56}Fe + \gamma \rightarrow 13He + 4n \tag{1.3} $$

a process that absorbs ~ 2 MeV of energy per nucleon and allows the core to collapse at near free-fall velocity. Core temperature and pressure continue to increase until

photo-disintegration of helium begins,

$$^4He + \gamma \rightarrow 2p + 2n. \tag{1.4}$$

This process absorbs a further $\sim$ 6 MeV of energy per nucleon and the collapse continues until the density is high enough to force the free electrons to be absorbed by protons,

$$p^+ + e^- \rightarrow n + \nu_e \tag{1.5}$$

in effect creating a pure neutron core. This process reduces the number of electrons, which further lowers the core pressure – which can continue until the core density reaches $\sim 10^{18}$ kg m^{-3} and neutron degeneracy pressure halts the collapse. Conservation of the lepton number in the electron absorption leads to the production of as many as 10^{57} neutrinos in the core. Although neutrino cross sections are notoriously small, the high densities will build up a non-negligible optical depth, and neutrinos will deposit some fraction of the total energy in the outwards bounced shell (see e.g. Janka et al., 2007, for a review.).

In the above narrative we focused only on the evolution of the stellar core as it evolves from hydrogen burning on the main sequence to iron core collapse. Although the mass of the core is the major discriminator between different remnant types, several other factors also influence the evolution of massive stars.

Although the simple spherically symmetric case discussed above is a good description of systems with negligible rotation, asymmetries introduced by rapidly rotating progenitors can significantly change this picture. The formation of rotationally supported accretion discs for example, can have profound implications on the nature of the core-collapse explosion, as I will discuss further in Section 1.3. The observational signature depends on how much of the hydrogen envelope has

been retained by the core (e.g. Georgy et al., 2009, see also Figure 1.2). Such as, if a hydrogen envelope of significant mass is still retained, the resulting spectrum will show a signature of Balmer lines. These tend to be the result of relatively low mass stars, $\sim 8 - 30 M_{\odot}$ (though see Smartt et al., 2009; Crowther, 2007, for more discussion on the upper limit of this range) , or stars with initially relatively low metallicities, that are unable to support high wind driven mass loss rates. Stars more massive than this, in particular those with strong winds, possibly supported by high metallicities, are generally able to eject most of their hydrogen envelopes before they explode and their spectra will lack any signature of hydrogen.

Producing gamma-ray bursts, may however need more unusual routes of stellar evolution. In the current paradigm, long duration GRBs are formed during core-collapse of massive progenitors. They differ from ordinary SNe, in that the central engine most likely consists of the core of the progenitor which is surrounded by an accreting torus. Breaking the spherical symmetry, this configurations launches ultra-relativistic bipolar jets along the rotational axis. Although this is similar to a core-collapse supernova, it requires additionally that **i)** the progenitor is rapidly rotating in order to support an accretion disk, and **ii)** that the core has shed the majority of its envelope so that the jets can be launched. Making the evolution of GRB progenitors even more alluring, standard (single) stellar evolution suggests that it is indeed difficult to both retain a rapid rotation and eject the envelope at the same time since winds tend to drain angular momentum. A few solutions have been suggested (e.g. Woosley and Heger, 2006), including evolution of GRB progenitors in binary systems (e.g. Levan et al., 2006b), and non-standard evolution with complete mixing of the envelope on the main-sequence (e.g. Heger et al., 2000; Yoon et al., 2006). In the first scenario, the binary system solves the problem of removing the hydrogen envelope by ejecting it in a common envelope phase. Secondly, common envelopes are ejected by taking angular momentum from the

binary orbit, hence this type evolution is effective at creating tight binary systems. Given a small binary separation, the final requirement of rapid rotation is enabled by tidal locking of the He core and its companion. In the second scenario, rotationally induced mixing counteracts the chemical gradient supported by nuclear burning. If successful, the entire hydrogen envelope will be mixed into the star and the red supergiant phase (RSG) bypassed. Becoming a Wolf Rayet star immediately after the main sequence means preventing mass loss in the RSG phase, and leaving a massive, rapidly rotating GRB progenitor. In the following sections we discuss observations and theory of supernovae and gamma ray bursts, and what we can expect to learn from studying their host environments.

1.2 Supernovae

Although the evolution leading to a collapsing iron core, and indeed the physics that govern the continuous in-fall to a nuclear density central object, are largely well understood, much uncertainty remains as to how the explosion occurs. Only in the recent years have two dimensional (radius and latitude) computer models with realistic input physics managed to simulate the explosion itself (e.g. Woosley and MacFadyen, 1999; Zhang et al., 2006a). The shock wave deposits $\sim 10^{44} - 10^{45} J$ of energy in the stellar envelope (Prialnik, 2000), ejecting the outer layers and heating the inner part so that renewed nucleosynthesis begins. At the peak luminosity of the lightcurve the energy is thermal. This cannot be sustained for long, and the later decay of the lightcurve is powered initially by the inverse β-decay of the radioactive nickel-56 isotope into cobalt-56,

$$^{56}Ni + e^{-} \rightarrow ^{56} Co + \nu_e + \gamma, \tag{1.6}$$

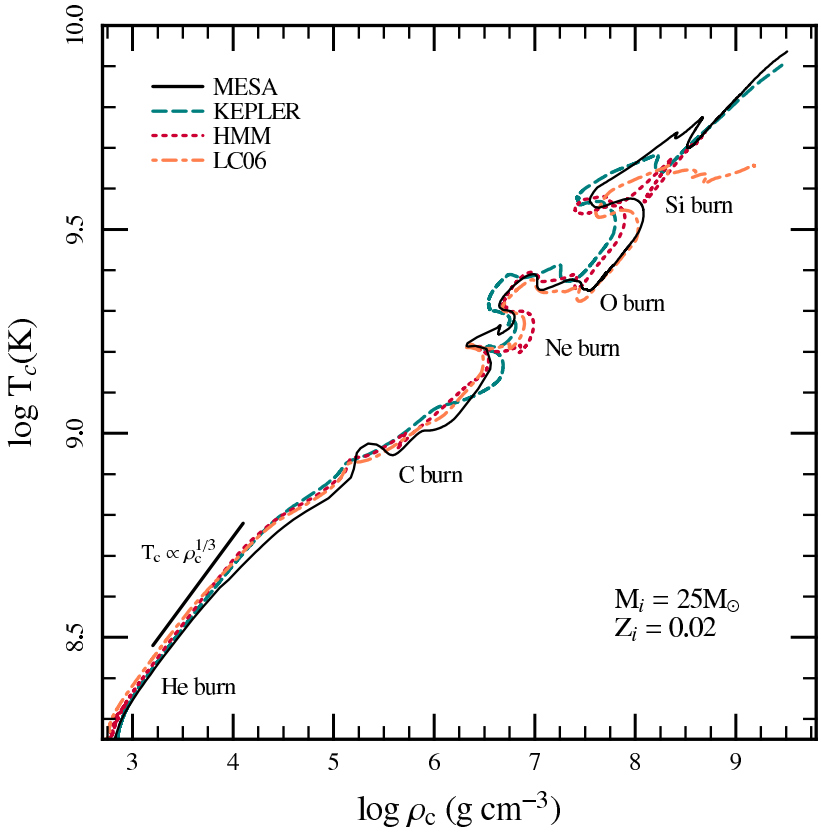

Figure 1.1: The evolution of a $25M_\odot$ star in the $\log T_C - \log \rho_C$ plane modelled by four different stellar evolution codes (See Paxton et al. (2010) page 79 for more detailed description and references.) The evolution starts on the main sequence with comparatively low core temperature and density, the figure shows the $T_C \propto \rho_C^{1/3}$ powerlaw slope expected on the MS from simple polytropic solutions to the equations of state in equilibrium. Off the main sequence the tracks show the evolution to higher core temperatures and densities, interrupted by quick flashes when burning of heavier elements (carbon, neon, oxygen and silicon) begins. Figure taken from Paxton et al. (2010)

which releases energy in the form of gamma ray photons ($\sim$ 1.72 MeV) when it decays to the ground state. The process in equation 1.6 has a half life time $\tau_{1/2} =$ 6.1 days, setting the early time decay slope of the lightcurve to $\sim$ 0.06 magnitudes/day. In the late time lightcurve the energy release is dominated by the decay of cobalt-56 into iron-56 by either inverse β decay or β^+ decay. I.e.

$$^{56}Co + e^- \rightarrow ^{56} Fe + \nu_e + \gamma \text{ or: } ^{56}Co \rightarrow ^{56} Fe + e^+ + \nu_e + \gamma, \tag{1.7}$$

with a half life $\tau_{1/2} = 77.7$ days, giving the late time lightcurve a slope of $\sim$ 0.01 magnitudes/day

Classically, supernovae are classified after prominent line features in their spectra (Minkowski, 1941). SNe type I lack hydrogen lines in the their spectra, while SNe type II have strong hydrogen Balmer lines. Type I's are further subdivided based on secondary line features in their spectra. Ia's have an absorption feature from silicon at $\lambda = 6150$ Å, while type Ib show He I lines and Ic have no strong absorption features at all. Type II are classified after lightcurve features as II-L if they decay linearly or as II-P if the lightcurve display a plateau of almost constant brightness before continuing to decay. For the purposes of the thesis however, it shall be more convenient to group all SNe that have massive stellar progenitors as core-collapse SNe (CCSN), these are SN Ib, SN Ic and SN II with all its subgroups. On the contrary, SN Ia progenitors are not massive stars, instead, most likely they are white dwarfs in interacting binary systems that explode once they have accreted mass to reach the Chandrasekhar limit. As opposed to SNIa's, which may be detached from star formation by the long timescales of binary evolution (e.g. Webbink, 1984; Stanek et al., 2006), core collapse SN progenitors are massive and short lived, hence the CCSN rate R_{SN} is proportional to the instantaneous star formation rate (SFR) by the fraction of stars in the supernovae progenitor mass range, assuming some lower

and upper limit of stellar masses.

$$R_{SN} \propto SFR \frac{\int_{8}^{100} \xi(M_\star) dM_\star}{\int_{0.1}^{100} M_\star \xi(M_\star) dM_\star}. \tag{1.8}$$

This suggests that $R_{SN} \sim 0.007$SFR yr^{-1}, which for a Milky Way star formation rate of $\sim$ a few solar masses per year is equivalent to a SN rate ~ 0.01 yr^{-1}. This is broadly consistent with the 2-5 core collapse supernovae recorded over the previous few thousand years (SN1054 and SN1680; SNe 386,393,1181 are of unknown type), given that our position inside the Galactic disk will hide a significant fraction of Galactic SNe behind obscuring dust (also compare to Diehl et al., 2006; Robitaille and Whitney, 2010). With such few events observed in our local galaxy, SN surveys are typically forced to look outside the Galaxy where SNe are both more numerous, and easier to detect. Early surveys targeted known, bright galaxies in the relatively nearby universe and were successful in uncovering a large number of SNe. The main shortcoming of targeted surveys is that they are inherently biased to discover SNe in known bright galaxies which may be more chemically evolved than the general star forming population. Rather, understanding the true nature of the environmental effects on SNe would require an unbiased selection method. Hence, more recent SN surveys have, instead of targeting bright galaxies, been implementing deep observations of blank fields at regular time intervals aiming to detect and/or measure the lightcurve near peak light. Utilising these methods, the SDSS Supernova Survey (Frieman et al., 2008; Sako et al., 2008) uncovered hundreds of SNe Ia, and $\sim$ 80 CCSN at low low redshifts (< 0.4). The Palomar Transient Factory (PTF) (Law et al., 2009; Arcavi et al., 2010) is a fully automatic wide field survey, currently boasting nearly one thousand spectroscopically confirmed SN, including about 300 core-collapse SNe. In Chapter 2 we will look in more detail on the SNe discov-

ered by the GOODS SN survey and PANS, both operating in the GOODS fields. Together they have discovered $\sim$ 60 CCSN and many more Ia's, stretching limits of detectability to $z \sim 2$ for the brighter type Ia's, although few CCSN are found above redshift ~ 1. Other missions to detect optical transients include Pan-STARRS (Kaiser et al., 2002), which is currently observing, and finding SNe (e.g. SN 2009kf Botticella et al., 2010), with one prototype telescope, but when fully operational will consist of a four telescope array in a wide-field setup covering the entire sky on an approximately weekly cadence.

We have already mentioned that the progenitors of CCSN are massive stars and described how they reach their core instabilities in order to collapse. But what different properties do they acquire to produce the different types of CCSN that are observed? Imaging of SN progenitors before they explode is of course is the most direct method to answer this. However, this is often very difficult due to the unexpected nature of these events, and deep pre-explosion images resolving the progenitor star have often been serendipitous. There are a number of studies in the literature to take note of though, beginning with the type II SN 1987A in the Large Magellanic Cloud (LMC), the first occasion on which the progenitor was resolved prior to the explosion, and clearly missing after the SN light had faded. In contrast to the predictions of standard stellar evolution models however, the exploding star was a blue, not red, supergiant (BSG) with a mass $\sim 18 M_{\odot}$ (Sonneborn et al., 1987) – leading to a re-examination of the stellar evolutionary models of massive stars (e.g. Langer et al., 1989) to include convection to produce BSG SN precursors. Clearly, the stellar evolution leading up to supernovae explosions is not simple, and most likely the details vary for the different SN types. The type II-P supernovae SN 2005cs had a relatively low mass red giant progenitor (Li et al., 2006), which has also been found for e.g. SN2003gd (Smartt et al., 2004; Maund and Smartt, 2009) and SN2008bk (Mattila et al., 2008) – suggesting a trend towards $8 - 15 M_{\odot}$

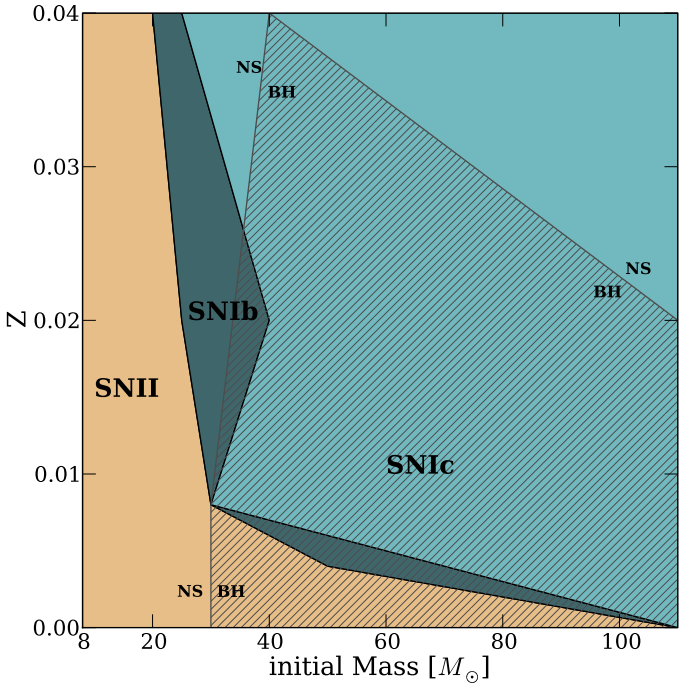

Figure 1.2: The end of stellar evolution in the initial metallicity vs. mass plane for single massive stars. The darker shaded area indicates where the explosion remnant is likely to be a black hole instead of a neutron star. (adapted from Figure 2 in Georgy et al., 2009)

stars exploding in the red giant phase (see also Smartt et al., 2009, for a review). Pre-explosion images of the type IIb[2] SN 1993J suggested that the progenitor was a red supergiant in an interacting binary system (Aldering et al., 1994) which was successfully confirmed after the supernovae had faded (Maund et al., 2004). Although not yet conclusive, binary progenitors are also suggested for SN2001ig (Ryder et al., 2004) and SN2008ax (Crockett et al., 2008), both of type IIb – suggesting that at least some hydrogen deficient SNe might have their envelopes stripped by a binary companion rather than ejected by a stellar wind.

[2]A classification used for SNe switching from type II to type Ib

In Figure 1.2 the properties of the different supernovae progenitors are drawn out in the initial mass vs. metallicity plane (Georgy et al., 2009). Although observations have indicated that many progenitors are found in binary systems, this simplified picture assumes evolution without interaction with a close companion. Indeed adding a companion would only lower the mass limits for making Ib and Ic's by replacing the inefficient mass loss by stellar winds with binary mass transfer. Qualitatively, the results agree. SNII progenitors are of lowest mass, although at extremely low metallicities even the most massive stars wont be able to support winds to remove the hydrogen envelope, hence towards zero metallicity only SNII are produced [3] . In the next section we discuss gamma-ray bursts, core collapse events related to supernovae but beamed in ultra relativistic jets emitting immense levels of γ-rays. Although their progenitors are elusive, it's now thought that they are closely related to certain types of supernovae.

1.3 γ-ray bursts

Until the mid twentieth-century, astronomy had been restricted to the optical range of the spectrum. In part this was due to complications of atmospheric absorption at other wavelengths, but also because of the lack of suitable detectors. With the development of more effective detectors for ionising radiation, exploring the high energy range of the electromagnetic spectrum largely began in the 1950's when sub-orbital sounding rockets were given X-ray capabilities. Though this was mainly motivated in order to study solar or lunar X-rays, the discovery of the first X-ray source outside of the solar system[4] started the era of high energy astrophysics in 1962. Then, in the midst of the cold war, during the 1960's, the American Vela satellites were put

[3] unless complete mixing during the main sequence depleted all the hydrogen, i.e. chemically homogeneous evolution (Maeder, 1987)

[4] i.e. Sco-X1,(Giacconi et al., 1962)

in orbit to monitor the nuclear disarmament treaty with the Soviet Union. These were the first space-born detectors with gamma-ray capabilities, and although their primary mission was not one of astronomical interest, their greatest legacy would be to discover a completely new and extremely energetic class of astronomical objects. Between 1969 and 1972 the Vela 5A, 5B, 6A and 6B satellites detected numerous short flashes of gamma rays. These events did not correspond to the signature of a terrestrial nuclear weapons explosion, and indeed even with the limited spatial resolution it could be determined that they did not originate from either the Earth or the Sun. When this discovery was released to the scientific community in 1973 (Klebesadel et al., 1973), a several decade long debate began as to the origin of these events.

The Compton Gamma Ray Observatory (CGRO) was launched in 1991 with the Burst Alert and Transient Explorer (BATSE) instrument on-board. BATSE achieved two main results that revolutionised the understanding of GRBs. Firstly, by accurately measuring the lightcurves (e.g. Figure 1.3) and durations of the gamma ray emission, it became apparent that there are two classes of GRBs separated in a bi-model distribution of the typical prompt emission duration (Kouveliotou et al., 1993), i.e. short bursts and long bursts as shown by Figure 1.4. Secondly, by localising the bursts on the sky to an accuracy $\sim 5-15$ degrees (Fishman et al., 1994), the spatial distribution was shown to be statistically isotropic (Meegan et al., 1992). One of the great controversies of GRBs was whether they were of Galactic origin or if they were extragalactic events. The arguments for a Galactic origin were mainly that extragalactic distances would imply luminosities several orders of magnitude greater than that observed in any supernovae. Although an isotropic distribution made theories of solar system or Galactic disc origin unfeasible, the question was not yet settled as theories of GRBs occurring in the spherical Galactic halo were still quite possible.

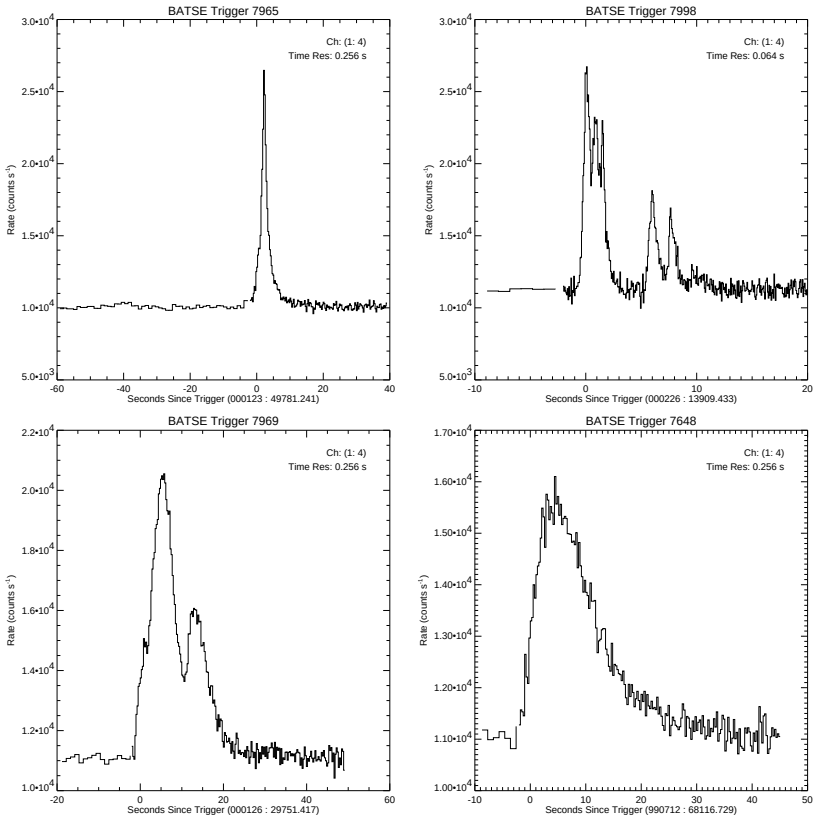

Figure 1.3: Prompt emission lightcurves from BASTE, showing a composite of four energy channels, $E > 20$ keV for each burst. Prompt emission lightcurves clearly exhibit a wide range of behaviours including short single peaks, multiple irregular or quasi-periodic variability and "fast rise exponential decay" shapes, and many burst display variability down to millisecond timescales, suggesting that the central engine must be a stellar sized object. Figures from http://www.batse.msfc.nasa.gov/batse/grb/ (Meegan et al., 1998)

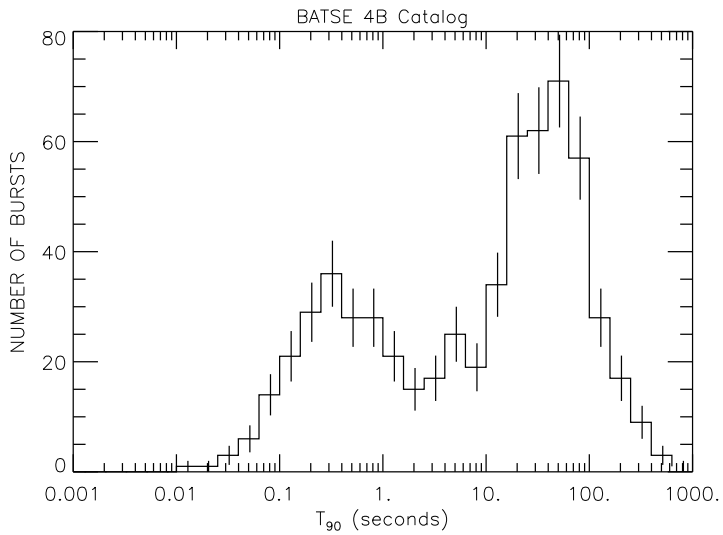

Figure 1.4: Distribution of T_{90} durations as measured by BATSE. Two distinct peaks can be recognised signifying that GRBs come in two different types with short or long duration. Figure from http://www.batse.msfc.nasa.gov/batse/grb/ (Meegan et al., 1998)

Whereas BATSE was mainly sensitive to the prompt and short lived γ-rays, the next step in understanding the origin of GRBs would come from discovering the panchromatic *afterglow* radiation. Enduring for much longer timescales, the afterglow had been predicted by theory to be the inevitable result of the deceleration of an ultra relativistic shock wave. Finally settling the question of the distances of GRBs, GRB 970228 was the first burst for which the theorised afterglow was actually detected (van Paradijs et al., 1997; Wijers et al., 1997). The burst was detected by the BeppoSAX satellite, which had the ability to promptly relay the burst location to the ground, serving observers with the information needed to follow up the event with ground, or space based optical observations. The optical afterglow of GRB 970228 did not reveal the redshift of the source, like many GRB afterglows would provide in the future, but it allowed an accurate position to be determined – which coincided with a faint blue galaxy at redshift 0.695 (Bloom et al., 2001).

Like SNe, GRBs are classified into subgroups, although here the classification is based on the duration [5] and the spectral hardness (Kouveliotou et al., 1993). The short and spectrally hard bursts typically have $T_{90} \lesssim 2$ s. They can be found in stellar populations of all ages, including passive elliptical host galaxies (e.g. Bloom et al., 2006, 2007), suggesting that their progenitors are most likely linked to older stellar populations, e.g. the coalescence of black holes or neutron stars in binary systems (e.g. Davies et al., 1994; Ruffert and Janka, 1999). The long and soft class of bursts, typically with 2 s $\lesssim T_{90} \lesssim$ 1000 s, are in contrast only found in star forming regions and have been firmly associated with the core collapse of massive stars (e.g. Stanek et al., 2003).

1.3.1 The Collapsar model

Explaining the unprecedented luminosities displayed by long GRBs has proved to be a challenge for theory. The high energies involved and the short time scale variability observed in the prompt emission lightcurves suggest that **(i)** they are most likely powered by gravitational energy, and **(ii)** the central engine must be small, such that the light crossing time is order of lightcurve variability, i.e. order of a millisecond (Morsony et al., 2010). The long and soft type of GRBs have readily been associated with both star forming regions and SN Ibc, suggesting that they indeed share some characteristics with core-collapse SN. The "failed" SN (Woosley, 1993), or hypernova (Paczynski, 1998), scenario, where a massive star undergoing core collapse fails to eject its shell and instead forms an accretion disk, leads to the standard collapsar theory of GRBs. Independent of the exact nature of the progenitor star or system, the collapsar model (Woosley, 1993; MacFadyen and Woosley, 1999) has seen success predicting the association of GRBs with star forming

[5] Most commonly measures by the length of the time interval during which 90% of the gamma energy is observed: T_{90}.

regions and core-collapse supernovae.

The standard model describes the general physics of the event, although each individual burst can exhibit variations or even deviations from this. Variations in initial mass of the collapsing core, rotational velocity, and the geometry of the jets can produce bursts with seemingly very different properties. Furthermore, the collapsar model has been successful in predicting that the GRB should be accompanied by a supernovae type Ib/c. Indeed, several nearby long bursts have shown evidence of supernovae signature in their lightcurves and/or spectra. e.g the GRB-SN pairs GRB 980425-SN1998bw (Galama et al., 1998a), GRB 030329-SN2003dh (Hjorth et al., 2003b), GRB 031203-SN2003lw (Malesani et al., 2004) and GRB 100316D-SN2010bh (Starling et al., 2010; Chornock et al., 2010). Although supernovae features are only expected to be seen in relatively nearby events, and certainly the majority of detected GRBs have been out of reach to attempt such observations, two nearby long GRBs lacking any trace of SN have challenged the standard classification scheme; GRBs 060505 and 060614 (e.g. Fynbo et al., 2006; Della Valle et al., 2006) at $z = 0.089$ and $z = 0.125$ (though see Cobb et al. (2006) for discussion on the possibility of mistaken identity of the GRB 060614 host galaxy – a higher redshift could render the SN issue moot). How these events relate to the collapsar model is still a matter of discussion, and apart from the lack of SN their afterglows are consistent with those of other long bursts (Xu et al., 2009). Furthermore, GRB 060505 is hosted by a spiral with low metallicity at the explosion site, high star formation rate and a young stellar population indicative of an origin from a collapsing massive star (Thöne et al., 2008a). The collapsar origin of GRB 060505 is also supported by its spectral lag [6] (McBreen et al., 2008), which is inconsistent with that of other short bursts (e.g. Zhang et al., 2006b) at the $\sim 3\sigma$ level, sug-

[6] I.e. the temporal correlation of the prompt emission at different photon energies (e.g. Band, 1997). Long bursts are typically observed with spectral lags ranging from 0 to several seconds, while short bursts are typically consistent with no spectral lag.

gesting that its massive progenitor exploded without producing a bright supernovae (e.g. Heger et al., 2003; Fryer, 2006, 1999). On the contrary, GRB 060614 appears to originate in a passive host, which is not a typical environment to find long bursts in, which along with the apparent lack of spectral lag (Xu et al., 2009) might suggest that perhaps the merger of compact objects with long lived central engine could be responsible (e.g. Kluźniak and Ruderman, 1998; Rosswog et al., 2003; Gal-Yam et al., 2006).

The collapsar begins to form as the iron core of a massive and rapidly rotating star collapses. Although the exact mass distribution of the progenitors is unknown, estimates suggest $M \gtrsim 20M_{\odot}$ (e.g. Larsson et al., 2007). Irrespective of the progenitors mass, it must be able to form an iron core with $M_C \gtrsim 2M_{\odot}$ – massive enough that it will collapse to a black hole, which will start accreting from the stellar envelope. Provided that the rotation is sufficient, a centrifugally supported disk will form. The polar regions of the envelope are less supported by the rotation and will be accreted first. The collapsar model is not specific on how energy is extracted to fuel the burst, although theoretical simulations, e.g. Figure 1.5 suggest that either magneto-hydrodynamic effects (e.g. Bucciantini et al., 2009) or neutrino-antineutrino annihilation (Woosley, 1993) is responsible for powering the launch of the ultra relativistic beamed jets.

1.3.2 Afterglows

Since the first discovery of GRB afterglows (Wijers et al., 1997), they have become one of the most important diagnostic tools for understanding a wide range of GRB behaviours (e.g. Rykoff et al., 2009) and tracing the immediate line of sight circumburst region (e.g. Schady et al., 2007, 2010; Perley et al., 2010a, and many others).

The afterglow is panchromatic with a broken powerlaw spectrum. The peak

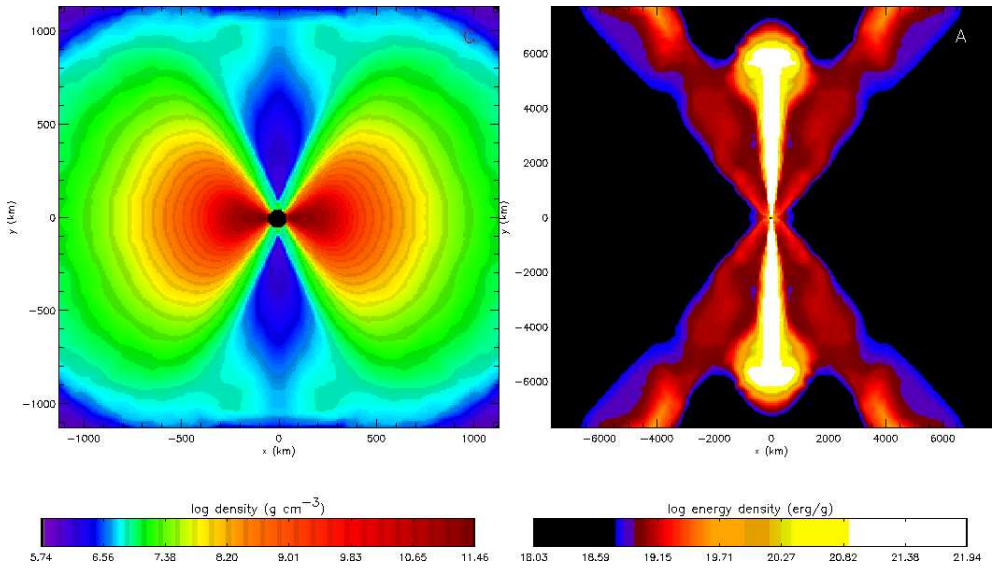

Figure 1.5: Structure of the accretion disk and jet forming around a rotating GRB progenitor. Right panel shows the disk density structure at 7.5 s after collapse of the iron core. Left panel shows the energy density of the polar jets. Figures adopted from Woosley and MacFadyen (1999)

.

energy moves from being initially in the X-ray band, through UV, optical, IR to radio as the jet is decelerated. Afterglows have been detected and studied across the electromagnetic spectrum. The X-ray afterglows are typically bright beginning a few seconds after the prompt emission, and often give the first insights into the nature of the burst, e.g. position, brightness, temporal decay and often give a measure of the absorption by neutral hydrogen along the GRB line of sight – providing valuable first clues as to the local environment of the burst. Although *Swift* can locate the X-ray afterglow to an accuracy of a few arcsec (e.g. Evans et al., 2009), optical afterglows are often necessary to uniquely identify the host galaxy. Furthermore, (absorption) spectroscopy of the optical transient is often vital to identify the redshift of the burst, and frequently also give deeper insight in the host environment by allowing direct study of the metal abundances e.g. Figure 1.6.

For both the spectral and temporal evolution of the afterglow, a powerlaw behaviour is prescribed, generally speaking,

$$F_\nu(t) \propto t^{-\alpha}\nu^{-\beta} \tag{1.9}$$

where α is the slope of the lightcurve and β is the spectral slope. The values of these parameters are intricately linked to the physical behaviour of the central engine and jet. The canonical X-ray afterglow lightcurve can be described by four segments of powerlaws (e.g. Figure 1.7) tracing the temporal evolution of the central engine and forward shock-wave (e.g. Zhang et al., 2006a);

i) The initial powerlaw decays steeply, typically with $\alpha \sim 3$, until $\sim 100 - 1000$ s post-burst. This is most likely the tail end of the prompt emission (Barthelmy et al., 2005).

ii) A shallow decay, indicating a steady continuous energy injection by the central engine (e.g. Jóhannesson et al., 2006; Zhang et al., 2006a; Nousek et al., 2006) typ-

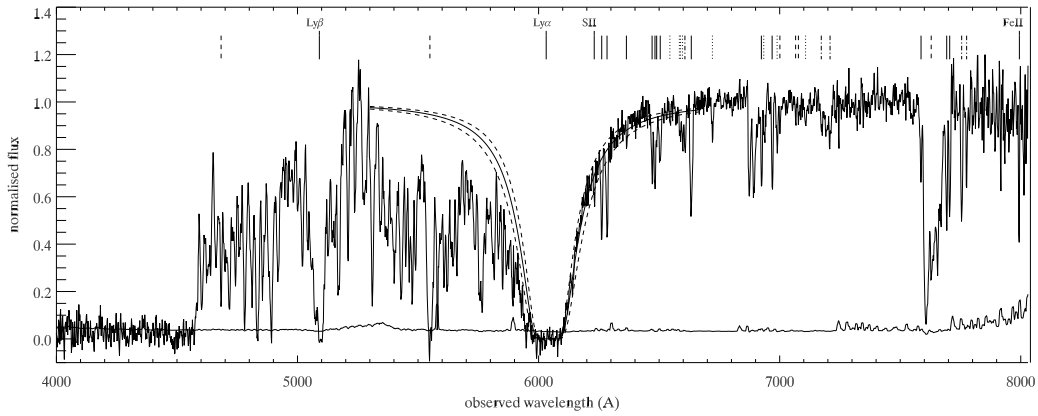

Figure 1.6: Optical spectra of GRB afterglows are often useful diagnostics of otherwise very faint systems – even when the host is too faint to be observed in emission; redshift, metallicity and hydrogen column can be constrained from the afterglow. Here showing the optical afterglow of GRB 050730 (Starling et al., 2005) with a dampened Lyman alpha line profile and several absorption features of the host at redshift $z = 3.97$ (solid marks) and intervening absorption systems at redshifts $z = 3.56$ and $z = 1.77$ (dot-dashed and dotted marks respectively). Spectral lines attributed to hydrogen, silicon and iron in the GRB hosting system are labelled. Note the wealth of information about the host extracted from the afterglow. Such detailed study would not be possible for this $i > 28.8$ (Levan, private communication) host without the GRB. Figure taken from (Starling et al., 2005).

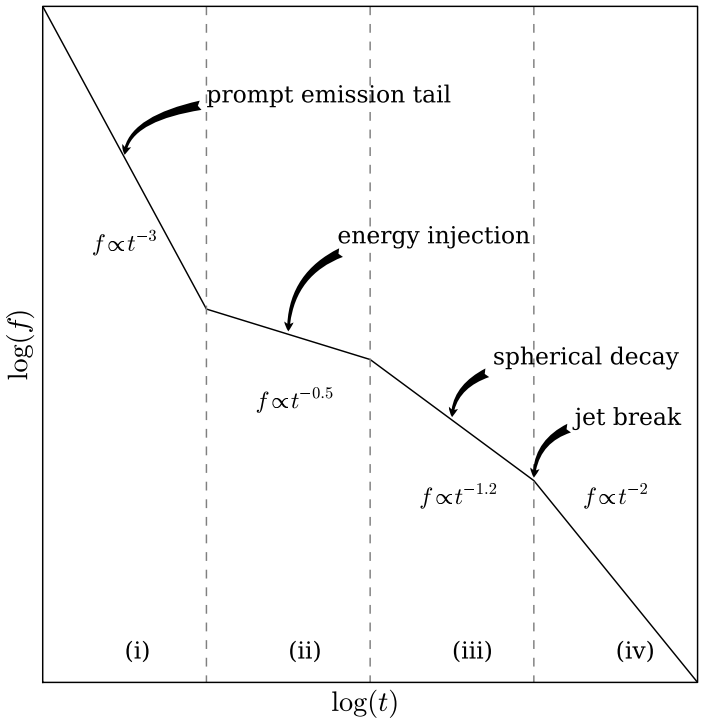

Figure 1.7: X-ray afterglow of the canonical gamma ray burst. Temporal decay indices are typical observed values. Continuous energy injection in segment ii) and the achromatic jet break between iii) and iv) are not always observed or detected. Figure is adapted from Zhang et al. (2006a) and Racusin et al. (2009)

ically decays with $\alpha \sim 1/2$ and last until 10^3 to 10^4 s, although this phase is not observed or present in all bursts.

iii) The normal spherical decay of the afterglow, typically $\alpha \sim 1.2$ until 10^4 to 10^5 s post-burst.

iv) Post jet break decay, i.e. an increased rate of decay caused by the jet slowing down and widening. The post jet-break typically decays with $\alpha \sim 2$.

In addition to these regions of powerlaw decay, a large fraction of GRB lightcurves also show one or several X-ray flares. Phase **i)** sometimes have a softer spectrum than the late time phases, while during phases **ii)** - **iv)** the spectral index is generally unchanged.

Sari et al. (1998) describe the spectral index as

$$\beta = \begin{cases} 1/2 & \nu_c < \nu < \nu_m \\ (p-1)/2 & \nu_m < \nu < \nu_c \\ p/2 & \nu_c, \nu_m < \nu \end{cases} , \tag{1.10}$$

where p is the powerlaw index of the electron electron distribution, $N(E)dE \propto E^{-p}dE$, and ν_c, ν_m are the the cooling and peak synchrotron frequencies. $2 < p < 2.5$ usually applies (though Dai and Cheng, 2001, solve the unbounded electron energy distribution also for $p < 2$ with a high energy cutoff), so that $0.5 < \beta < 1.25$. This restriction on the spectral slope have been tested observationally by multi-wavelength studies of burst afterglows, which are generally in excellent agreement with the theory (e.g. Galama et al., 1998b; Willingale et al., 2007). However, it is also apparent that some systems have spectral slopes more shallow the the $0.5 < \beta$ limit, suggesting that the optical flux is suppressed relative to the X-ray (i.e. dark bursts Jakobsson et al., 2004). In Chapter 4 we return to the subject of dark bursts

and their host galaxies with a more in depth discussion and new results.

Since the afterglow is emitted when the external shock wave interacts with the circumstellar medium, it is, in theory, possible to test for the signatures of different progenitors. Massive stars eject significant amounts of matter through their stellar winds, from which it is likely that the radial density profile of the circumstellar medium becomes $n(r) \propto 1/r^2$ rather than roughly constant, as expected from the interstellar medium. Although testing this observationally is challenging, theoretical calculations in the afterglow evolution in wind-like mediums suggest that cooling breaks will vary in magnitude for the two cases (e.g. Chevalier and Li, 2000; Panaitescu and Kumar, 2002). Although a wind-like medium finds favour with several bursts, many do not, and so require either different progenitors, or some mechanism, such as high ISM pressure, to transform a wind-like medium into a constant density profile.

The jet break is a geometric effect, and hence it is always achromatic. Multicolour observations are usually required to differentiate it from a *cooling* break, which occurs when the cooling frequency, ν_c moves through the observed frequency ν in equation 1.10 (e.g. Sari et al., 1998). A cooling break will have $\Delta\beta = 1/2$, the break size in the lightcurve can be estimated from the theoretical relationships between α and β known as the closure relations (e.g. Sari et al., 1998).

1.4 GRBs as cosmic probes

Owing to their extremely high luminosities, gamma-ray bursts can be used to probe the conditions of the early universe. Their connection with core-collapse SNe means that they trace star formation, although questions remain if this relationship is direct or if it is altered by GRB progenitors being biased towards low-metallicity environments. Nevertheless, high redshift bursts will offer unique opportunities to

study many interesting aspects of the cosmic history; from the era of re-ionisation (McQuinn et al., 2008) and the first population III stars (Sivaram and Arun, 2010), the formation and evolution of galaxies, the luminosity function (Jakobsson et al., 2005) and the chemical enrichment history of star forming galaxies. The ability to detect high redshift GRBs is a great improvement of what is possible even with the brightest of SNe (see Figure 1.8 for a comparison between the peak absolute magnitude of SNe, and the discovery magnitudes of GRB optical afterglows), offering considerable benefits for using them as probes of high redshift galaxy populations. While the luminosity function and cosmic star formation rate history (Figure 1.9) are well constrained at low redshift, it becomes increasingly difficult beyond redshift $z \sim 2$. Hence, GRB selection of star forming galaxies would in principle be ideal to help improve this by being able to probe even faint galaxies. While SNe are helpful at low redshift, GRBs would allow pinpointing the locations of galaxies beyond $z \sim 8$.

Although GRBs are promising for studying the evolution of the universe, we also realise the limits of our current knowledge. In reality, much remains unknown or poorly understood of how GRB progenitors evolve and how it is dependent on their environments. Without first having a solid understanding of how GRB selection works, i.e., how and why some massive stars end their lives as GRBs instead of core-collapse SNe, we can't use their full potential as cosmic probes. Hence, the goals of this thesis are to improve the understanding of GRB host galaxies and how their selection is dependant on their star formation rates, masses and metallicities. This serves as a calibration of a GRB selected sample in relation to fundamental properties.

In their full potential, the advantages of using GRB selection of star forming galaxies can be summarised as follows.

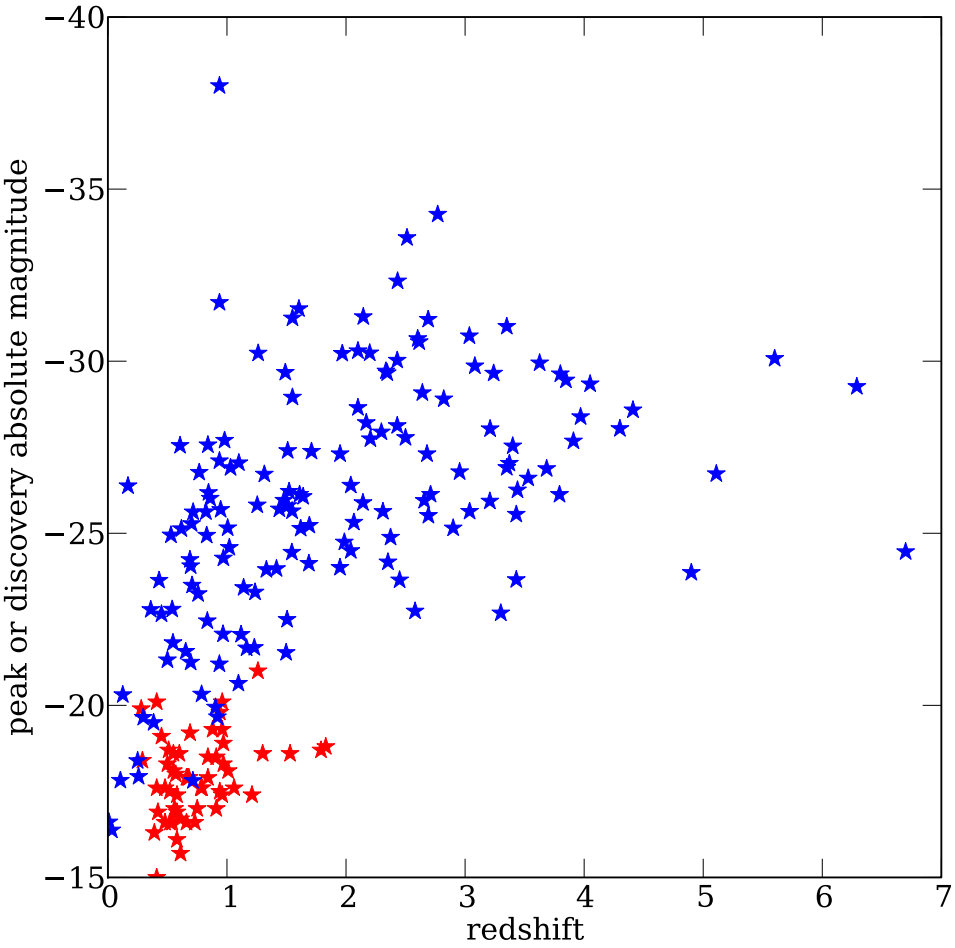

Figure 1.8: Comparison of absolute magnitudes on discovery of optical GRB afterglows (blue stars) with peak absolute magnitude of core-collapse SN lightcurves (red stars). The CCSN in this figure are found by an optical transient survey in in the GOODS North and South fields (see e.g. Strolger et al., 2004, note that core-collapse was data acquired in private communication.). The GRB sample include 153 GRBs with known redshift and discovery magnitudes reported through the GCN network, compiled by the GRBlog project. Absolute magnitudes of the GRB optical transients include first order k-correction but no spectral shape correction.

- The GRB is produced by a single stellar progenitor, allowing selection across the galaxy luminosity function.
- The afterglow is bright enough to be detected at great cosmological distances and with an intrinsic featureless powerlaw spectrum.
- The GRB event is relatively short and localised, unlike QSOs or AGNs they don't affect their host galaxies on scales larger than a few tens of parsecs.
- The afterglow fades on timescales of days to months, leaving the clean host galaxy to be observed.
- The high energy γ- and X-ray emission can easily penetrate obscuring dust and gas, meaning that GRB selected samples are less affected by extinction than optical observations.

1.5 Organisation of the thesis

Owing to their extreme luminosities, GRBs have already enabled detailed study of high-redshift star forming regions. Future prospects suggest that GRB selected sampled galaxies will reveal the nature of star formation through the evolution of the universe, essentially providing a homogeneous sample selection from the present day to redshift above $z = 8$ where the first stars and galaxies form. In this thesis I will present *new and interesting results* of research on the nature of GRB hosting galaxies, how their galactic environments compare to those of core-collapse SNe in the local universe and how future sample selections can be enhanced to improve the completeness. Briefly, the organisation of the thesis is as following:

- In **Chapter 2** I study the physical restframe properties of low redshift GRB hosts in order to statistically compare their distributions to that of classical

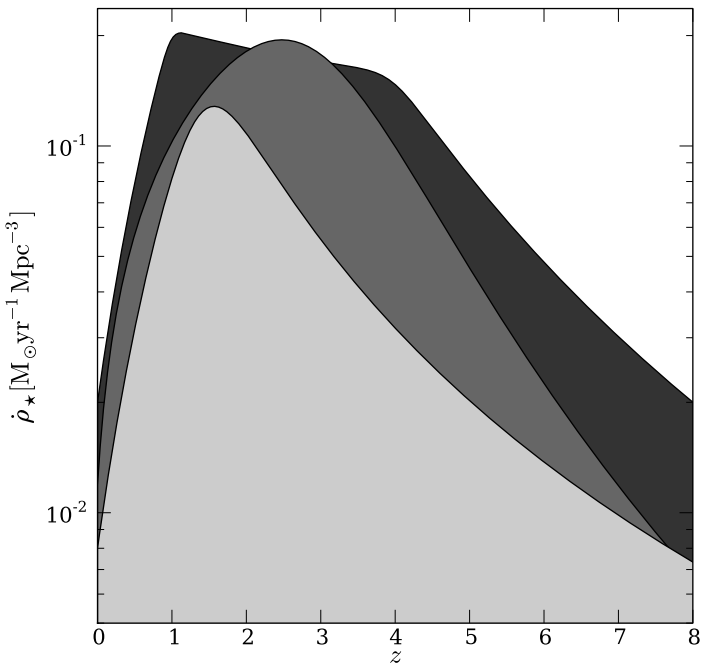

Figure 1.9: The evolution of the cosmic star formation rate as represented by three different studies. In order from light shading to darker: **(1)** The original "Madau plot" (Madau et al., 1998b) modelling the SFR from the integrated light of faint field galaxies and a Salpeter IMF. Uncertainty is increasing above $z \sim 4 - 5$. **(2)** A compilation of measurements from UV to radio by Hopkins (2004); Hopkins and Beacom (2006) modelled with the functional form of Cole et al. (2001). **(3)** Yüksel et al. (2008) incorporating high redshift GRBs scaled by local GRB-SFR ratios to extend the model of the cosmic star formation history, here using a double broken powerlaw.

CCSNe. Here I utilise multiwavelength photometry to model the spectral energy distributions and to extract absolute magnitudes and estimate host masses and star formation rates. I study the distributions of morphological properties; galaxy sizes, surface luminosities and the relative brightnesses of the GRB or SNe site on their galaxies in order to understand *how and why GRB hosts differ from those of CCSN.*

- In **Chapter 3** we study the mass and metallicity distributions of the high-redshift GRB host population. I will show that, although low redshift hosts are typically less chemically evolved than suggested by the mass-metallicity relation, at higher redshift this trend is less obvious. This also coincides with the redshift range were M^* of the galaxy mass function is sampled by a larger fraction of the hosts due to the decrease of the global metallicity, suggesting that above redshift $z \gtrsim 3-4$, GRBs are unbiased tracers of star formation. Comparing with the mass-metallicity relation of high redshift galaxy populations, these results indicate that GRBs are consistent with the chemical enrichment history probed by Lyman-break galaxies.

- In **Chapter 4** I discuss the growing evidence that *dark* bursts have evolved in significantly different environments than the bulk of the host sample studied before. I perform a case study of the dark GRB 080207 in which we model the afterglow and spectral energy distribution from X-ray to optical and show that the properties can be adequately explained by extreme amounts of intervening dust and gas in the direct line of sight. I study the multiwavelength properties of the extremely red host galaxy using observations from the best available ground and space based observatories and show that the host is an extremely dust obscured star forming galaxy with a disturbed morphology. I add this to the growing evidence that most dark bursts show extinction, and draw

more general conclusions on the implications on the dark burst hosting galaxy population, including how their omission from optically selected samples at low redshift may affect our view of e.g. metallicity biases of GRB progenitors.

Chapter 2

The host galaxies of Core-collapse supernovae and long gamma ray bursts

2.1 Introduction

Core-collapse supernovae (CCSN) mark the end-points in the lives of short-lived (lifetime $\lesssim$ few$\times 10^7$ years), massive stars (M $\gtrsim 8 M_\odot$). The selection of galaxies via the presence of a CCSN thus provides, in principle, an ideal mechanism for the detection of star forming galaxies at a range of redshifts. Long duration GRBs are closely related to CCSN, and offer similar advantages as tracers of star formation, which have been widely discussed in e.g. Jakobsson et al. (2005, 2006); Madau et al. (1998a). Specifically, both CCSN and GRB production requires only a single stellar progenitor, and so they select galaxies *independently* of the galaxy luminosity. By doing so they can point out galaxies too faint to be included in flux limited surveys, potentially providing a handle on the faint end of the galaxy luminosity function at high-z. Unlike GRBs however, CCSN are less affected by metallicity effects, and

hence they provide a more complete selection of the collapse of stars with initial main sequence masses in excess of $\sim 8 M_{\odot}$. Therefore, a census of supernova host galaxies is providing a census of essentially all massive star formation sites at a given redshift.

One drawback in the use of supernovae as a direct probe of star formation has been the inability to pursue searches for CCSN beyond $z \sim 1$, due to the limitations of current technology. Out to this distance the luminosity function, and star formation rate are reasonably well constrained through other methods. However, the recent installation of Wide Field Camera 3 (WFC3) on the *Hubble Space Telescope* (*HST*), and in the longer term the launch of *JWST* offer the opportunity to push this to much higher redshift. Nonetheless, in the interim period their potential use to "calibrate" environmental dependencies in nearby GRBs, and other star-forming galaxy samples, motivates their study.

A complication in the use of SN comes from understanding biases in their observed rate introduced by dust extinction within their hosts. While the highly penetrating γ and X-ray's from GRBs can largely circumvent problems with local extinction this is not necessarily the case for their optical afterglows. CCSN, which are several magnitudes fainter at peak than a typical GRB optical afterglow (e.g. Tanvir et al. (2010); Bloom et al. (2009) and Figure 1.8), are even more prone to non-detection due to host galaxy extinction. In practise, the extent to which extinction biases the detection of either GRB optical afterglows or CCSN remains poorly understood, although it is likely to impact both (e.g. Mannucci et al., 2003; Fruchter et al., 2006; Rol et al., 2007; Levan et al., 2006a).

Effort has already been invested in studying SN hosts, and the locations of SN within them. In particular this has focused on large samples of SN at low redshift, for example those found by, or overlapping with, the Sloan Digital Sky Survey e.g. Prieto et al. (2007) or those found in galaxies targeted by other surveys e.g.

James and Anderson (2006). These surveys offer insight into SN host properties and locations, and using local SN, with small angular distances, allow the environments to be probed in detail. However, locally discovered supernovae have historically been found by targeted searches of specific galaxy catalogues, producing a bias towards brighter host galaxies. More recent searches (e.g. SDSS, SN Factory, Skymapper and Pan-STARRS) avoid this by repeatedly tiling blank regions of sky, although they typically find more distant SN. Comparisons of these hosts suggest that while SN globally trace star formation the relative fractions of Ib/c increase in highly metal enriched environments, likely reflecting the tendency for massive stars to loose their hydrogen envelopes via radiatively driven winds at higher metallicity (Prieto et al., 2007).

All CCSN, by their nature, indicate the formation of massive stars in their hosts, while the locations of the supernovae within their hosts can also be strongly diagnostic. Fruchter et al. (2006)(hereafter F06) used a new pixel statistic (essentially the fraction of light contained in regions of lower surface brightness than the region containing SN or GRB) to show that GRBs are highly concentrated on the light of their hosts, and likely favour a much more massive and shorter lived progenitor than CCSN, which trace blue light within their host galaxy. Utilising this technique on a lower redshift sample of CCSN found in the SDSS fields, Kelly et al. (2007) show that SN Ic are also highly concentrated on the brightest regions of their hosts, a distribution very similar to GRBs. This may suggest that both GRBs and SN Ic originate only from the most massive stars (Larsson et al., 2007). James and Anderson (2006) take an alternative approach of using Hα images and similarly find that SN Ib/c are more concentrated on their hosts. They suggest that this may be due to the expulsion of SN II progenitors from their star forming regions with moderate velocities, rather than an intrinsic tendency for SN Ib/c to lie on brighter regions of their hosts. Should SNII typically originate from less massive stars than

SN Ib/c then this may be expected since the transverse distances travelled over the stellar lifetime would be larger for less massive (and hence longer lived) stars.

Although there is a growing consensus that GRBs originate from different environments than the bulk of CCSN, it is not yet clear how well the global properties of the whole host galaxy are evidence of this. Savaglio et al. (2008) note that global metallicity measurements of GRB hosts are predominantly subsolar[1]. This agrees with theoretical models of GRB production, which favour lower metallicity environments (e.g. Heger et al., 2003). Furthermore, a study by Modjaz et al. (2008) suggested that SN Ic not associated with GRBs tend to originate from more metal rich environments than SN Ic with a GRB associated. These authors also suggested that sub solar (20 to 60 percent of solar) metallicity is required to produce a GRB. A complication of testing this hypothesis is that metallicity can vary by several tenths of a dex within the hosts, both by localised enrichment (e.g. the IFU measurements by Christensen et al., 2008) and due to a radial gradient (e.g. Garnett et al., 1997; Rolleston et al., 2000). This makes spatially resolved spectroscopy, or direct measurements of metallicity from the afterglow spectrum valuable. However, this is impossible for a significant fraction of GRBs, since the angular distances are too small to resolve the hosts into many resolution elements. Thus, while not an ideal measure, estimates of the stellar mass or luminosity of the hosts can be used as a proxy for metallicity, and when averaged over a large number of hosts should still provide robust statements about CCSN and GRB environments.

Here I investigate the multi-wavelength properties of a sample of CCSN host galaxies observed by the GOODS (Great Observatories Origins Deep Survey), and PANS (Probing Acceleration Now with Supernovae) surveys, and compare these to those of GRBs. These galaxies, lying at comparable redshift to many GRBs,

[1] Although at times this conclusion depends on an assumption about the ionisation parameter within the host

although at distinctly lower-z than the mean GRB value of ~ 2.5 (Jakobsson et al., 2006), offer the opportunity for direct comparison of derived physical properties (e.g. mass, star formation rate), without the need to worry about evolutionary effects in either the galaxy luminosity function, or, in the case of GRBs, the universal evolution of metallicity. Using a large, multi-wavelength (optical through mid-IR) dataset I derive physical parameters for the host galaxies of CCSN and GRBs. This includes, rest frame luminosities, star formation rates, stellar mass and surface brightness at the GRB or SN location. Considering possible bias effects that might be present in both samples, my results broadly echo those of previous work that GRB hosts are typically smaller and less massive than those of CCSN, most likely due to metallicity bias. GRBs also originate in brighter locations, consistent with their origin in more massive stars.

2.2 Host galaxy samples

See Table 3.1 for a brief summary of the data samples and sources used in this chapter. The following sections describe the sample construction and data analysis in more detail.

2.2.1 Supernovae in GOODS and PANS

The GOODS (Giavalisco et al., 2004) survey undertook observations in two fields, centred on the Hubble Deep Field North and Chandra Deep Field South. These observations included deep observations with the *HST* using the Advanced Camera for Surveys (ACS) in the F450W(B), F606W(broad V/R), F814W(I) and F850LP(Z) filters. Rather than obtain the images in a single epoch, the observations were made roughly every 45 days, to be sensitive to the rise time of SN Ia at $z \sim 1$ (see e.g. Riess et al., 2004). As well as detecting a number of SN Ia, these observations also located

Table 2.1: Summary of GRB and CCSN data sources.

CCSN host Sample	
Sample size	58
Redshift sources	Wirth et al. (2004), Vanzella et al. (2005), Vanzella et al. (2006),Vanzella et al. (2008), Strolger et al. (2004) and Strolger (private communication).
Public photometry sources	Chary et al. (2005), Giavalisco et al. (2004)
New photometry in this thesis	Tables 2.2, 2.3 and 2.4 NB: Optical data is catalog sourced, but not previously published.
Selection Criterion	CCSN in GOODS North or South.
GRB host Sample	
Sample size	34
Redshift sources	See Savaglio et al. (2009, 2006) and sources within.
Public photometry sources	See Savaglio et al. (2009, 2006) and sources within.
New photometry in this thesis	Table 2.5 (IRAC photometry)
Selection Criterion	Long burst at z ¡ 1.2 with host detected in at least one band.

numerous core collapse supernovae (e.g. Strolger et al., 2004; Dahlen et al., 2008, and Dahlen et al. in prep) with a mean redshift of $z \sim 0.6$ (CCSN are generally less luminous at maximum than SN Ia, and so visible over a smaller volume in a flux limited sample). These SN host galaxies form an excellent sample for further study, by virtue of their selection in a blind survey, independent of galaxy luminosity (in contrast to many low-z SN searches which are targeted at specific galaxy catalogues), and because of the wide range of supporting data covering the blue optical to mid-IR regions.

These data, in addition to that secured by *HST* and described above, encompassed large programmes with *Spitzer* and also a concerted effort from ground based observatories to secure complementary near-IR observations and redshift catalogues. ACS V-band images of the resulting sample of CCSN hosts are shown in Figure 2.1.

Each SN discovered in GOODS or subsequently PANS is typed based on the available photometric and spectroscopic data on both the SN and its host galaxy.

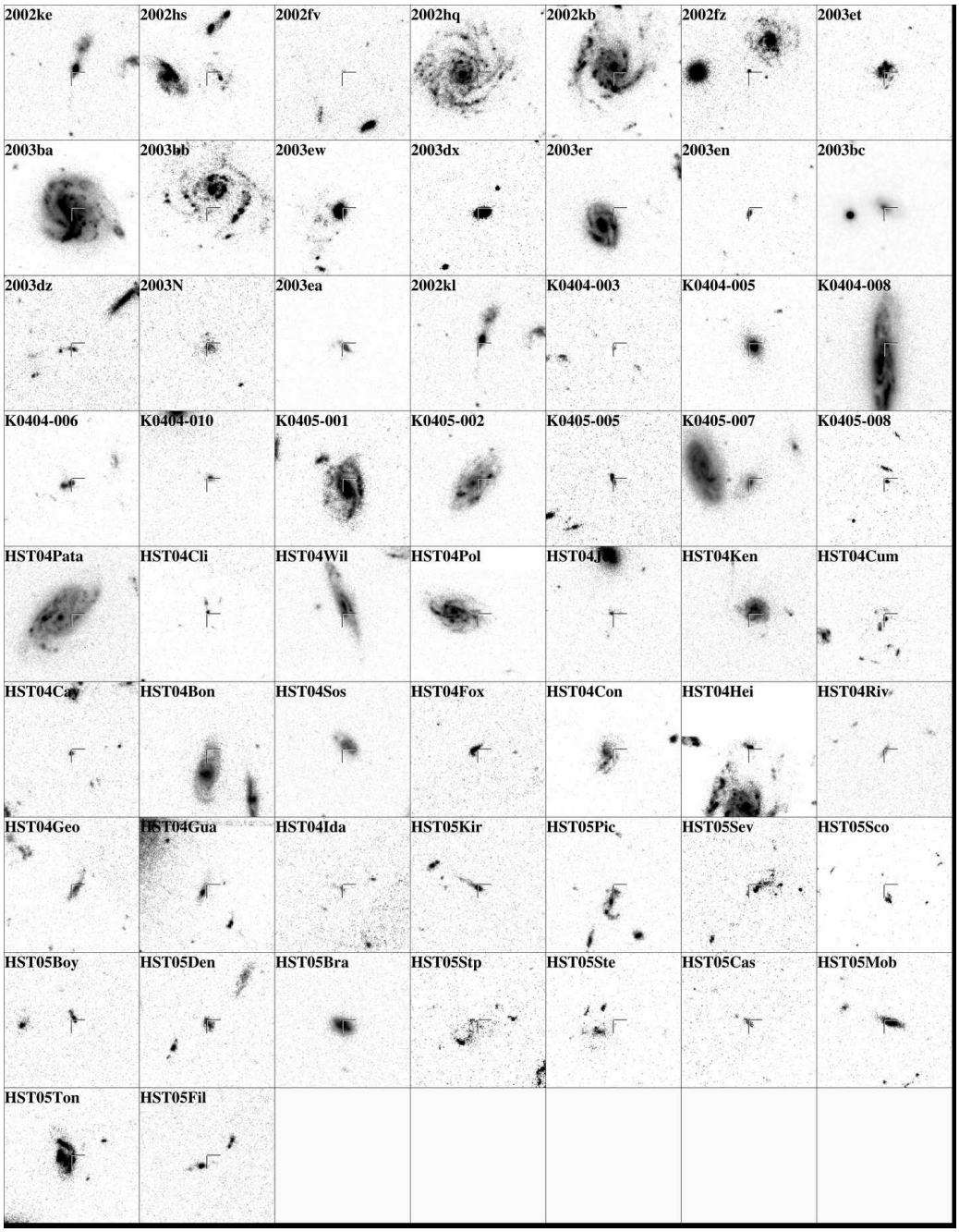

Figure 2.1: Mosaic image of the 58 CCSN host galaxies in the GOODS fields. These V-band images have a width of 7.5 arcseconds and the location of the Supernovae on the host is marked with a cross-hair.

The means of this typing is described in Strolger et al. (2004), its outcome is that the confidence in the typing of a given supernova is given by the assignation of a "medal". These medals, termed Gold, Silver or Bronze reflect both the quality and quantity of data available to type the SN. The optimal diagnostic is obviously a spectrum of the SN itself, demonstrating the clear presence (or absence) of hydrogen. Spectroscopically typed SN are given a Gold medal. In the absence of a spectrum the diagnostics used are the lightcurve shape, its peak absolute magnitude, the type of host galaxy and its U-B colour. Initially the lightcurve shape is compared to that of a SN Ia. If this fit is poor, but the lightcurve well sampled then the transient is assigned as a CCSN with a Silver medal. If the lightcurve is inconclusive, but the host galaxy appears to be star forming then (in general) the SN is typed as CCSN with a Bronze medal. Hence, it is possible that the inclusion of Bronze CCSN introduces a small number of SN Ia into the CCSN sample. I will discuss this issue, and other selection effects, further in section 8. For further details on the algorithms for the classification of each SN the reader is referred to Strolger et al. (2004).

2.2.2 GRB host galaxies

The mean redshift of GRBs in the *Swift* era is ~ 2.5 (Jakobsson et al., 2006), however a number of GRB host galaxies have been observed at redshifts across the same, or very similar range as that of the GOODS CCSN sample. To approximately match the redshift distributions I use all GRB host galaxies at $z < 1.2$. Images of the resulting sample, which have *HST* observations, are shown in Figure 2.2, the subset of the hosts for which I present *Spitzer* fluxes is shown in Figure 2.3. A comparison of the resulting redshift distributions is shown in Figure 2.4. Using this sample enables me to create a consistent dataset for CCSN and GRB hosts to perform the analysis on. This is crucial in order to be able to compare the results in a methodical way. The majority of the photometry for GRB host galaxies fitted here

is taken from F06 and Savaglio et al. (2008). However, I have supplemented this data with *HST* observations of 4 GRB host galaxies at $z < 1.2$ (GRB/XRF 050416, GRB 050525, GRB 060218 and GRB 080319B[2]) and *Spitzer* IRAC observations of a further 13 hosts. The use of *HST* makes it possible to spatially resolve these galaxies and thus enables a comparison of not only their luminosities but also physical sizes and the locations of the transients on the host. The *HST* data was reduced in the standard fashion via `multidrizzle`, and magnitudes and radii were determined following the method described in F06. See section 2.3.1 for a description of the IRAC photometry. Although deep imaging across multiple bands is available I do not include the ambiguous GRBs 060505 and 060614, whose membership of the long duration category of GRBs is controversial (e.g. see Gehrels et al., 2006; Fynbo et al., 2006; Thöne et al., 2008a; McBreen et al., 2008, for a discussion of different viewpoints).

Although the above selection largely removes any redshift bias from the observed population, there do remain important selection differences between the GRB and CCSN host population. Whilst these are difficult to quantify they should be considered before conclusions regarding the two populations are drawn. The first effect is that the CCSN have been located in a blind field search, and have a wide range of complementary data. This means that it is possible to derive at least a photometric redshift for every CCSN within the sample. In contrast there are a number of very faint GRB host galaxies, which do not have spectroscopic redshifts, and have insufficient bands for photometric redshifts to be plausible. Should these lie in the range of redshift I consider here ($z < 1.2$) their non-inclusion would tend to bias the observed population to higher luminosity. Indeed, even for the systems with measured redshifts, the majority of the low-z sample, (~ 28 from 34) come via emission line measures in their host systems, rather than absorption lines in the af-

[2]Host photometry extracted after subtraction of point source, see also Tanvir et al. (2010)

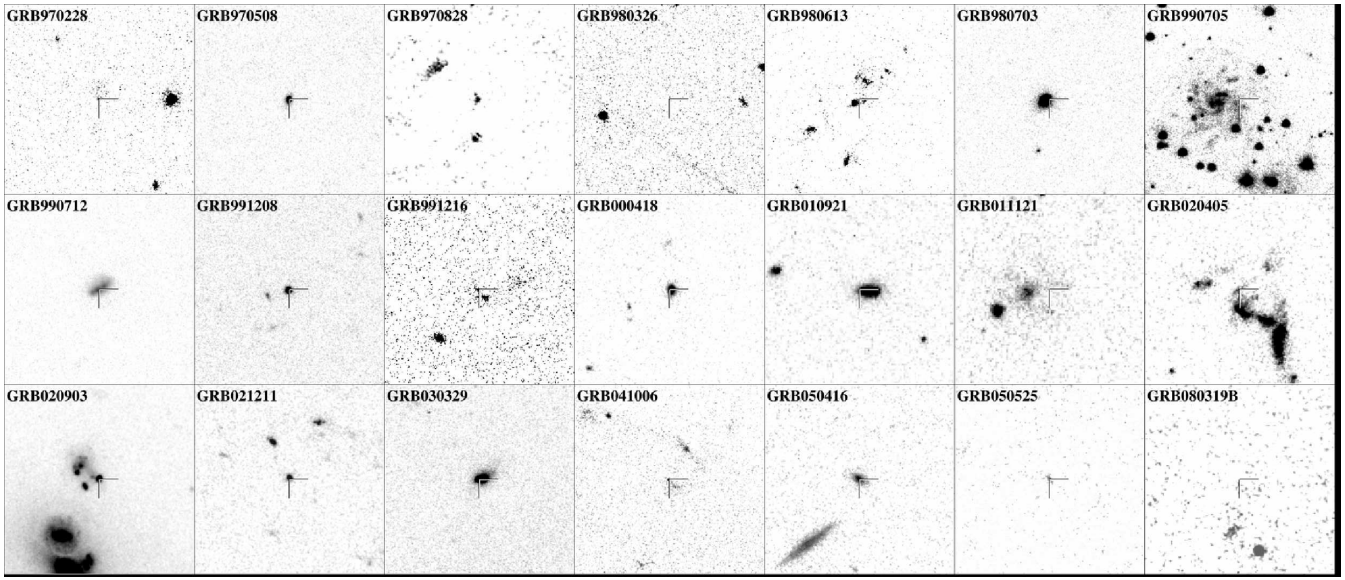

Figure 2.2: Mosaic image of GRB host galaxies with *HST* imaging. The images are 7.5 arcseconds wide, and the locations of the GRBs on the host is marked with a cross-hair.

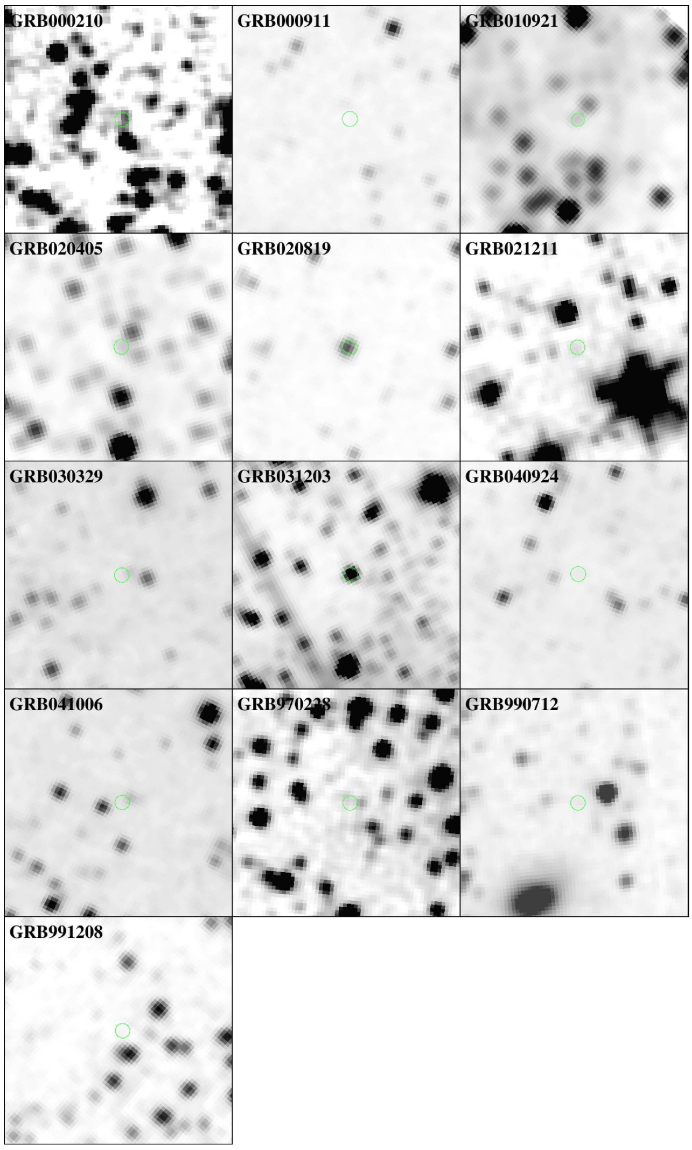

Figure 2.3: Mosaic image showing the GRB hosts observed with *Spitzer* IRAC. Images are in $3.6\mu m$ where available, otherwise in $4.5\mu m$. The width of each tile is ~ 80 arcseconds.

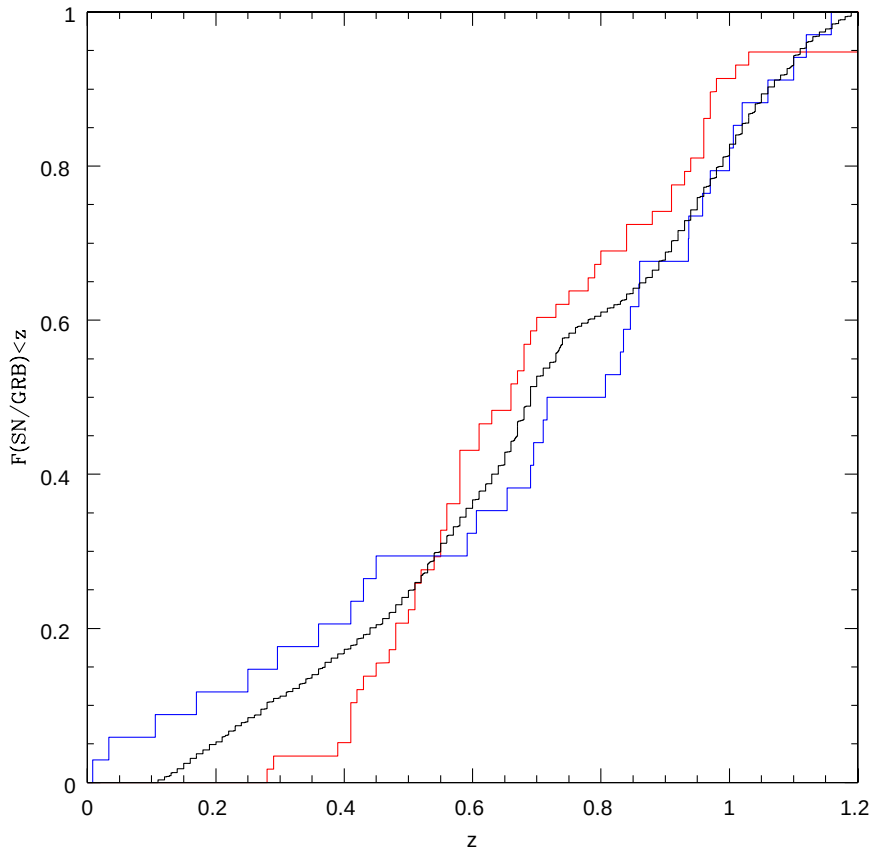

Figure 2.4: The redshift cumulative distributions of the GRB (blue) and SN (red) samples used in this chapter. To provide similar redshift distributions I only consider GRBs with $z < 1.2$. The redshift distribution of 6900 MUSIC field galaxies is plotted in black.

terglow, which may well create a bias towards brighter hosts, and will be considered in more detail later. In a similar spirit I have included GRBs with hosts identified both by their optical afterglows and where the X-ray afterglow is sufficient to unambiguously locate the host, however it should be noted that bursts with particularly faint optical afterglows (by dust extinction) could be missed from the sample.

Finally, there are a number of host galaxies at known redshift (GRBs 980326, 990705, 991216, 050416A, 050525A, 050824 and 051016B), which have observations in a single photometric band, precluding a detailed analysis of their spectral energy distributions. Excluding these would create a further bias within the samples, and so, rather than omitting them I derive physical parameters by assuming they can be fit with the spectral template which provides the best fit of the majority of the GRB hosts. Although this produces potential systematic errors into the analysis (for example the fainter galaxies may typically have different colours than the brighter systems where the templates are derived) it is preferable to their complete omission.

2.2.3 GOODS-MUSIC: A comparison sample

The GOODS-MUSIC (MUltiwavelength Southern Infrared Catalog) (Grazian et al., 2006) includes photometry ranging from U-band (2.2ESO and VLT-VIMOS) to the 8 μm IRAC band. Of the $\sim$ 14000 objects listed in the catalog, I select $\sim$ 6900 non-stellar, non-AGN objects with $0.1 < z < 1.2$ (redshift either spectroscopic or photometric) as a field galaxy comparison sample to the GRB and CCSN populations. The object selection for the MUSIC catalog is made in the ACS z-band with a secondary selection made in the Ks-band to obtain a higher completeness. The limiting magnitudes are reported to be $z_{lim} \sim 26$ or $K_{lim} \sim 24$ (AB magnitudes) at a completeness level of 90 %.

Although this is a magnitude limited catalog, whereas the GRBs and CCSNe are are detected independent of host magnitude, I consider this a good sample of

field galaxies at similar redshifts to those of the GRBs and CCSNe described above. It should also be noted that method of selecting the MUSIC galaxies does not bias towards highly starforming galaxies like the selection based on core-collapse events does. The MUSIC galaxies are hence bound to give a representation of all Hubble types, i.e. include starforming spiral and irregular galaxies as well as passive elliptical galaxies.

2.3 Photometry

Image data from GOODS is used to assemble photometry in up to 12 bands. B, V, I and Z bands are taken from *Hubble*'s Advanced Camera for Surveys (ACS). Near infrared J, H and K bands from ground based Very Large Telescope (VLT) using the Infrared Spectrometer And Array Camera (ISAAC). Infrared images come from *Spitzer*'s InfraRed Array Camera (IRAC) at 3.6, 4.5, 5.8 and 8 μm wavelength. Further infrared magnitudes at 24 μm (*Spitzer* MIPS) are adopted from Chary et al. (2005). The ACS data comes in high resolution (0.03 arcseconds per pixel) drizzled images. I use the online cutout-service [3] to extract only the galaxy and it immediate surroundings from the larger mosaic image. The *Spitzer* images are lower resolution and one image of manageable size covers the entire field.

Photometry on the ACS images for the 16 hosts in the original sample (F06) is initially done with the qphot package in IRAF. I then compared this photometry with the GOODS source catalog (Giavalisco et al., 2004), and finding a good agreement between them, I adopted catalog values for all of the hosts (see Table 2.2). Photometry on the ISAAC data, J, H and K bands was also checked for consistency between automatic source detection via SExtractor (Bertin and Arnouts, 1996) and manual aperture photometry, after which I create a source catalog, and adopt

[3] http://archive.stsci.edu/eidol.php

values from this for all of the hosts (see Table 2.3).

Due to the high amount of blending in the IRAC bands, automatic source detection is more challenging than for the optical and NIR bands. Photometry of the IRAC data is performed by hand, see below for a more detailed description.

In addition to photometric data I also extract measured radii from the GOODS catalogue values. These are converted into physical sizes using the assumed cosmology (ΛCDM, Ω_M =0.27, $\Omega_\Lambda = 0.73$, $H_0 = 71$ km s^{-1} Mpc^{-1}).

The majority of the host galaxy photometry for the GRB host galaxies is collected from the GHostS project, where the photometry is compiled from numerous sources, see Savaglio et al. (2008) and references within. All photometry has been corrected for galactic extinction following Schlegel et al. (1998).

2.3.1 IRAC photometry

The GOODS fields have been imaged in the *Spitzer* IRAC bands, from which I have measured and report photometry for 56 of the 58 CCSN hosts in Table 2.4. A number of GRB hosts have also been imaged in the IRAC bands, in addition to the reported magnitudes collected from the GHostS project. I have analysed these images and report 26 new $3.6\mu m - 8.0\mu m$ magnitudes or magnitude limits for GRB hosts in Table 2.5.

Note that, due to the amount of blending between sources at IRACs resolution, for some galaxies reliable photometry could not be achieved. In these cases the catalog entry is left blank.

The GOODS Spitzer/IRAC observations have been mosaiced and drizzled to a pixel scale of 0.6 arcsec/pixel, limiting magnitudes are $\sim 24 - 25$ depending on the IRAC band and extent of the source, as estimated from *HST* imaging. The GRB observations are reduced by the standard IRAC pipeline, and have the native pixel scale of 1.2 arcsec/pixel. Limiting magnitudes are $\sim 19 - 23$ depending on

exposure times and bands of the individual observations.

The photometry is performed with a program coded in Python, using the PyFITS module provided by STScI to interact with FITS images, to extract (normal extraction) the flux inside a circular aperture with sub-pixel accuracy. The background is measured from blank apertures outside the host, which also provide the background standard deviation for determination of limiting magnitudes. Quoted limits are 3-sigma.

At the resolution of IRAC, the majority of the hosts are unresolved; in which case I use small aperture photometry and aperture corrections according to the official IRAC calibration (for the GRB hosts) or as determined from the curve of growth (CCSNe in the GOODS mosaic). If the source emission is determined to have a FWHM larger than the FWHM of the PSF, I extract the photometry from a large aperture enclosing all of the flux.

2.4 Spectral Energy Distribution fitting

The collected photometry covering wavelengths from 0.4 μm (ACS B-band) to 24 μm (*Spitzer* MIPS), allows me to fit template spectral energy distributions that are close representations of the true SED within these limits. Redshifts for the CCSN hosts are determined spectroscopically in 41 cases and photometrically in 17. Spectroscopic redshifts are adopted either from Strolger et al. (2004) where available, or by querying the Team Keck Treasury Redshift Survey (TKRS) (Wirth et al., 2004) for the GOODS north field, or the GOODS/FORS2 release 3 (Vanzella et al., 2005, 2006, 2008) online redshift catalog in the south field. Photometric redshifts are calculated with the HyperZ photometric redshift code (Bolzonella et al., 2000) [4]. The SED fitting includes only two degrees of freedom: a wavelength

[4]Consistency is checked using objects overlapping with the MUSIC catalog.

Table 2.2: Photometric catalog over CCSN host galaxies in the GOODS fields. Errors are 1 sigma standard errors, limits are 3 sigma limiting magnitudes estimated from the sky background.

SN name	B	V	I	Z
2002fv	28.94 ± 0.53	28.16 ± 0.21	26.78 ± 0.12	26.89 ± 0.17
2002fz	23.23 ± 0.19	22.4 ± 0.07	21.45 ± 0.07	21.11 ± 0.08
2002hs	24.17 ± 0.17	23.93 ± 0.12	23.51 ± 0.18	23.06 ± 0.17
2002hq	21.93 ± 0.18	21.08 ± 0.06	20.19 ± 0.07	19.90 ± 0.08
2002kb	21.47 ± 0.14	20.64 ± 0.05	20 ± 0.07	19.78 ± 0.08
2002ke		21.45 ± 0.05	20.72 ± 0.07	20.47 ± 0.08
2002kl	23.32 ± 0.13	22.69 ± 0.06	22.28 ± 0.1	22.18 ± 0.13
2003ba	21.07 ± 0.04	20.06 ± 0.01	19.63 ± 0.02	19.43 ± 0.03
2003bb	22.32 ± 0.29	21.62 ± 0.12	20.71 ± 0.13	20.24 ± 0.12
2003bc	22.6 ± 0.05	21.78 ± 0.02	21.29 ± 0.03	21.14 ± 0.04
2003dx	24.02 ± 0.04	23.31 ± 0.02	22.78 ± 0.02	22.65 ± 0.03
2003dz	25.51 ± 0.18	25.28 ± 0.14	24.79 ± 0.19	24.57 ± 0.24
2003en	25.78 ± 0.06	25.34 ± 0.04	24.53 ± 0.04	24.49 ± 0.04
2003er	22.65 ± 0.12	21.40 ± 0.03	20.41 ± 0.03	20.05 ± 0.03
2003et	23.34 ± 0.04	23.09 ± 0.03	22.73 ± 0.04	22.25 ± 0.04
2003ew	23.55 ± 0.14	22.61 ± 0.05	21.76 ± 0.05	21.45 ± 0.06
2003N	24.96 ± 0.16	24.7 ± 0.11	24.32 ± 0.17	23.88 ± 0.17
K0404-005	24.95 ± 0.08	22.88 ± 0.01	21.23 ± 0.01	20.57 ± 0.0
K0404-003	27.19 ± 0.14	27.13 ± 0.14	26.53 ± 0.16	26.43 ± 0.17
K0404-006	24.03 ± 0.02	23.45 ± 0.01	23.02 ± 0.02	22.77 ± 0.02
K0404-008	21.15 ± 0.01	19.84 ± 0.0	19.16 ± 0.0	18.83 ± 0.0
K0404-010	27.45 ± 0.44	25.26 ± 0.05	23.76 ± 0.03	23.22 ± 0.02
K0405-001	22.39 ± 0.01	21.66 ± 0.01	21.04 ± 0.01	20.87 ± 0.01
K0405-002	22.39 ± 0.01	21.62 ± 0.01	21 ± 0.01	20.83 ± 0.01
K0405-005	26.04 ± 0.11	25.24 ± 0.04	24.37 ± 0.04	24.33 ± 0.05
K0405-007	24.14 ± 0.03	23.03 ± 0.01	22.21 ± 0.01	21.91 ± 0.01
K0405-008	27.02 ± 0.23	26.22 ± 0.09	25.59 ± 0.1	24.89 ± 0.06
HST04Pata		20.13 ± 0.0	19.56 ± 0.0	19.26 ± 0.0
HST04Cli	26.92 ± 0.16	25.85 ± 0.05	25.42 ± 0.06	25.47 ± 0.08
HST04Wil	22.65 ± 0.01	21.72 ± 0.01	21.27 ± 0.01	21.08 ± 0.01
HST04Pol	22.22 ± 0.01	21.43 ± 0.0	20.74 ± 0.0	20.5 ± 0.0
HST04Jef	25.7 ± 0.1	25.83 ± 0.1	24.99 ± 0.09	25.04 ± 0.13
HST04Ken	23.05 ± 0.02	22.21 ± 0.01	21.56 ± 0.01	>24.43
HST04Cum	25.17 ± 0.05	25.04 ± 0.04	24.58 ± 0.05	24.50 ± 0.05
HST04Cay	26.75 ± 0.1	25.74 ± 0.03	25.58 ± 0.06	25.39 ± 0.06
HST04Bon	23.56 ± 0.03	21.94 ± 0.01	20.67 ± 0.0	20.23 ± 0.0
HST04Sos	23.90 ± 0.03	22.8 ± 0.01	22.05 ± 0.01	21.76 ± 0.01
HST04Fox	24.91 ± 0.04	24.6 ± 0.02	24.01 ± 0.03	>26.36
HST04Con	23.43 ± 0.02	22.95 ± 0.01	22.08 ± 0.01	21.76 ± 0.01
HST04Hei	21.47 ± 0.14	20.64 ± 0.05	20.00 ± 0.07	19.78 ± 0.08

SN name	B	V	I	Z
HST04Riv	26.45 ± 0.13	25.64 ± 0.05	24.80 ± 0.05	>26.18
HST04Geo	24.26 ± 0.03	24.08 ± 0.03	23.36 ± 0.03	23.12 ± 0.02
HST04Gua	26.11 ± 0.17	24.36 ± 0.04	22.66 ± 0.01	21.66 ± 0.01
HST04Ida	27.10 ± 0.11	26.29 ± 0.08	26.49 ± 0.21	26.59 ± 0.3
HST05Kir	24.66 ± 0.04	24.43 ± 0.03	23.98 ± 0.03	24.10 ± 0.05
HST05Pic	23.60 ± 0.02	23.47 ± 0.02	22.81 ± 0.02	22.65 ± 0.02
HST05Sev	24.15 ± 0.05	24.18 ± 0.04	23.66 ± 0.04	23.32 ± 0.04
HST05Sco	25.20 ± 0.06	25.34 ± 0.06	24.58 ± 0.06	24.35 ± 0.06
HST05Boy	25.45 ± 0.05	25.29 ± 0.04	24.80 ± 0.05	>26.37
HST05Den	25.30 ± 0.07	24.78 ± 0.04	23.92 ± 0.03	23.53 ± 0.03
HST05Bra	23.32 ± 0.02	22.28 ± 0.01	21.63 ± 0.01	21.36 ± 0.01
HST05Str	24.03 ± 0.04	23.84 ± 0.04	23.21 ± 0.03	22.93 ± 0.03
HST05Ste	24.34 ± 0.23	23.75 ± 0.09	23.32 ± 0.1	23.51 ± 0.1
HST05Cas	26.33 ± 0.15	25.83 ± 0.08	24.98 ± 0.07	24.89 ± 0.08
HST05Mob	24.91 ± 0.05	23.93 ± 0.02	22.97 ± 0.02	22.66 ± 0.01
HST05Ton	23.22 ± 0.02	22.45 ± 0.01	21.45 ± 0.01	21.15 ± 0.01
HST05Fil	24.94 ± 0.04	24.73 ± 0.03	24.57 ± 0.04	24.38 ± 0.04

Table 2.3: Photometric catalog over CCSN host galaxies in the GOODS fields. Errors are 1 sigma standard errors, limits are 3 sigma limiting magnitudes estimated from the sky background.

SN name	J	H	K
2002fv	>27.82	>24.17	>26.96
2002fz	>23.78		20.01 ± 0.02
2002hs	23.25 ± 0.05	23.02 ± 0.62	22.70 ± 0.05
2002hq	19.45 ± 0.02	19.23 ± 0.14	18.85 ± 0.02
2002kb	19.3 ± 0.02	19.18 ± 0.17	18.89 ± 0.03
2002ke			
2002kl			
2003ba			
2003bb			
2003bc			
2003dx			
2003dz			
2003en			
2003er			
2003et			
2003ew			
2003N			

SN name	J	H	K
K0404-005			
K0404-003			
K0404-006			
K0404-008			
K0404-010			
K0405-001			
K0405-002			
K0405-005			
K0405-007			
K0405-008			
HST04Pata			
HST04Cli	24.22 ± 0.5		23.28 ± 0.32
HST04Wil	20.83 ± 0.1	20.75 ± 0.1	20.61 ± 0.09
HST04Pol	20.15 ± 0.07	19.91 ± 0.07	19.62 ± 0.06
HST04Jef	>27.14	>23.63	>26.31
HST04Ken	20.91 ± 0.1	20.74 ± 0.1	20.45 ± 0.08
HST04Cum			
HST04Cay			
HST04Bon	19.59 ± 0.06	19.18 ± 0.05	18.81 ± 0.04
HST04Sos	21.37 ± 0.13	21.22 ± 0.12	20.96 ± 0.11
HST04Fox	23.92 ± 0.42	23.73 ± 0.39	23.43 ± 0.34
HST04Con			
HST04Hei	19.3 ± 0.02	19.18 ± 0.17	18.89 ± 0.03
HST04Riv	24.47 ± 0.56	25.18 ± 0.79	24.36 ± 0.53
HST04Geo			
HST04Gua			
HST04Ida			
HST05Kir			
HST05Pic			
HST05Sev			
HST05Sco			
HST05Boy	24.29 ± 0.51		24.24 ± 0.52
HST05Den			
HST05Bra			
HST05Str			
HST05Ste			
HST05Cas			
HST05Mob			
HST05Ton			
HST05Fil			

Table 2.4: Photometric catalog continued: *Spitzer* IRAC bands

SN name	3.6 μm	4.5 μm	5.8 μm	8 μm
2002fv	> 25.65	24.52 ± 0.14	> 23.58	> 24.69
2002fz				
2002hs	21.78 ± 0.01	21.79 ± 0.01	22.37 ± 0.06	22.53 ± 0.06
2002hq	18.89 ± 0.01		19.39 ± 0.03	
2002kb	19.28 ± 0.01	19.95 ± 0.0	19.8 ± 0.13	19.74 ± 0.01
2002ke	19.97 ± 0.01		20.47 ± 0.2	
2002kl	22.4 ± 0.03		23.17 ± 0.21	
2003ba		19.45 ± 0.01		18.55 ± 0.01
2003bb		18.97 ± 0.01		19.43 ± 0.03
2003bc				
2003dx		22.44 ± 0.02		22.46 ± 0.08
2003dz		23.35 ± 0.04		23.66 ± 0.2
2003ea	22.4 ± 0.07	22.78 ± 0.07	23.06 ± 0.38	> 23.25
2003en	24.58 ± 0.24	25.33 ± 0.25	> 22.93	> 25.44
2003er		19.55 ± 0.0		20.08 ± 0.03
2003et		20.89 ± 0.01		21.19 ± 0.02
2003ew		21.16 ± 0.01		21.34 ± 0.05
2003N	21.86 ± 0.02	21.86 ± 0.01	22.04 ± 0.07	22.2 ± 0.1
K0404-005	18.99 ± 0.0	19.52 ± 0.0	19.67 ± 0.01	20.13 ± 0.04
K0404-003		24.71 ± 0.16		23.44 ± 0.26
K0404-006	21.03 ± 0.01		20.79 ± 0.02	
K0404-008	18.02 ± 0.0		18.33 ± 0.01	
K0404-010	21.71 ± 0.02	23.52 ± 0.03	22.76 ± 0.19	22.9 ± 0.12
K0405-001		20.99 ± 0.01		21.19 ± 0.05
K0405-002		20.98 ± 0.01		20.97 ± 0.05
K0405-005	24.03 ± 0.07	24.29 ± 0.1	> 23.97	> 24.23
K0405-007				
K0405-008	23.1 ± 0.06		23.15 ± 0.2	
HST04Pata	18.86 ± 0.0	19.26 ± 0.0	19.25 ± 0.03	17.97 ± 0.02
HST04Cli	22.88 ± 0.13		22.47 ± 0.11	
HST04Wil	20.91 ± 0.03		21.43 ± 0.07	
HST04Pol	19.83 ± 0.01	20.2 ± 0.0	20.19 ± 0.04	20.28 ± 0.05
HST04Jef				
HST04Ken				
HST04Cum	23.21 ± 0.05	23.5 ± 0.05	23.69 ± 0.23	> 24.06
HST04Cay	23.65 ± 0.05	23.83 ± 0.08	23.11 ± 0.27	23.79 ± 0.32
HST04Bon	18.97 ± 0.0	19.32 ± 0.0	19.34 ± 0.01	19.51 ± 0.01
HST04Sos	21.21 ± 0.02	21.54 ± 0.01	21.76 ± 0.08	21.82 ± 0.06
HST04Fox		24.23 ± 0.09		> 24.54
HST04Con	20.77 ± 0.0	21.25 ± 0.01	21.2 ± 0.05	21.88 ± 0.07
HST04Hei	19.28 ± 0.01	19.95 ± 0.0	19.8 ± 0.13	19.74 ± 0.01
HST04Riv	23.89 ± 0.06		23.97 ± 0.44	

SN name	3.6 μm	4.5 μm	5.8 μm	8 μm
HST04Geo		23.13 ± 0.02		23.72 ± 0.23
HST04Gua	18.74 ± 0.03		19.18 ± 0.04	
HST04Ida		24.32 ± 0.16		> 24.21
HST05Kir				
HST05Pic	22.42 ± 0.03		22.69 ± 0.26	
HST05Sev	23.51 ± 0.08		23.47 ± 0.38	
HST05Sco	22.06 ± 0.03		22.7 ± 0.17	
HST05Boy		24.8 ± 0.26		> 24.47
HST05Den	22.65 ± 0.03	22.75 ± 0.02	23.05 ± 0.12	23.05 ± 0.17
HST05Bra	20.82 ± 0.0	21.04 ± 0.01	21.11 ± 0.03	20.93 ± 0.04
HST05Str	21.99 ± 0.07	22.4 ± 0.06	> 22.1	22.55 ± 0.13
HST05Cas		> 26.07		> 24.67
HST05Mob	21.3 ± 0.03	21.87 ± 0.01	21.85 ± 0.1	22.37 ± 0.09
HST05Ton	19.79 ± 0.0	20.28 ± 0.0	20.23 ± 0.03	20.51 ± 0.02
HST05Fil	23.32 ± 0.06		> 24.25	
HST05Ste	23.54 ± 0.09		> 23.81	

Table 2.5: GRB host photometry in the *Spitzer* IRAC bands. Limits are 3-sigma background estimates, errors are 1-sigma.

GRB	3.6 μm	4.5 μm	5.8 μm	8 μm
970228	22.02 ± 0.2		> 20.02	
990712		21.98 ± 0.4		> 19.42
991208		> 22.21		> 20.57
000210		21.76 ± 0.23		20.48 ± 0.25
000911		> 22.12		> 18.41
010921	21.74 ± 0.43		> 20.15	
020405	20.81 ± 0.15		> 19.82	
020819	18.96 ± 0.02		19.27 ±0.22	
021211		21.24 ± 0.24		> 18.57
030329	>22.59		> 18.96	
031203	18.19 ± 0.03		17.6 ± 0.06	
040924	>21.92		> 19.81	
041006	21.43 ± 0.19		> 20.0	

independent flux proportionality, and a reddening inside the host galaxy that is wavelength dependent and calculated in the host restframe. The reddening curve is adopted from Calzetti et al. (2000) which is derived to suit actively starforming galaxies.

Template spectral energy distributions are collected from the literature. They include both observed SEDs of local galaxies and SEDs produced with various spectral synthesis codes. Mean templates for local ellipticals and spirals galaxies are adopted from Coleman et al. (1980). Synthetic GISSEL98 spectra ranging along the entire Hubble sequence are adopted from Bruzual A. and Charlot (1993), and synthetic fits for local galaxies ARP220, HR10, M51, M82, M100, NGC 6090 and NGC 6946 are adopted using the GRASIL spectral libraries of Silva et al. (1998). I also include GRASIL synthetic templates fitted for submm selected GRB hosts by Michałowski et al. (2008).

The best fit is given by minimising

$$\chi^2 = \sum_{i=1}^{N_{filter}} \left(\frac{f_{i,obs} - b \times f_{i,template} \times 10^{\frac{k(\lambda)A_v}{R_v}}}{\sigma_{i,f}} \right)^2 \tag{2.1}$$

with respect to the scaling parameter b, and the reddening parameter A_v. The reddening curve $k(\lambda)$ and $R_v = 4.05$ are fixed by the reddening law. The optimum SED template is transformed to its restframe and analysed to estimate physical parameters of the host galaxy. For wavelengths between two photometric bands this means we derive the flux from a model fit that is more secure than a simple linear interpolation, or by assuming a globally flat SED. Some examples of the SED fits are shown in Figure 2.5. Having determined the best fitting spectral templates I derive absolute magnitudes in given photometric bands by integrating the spectrum over the response function of the filter. In Figure 2.6 I plot the derived M_V values against the radii of each host galaxy (here defined by r_{80} – the 80% light

radius).

In the following section I describe in brief the parameter-SED relations used to estimate stellar mass content ($M_\star$) of the hosts, their star formation rates (SFR) and metallicities ($12 + \log O/H$). Note that the spectral energy distributions are corrected for internal extinction added in the fitting procedure when estimating these properties. Estimating the uncertainties of the final parameters is, due to the nature of the SED fitting, difficult. The statistical errors of the final "best" fit model can be easily computed by allowing the normalisation constant of the fit to change, giving errors that are proportional to the photometry errors. A fully comprehensible estimate of the errors introduced by the fitting should rather involve a *model independent* treatment, i.e. not being limited to the best fit model. Such treatment would likely involve a much increased computational load deriving from the necessity for additional fitting in a Monte Carlo type of simulation. Such treatment it unfortunately outside the scope of this work. Nevertheless, it should be noted that the implicit uncertainties of all properties derived from the model fits involve both a statistical (i.e. deriving from the photometric uncertainty) and a systematical (i.e. introduced by the model fitting) component. Furthermore, it's important to note that the systematic component is highly dependent on the photometric coverage, and variable across the SED in such a way that it is small close to, or between, measured wavelengths, and grows far away, or outside the wavelength range sampled by photometry.

2.5 Deriving Physical Parameters

2.5.1 Stellar masses

The stellar component of the total mass in a galaxy, $M_\star$, can be estimated using the rest frame K-band luminosity, which samples the old stellar population with a

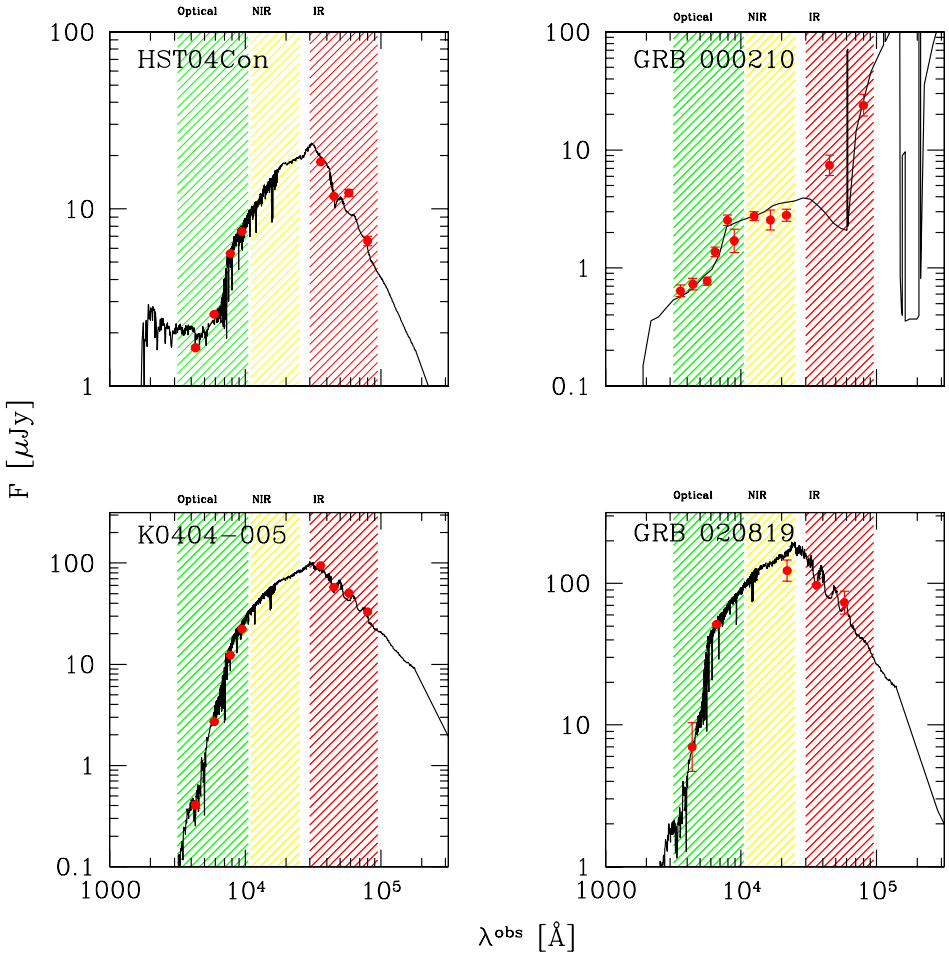

Figure 2.5: Example spectral energy distribution fits. Wavelengths are in the observed frame. Host galaxies of SNe HST04Con and K0404-005 have absolute V magnitudes of -21.37 and -22.53 respectively. The hosts of GRBs 000210 and 020819 have absolute magnitudes of -20.07 and -21.93 respectively

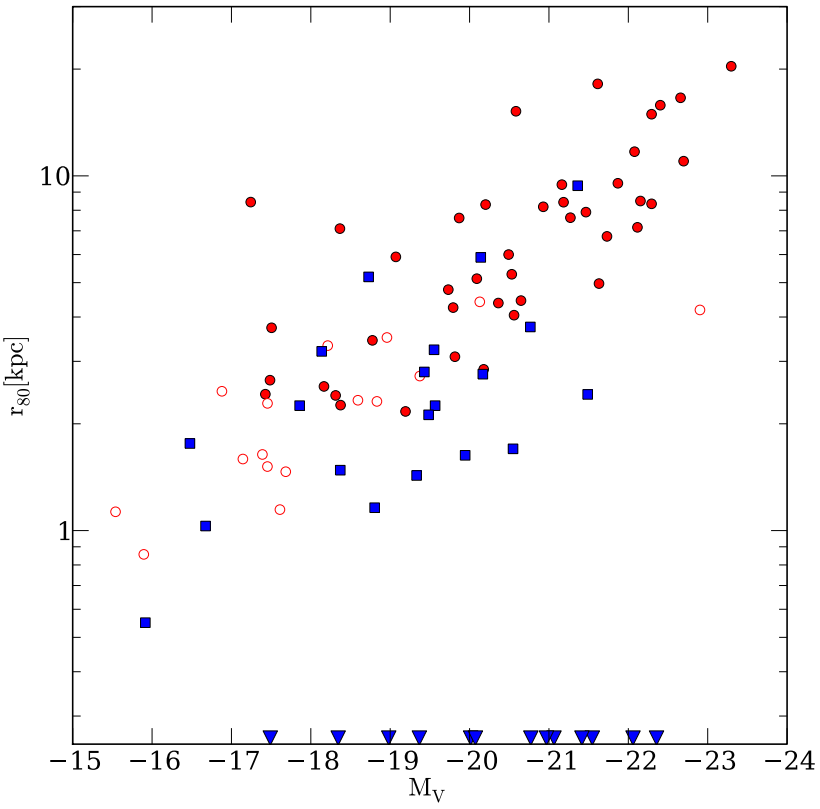

Figure 2.6: 80 % light radius versus absolute V band magnitude for GRB hosts (blue squares), CCSN hosts (red points, filled for hosts with spectroscopic redshifts). Blue triangles on the bottom axis are the absolute magnitudes for GRB without a measured radius (i.e. those without *HST* imaging).

much weaker contribution from hot and massive short lived stars. I note that some caution has been suggested when using this method on stellar populations dominated by young to intermediate aged stars, as red supergiants can become a significant source of enhanced K-band luminosity, and thereby lead to an overestimate of the stellar mass, e.g. Leitherer and Heckman (1995). A standard method of mass estimation is the mass to light ratio, where one assumes a proportional relationship between the stellar mass and the K-band luminosity. Castro Cerón et al. (2006) prescribe $M_\star/L_K \sim 0.1$ for the GRB host galaxies in their sample. Here I have chosen to estimate the stellar masses with the relation of Savaglio et al. (2009),

$$\log(M_\star/M_\odot) = -0.467 \times M_K - 0.179, \tag{2.2}$$

where $M_\star$ is the total stellar mass of the galaxy in units of solar masses. This relation is calibrated on the basis of GRB hosts, (see also Glazebrook et al. (2004) for details on this mass calibration) and give results that are consistent with the mass to light ratio in Castro Cerón et al. (2006).

2.5.2 Starformation rates

While the K-band luminosity is an indicator of the old stellar population in a galaxy, the U-band luminosity samples the SED contribution from the hot, massive and hence newly formed stars. Following Cram et al. (1998) the SFR is estimated by,

$$SFR_U(\mathrm{all}) = \frac{8.8 \times L_U}{1.5 \times 10^{22} \mathrm{Whz}^{-1}} \mathrm{M}_\odot \mathrm{yr}^{-1}. \tag{2.3}$$

Where L_U is the U-band luminosity in units of Whz^{-1}, and the factor 8.8 is introduced to correct from $SFR_U(M/M_\odot > 5)$ to account for all star formation. It should be noted that this SFR is not model independent, but rather it assumes a certain initial mass function (IMF). Cram et al. (1998) assume a Salpeter IMF.

Both stellar masses and star formation rates may be inaccurately estimated if the IMF is strongly deviating from that of Salpeter.

Further useful quantities are the specific star formation rate (SSFR) Φ,

$$\Phi = \frac{SFR}{M_\star} \ \mathrm{yr}^{-1}, \tag{2.4}$$

and the star formation surface density Σ,

$$\Sigma = \frac{SFR}{\pi r_{80}^2} \ \mathrm{M_\odot yr^{-1} kpc^{-1}}, \tag{2.5}$$

– star formation per unit stellar mass and unit area in the galaxy respectively. Since these indicate how intense the star formation is, they are in some regards a more interesting parameters to study than the SFR itself. GRB hosts are believed to have high SSFR in general, as the presence of GRB itself is evidence of the formation of massive stars. Indeed this is supported by Castro Cerón et al. (2006) who place the SSFRs of four $z \sim 1$ GRB hosts amongst the highest observed. In Figure 2.7 I plot the SSFRs vs the masses for the GRB and CCSN hosting galaxy populations, as well as a selection of other high-z galaxy populations.

2.5.3 Metallicities

The role of progenitor metallicity in determining the outcome of massive-star core collapse has been discussed by various authors. With the difficulties in making direct measurements of the metallicity at high redshift, mass or luminosity are commonly used as proxies. The existence of a relationship between galactic stellar mass and its metallicity has been known since Lequeux et al. (1979) published their results based on a sample of eight local galaxies. Their conclusion that low stellar mass galaxies also have lower metallicities, has since been confirmed and extended by using the

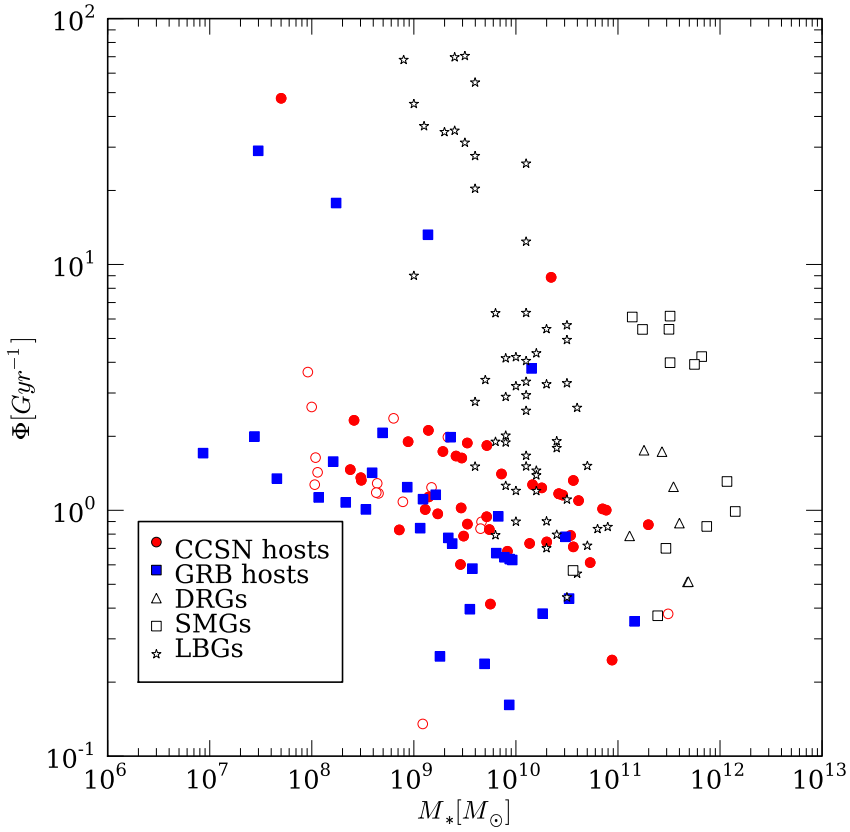

Figure 2.7: Specific star formation rates versus stellar mass for GRB hosts (blue squares), CCSN hosts (red circles, filled for hosts with spectroscopic redshifts) and a selection of distant red galaxies (DRGs), Sub-mm galaxies (SMGs) and Lyman-break galaxies (LBGs) compiled by Castro Cerón et al. (2006)

much larger samples of local galaxies allowed by the SDSS, e.g. Tremonti et al. (2004). The origin of the M-Z relation is still under investigation. Loss of metal enriched gas via galactic winds, accretion of low metallicity gas from the IGM, or lower starformation efficiencies in low mass galaxies could all effect the metallicity, and have been suggested as possible explanations, see e.g. Larson (1974) and Pei and Fall (1995).

Savaglio et al. (2005) calibrate the following mass-metallicity (M-Z) relationship using 69 Gemini Deep Survey and Canada-France Redshift Survey galaxies with redshifts between 0.4 and 1,

$$12 + \log(\mathrm{O/H}) = 0.478 \log M_\star + 4.062, \tag{2.6}$$

where $M_\star$ is given in units of solar masses. This M-Z relation is claimed to be an improvement from the use of luminosity-metallicity relations ($\sim$ 0.2 dex scatter), largely due to the small variations through the galaxies evolution in the K-band luminosity used to estimate the stellar mass in the galaxies. While short starburst and star formation history modify the B- and V-band luminosity greatly, the K-band remains relatively constant.

2.6 Locations

In addition to their galactic environments, the local environments of GRBs and SN can also provide strong constraints on progenitors. If spatially resolved spectroscopy is available then the chemical evolution of the progenitor region can be probed directly, however, this is only possible in a handful of cases (e.g. Christensen et al., 2008). In the absence of detailed spectroscopy the luminosities of the region containing the transient can also be a diagnostic (e.g. Östlin et al., 2008). These luminosities can be investigated both in relation to the overall host galaxy, and in

absolute terms. Fruchter et al. (2006) developed a pixel statistic, F_{light}, where the galaxy is defined by adjoining pixels above some signal to noise limit. These pixels are then sorted into ascending order, and the pixel containing the GRB or SN is located in this ranked list. It is then possible to record a simple statistic – the fraction of host light in pixels of equal or lower surface brightness than the pixel containing the GRB or SN. This technique has the significant advantage that it provides information on the location of a given transient which is broadly independent of the morphology of the galaxy. This is particularly important for high redshift hosts, which often show disturbed and irregular morphologies. The analysis of Fruchter et al. (2006) showed that GRBs are significantly more concentrated on their host light than the SN, and this is naturally interpreted as GRBs originating from more massive stellar progenitors (Larsson et al., 2007). A similar result was obtained by Kelly et al. (2008) for type Ic supernovae, also suggesting a higher mass origin for these systems (Raskin et al., 2008).

I have extended the analysis of Fruchter et al. (2006) to include more recent CCSN and GRBs. The GRB sample is only moderately enhanced from the sample of Fruchter et al. (2006), since the number of bursts with accurate positions and *HST* observations is not dramatically larger in the *Swift* era. However, the CCSN sample has increased by a factor of 4. To derive locations for the transients I co-align images taken at different epochs, one in which the SN/GRB is bright, and the other where it absent (for GRBs this is normally a very late time image, while for SN it is frequently a pre-explosion image). I then perform a direct subtraction of the two *HST* images and centroid on the variable source. I then create a galaxy mask via SExtractor and locate the pixel containing the GRB/SN in its cumulative distribution. The results for the F_{light} parameter are listed in Tables 2.6, 2.7 and 2.8.

An alternative approach is to investigate the surface brightness of these pix-

els, and thus of the region of the host galaxy containing the GRB or SN. By doing this, one can make a direct comparison of the local luminosities of GRB and CCSN, essentially measuring the luminosity of the populations which host them. Since the luminosity of a given star is roughly proportional to the cube of its mass $L_B \propto m_\star^3$, the mass (and hence age) of the stellar population dominates this statistic, more strongly than, for example, stellar number counts, where $L_B \propto N_\star$. Since the GRB and CCSN host galaxies lie at similar redshifts the physical scales probed by this are comparable[5].

I perform this analysis using the full sample of 58 CCSN shown in Tables 2.6 and 2.7. For the GRBs, I utilise a subset of the sample as F06, where the burst lies at $z < 1.2$ with a positional accuracy of $\lesssim 0.08$ arcsec, such that the location of the burst was known to better than the *HST* (WFPC2 or ACS) PSF, and thus the images did not require additional smoothing to emulate the observation of the host at the resolution of the error region. I have calculated the true surface brightness of the pixel that contained the CCSN or GRB event in units of $L_\odot$ kpc^{-2} for a subsample of hosts. To account for the differing redshifts of the sample I make K-corrections to these values assuming that the locations of the transient have the same colours indicated by global photometry of the host galaxy. This introduces a degree of error since the colour mapping across the galaxy is unlikely to be constant. However, the signal to noise of individual pixels is normally too low to place strong constraints on the pixel colours. I note that the application (or not) of this correction does not significantly impact the results. The resulting distribution in shown in Figure 2.8, and confirms that not only do GRBs trace a high power of light within their host galaxies, but also that GRB hosting regions are much brighter than those which host a CCSN.

[5]A pixel is roughly 150-200pc on a side

2.7 Results

The results of my analysis for CCSN and GRB hosts are shown in Tables 2.6, 2.7 and 2.8, where I have tabulated the parameters derived from the fits (absolute magnitudes, star formation rates, stellar masses and metallicities) along with directly measured parameters (r_{80}). The raw photometry used for the fits to the CCSN hosts is presented in Tables 2.2, 2.3 and 2.4. The median V band absolute magnitudes are -20.0 (CCSN) and -19.56 (GRB) respectively, median masses are $3 \times 10^9 M_\odot$ (CCSN) and $1.9 \times 10^9 M_\odot$ (GRB), median star formation rates and specific star formation rates are $3.6 M_\odot yr^{-1}$ (CCSN), $1.5 M_\odot yr^{-1}$ (GRB) and $1.2 Gyr^{-1}$ (CCSN), $0.97 Gyr^{-1}$ (GRB).

In Figure 2.6 I showed the distribution of r_{80} versus M_V, and in Figure 2.7 the distribution of SSFR versus stellar mass. I perform KS-tests on the cumulative distributions of all the parameters to formalise the probabilities that they are drawn from a single population. The KS probabilities are listed in Table 2.9, and a selection of the cumulative distribution functions are plotted in Figures 2.9 to 2.8.

I also compare the GRB/CCSN selected galaxies with the GOODS-MUSIC field galaxy sample. Since this sample is selected differently from the CCSN or GRB hosts, the field galaxy CDFs cannot simply be compared to the CCSN/GRB CDFs. Instead, for $M_\star$ I accumulate the mass in every step so that the step height is proportional to the mass of each field galaxy instead of constant. Hence, where the CDF for the CCSN/GRB hosts shows the number of galaxies with mass $< M_\star$ the accumulated function shows the *fraction of total mass in the field* that is accounted for by galaxies with mass $< M_\star$. The principle for the SFR and Φ is the same, but Φ weighted by SFR instead of Φ itself, i.e. this distribution function shows what fraction of star formation occurs in galaxies less active than Φ. In plotting the field galaxies in this way, agreement is expected between the field galaxy and GRB/SN

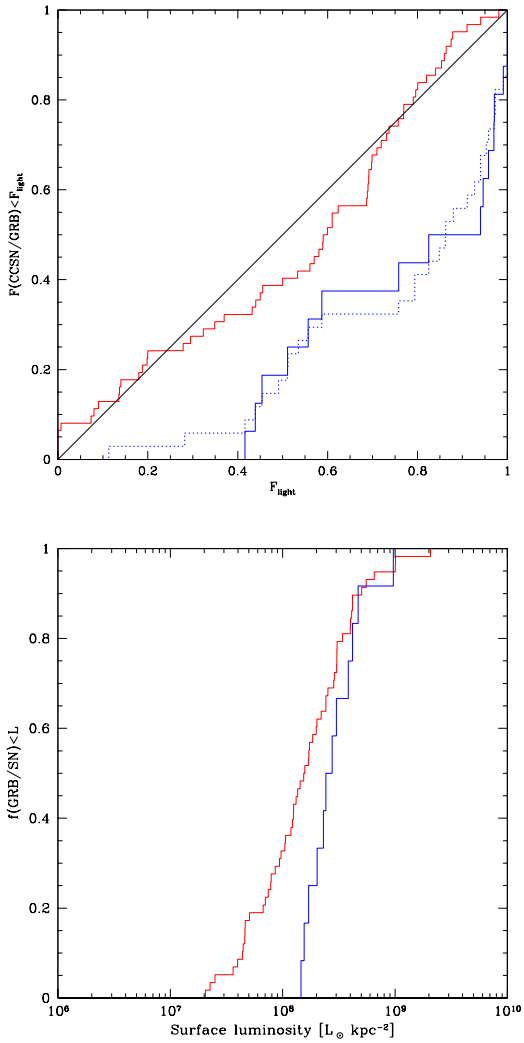

Figure 2.8: Local environmental properties of the GRB and CCSN sample. **Top:** The locations of SN (red) and GRBs (blue) on the light distributions of their host galaxy. The blue dashed line shows the locations for GRBs at $z < 1.2$, while the solid blue line shows all bursts in the sample of Fruchter et al. (2006). **Lower:** The absolute surface brightness under the transient location in units of $L_{\odot}$ kpc^{-2}. Both in relative and absolute terms GRBs appear more concentrated on their host galaxy light.

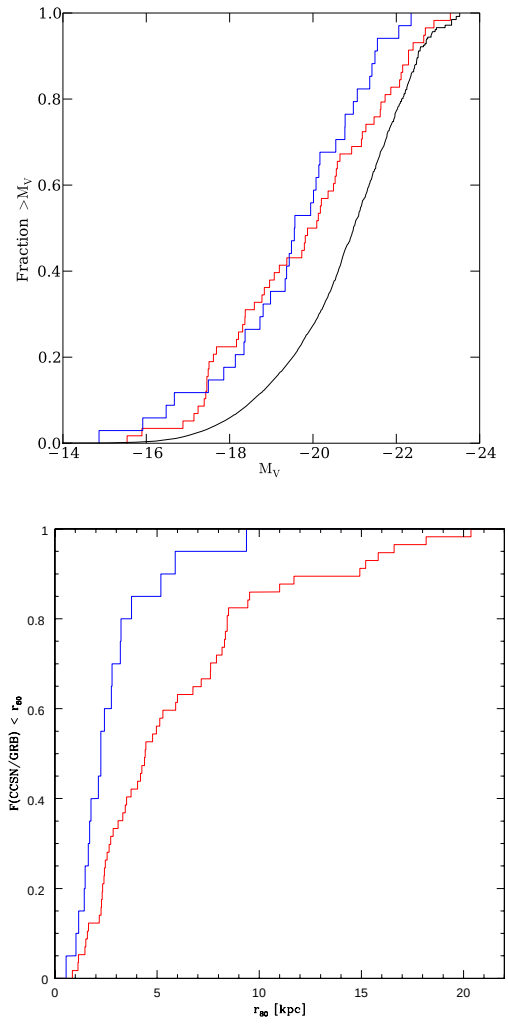

Figure 2.9: **Top:** Cumulative distribution of the absolute V-band magnitudes of GRB hosts (blue line), CCSN hosts (red) and the MUSIC field galaxy sample (black) with absolute magnitudes accumulated by luminosity. **Lower:** Cumulative distribution of the 80% light radius of GRB hosts (blue line) and CCSN hosts (red line).

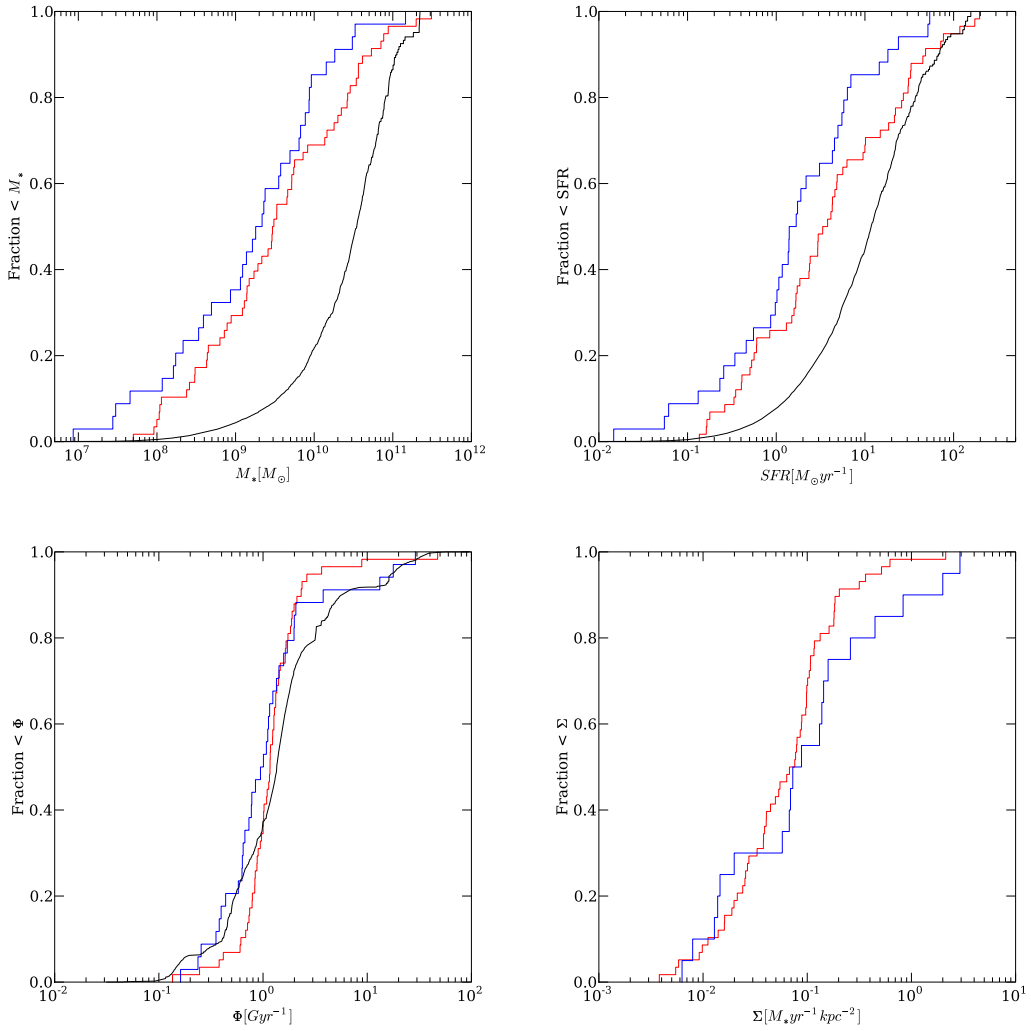

Figure 2.10: **Top left:** Cumulative distribution of CCSN (red) and GRB (blue) host galaxy masses along with fractional mass distribution in field galaxies (black). Note that for CCSN and GRB I plot the fraction of number of galaxies, while for the field galaxies, I plot the fraction of mass. **Top right:** Cumulative distribution of the star formation rates. The field galaxy sample is weighted by the individual galaxies SFR. **Lower left** Cumulative distribution of CCSN and GRB specific star formation rates. The field galaxies SSFR is weighted by the SFR in each galaxy. **Lower right** The surface star formation rates of GRB and supernova host galaxies, assuming a uniform distribution of star formation over r_{80}.

curves if the probability of a GRB or SNe occurring in a given galaxy were directly proportional to the SFR (or mass) of the galaxy.

Unlike previous work, I do not find any statistically significant differences between the absolute magnitudes of the GRB and CCSN host populations: the hypothesis that they are drawn from the same population is accepted with probability $P_{KS} = 0.43$ for both M_B and M_V, although the median M_V of the CCSN hosts is a factor of ~ 1.5 brighter in luminosity than that of the GRB hosts. Also the rest-frame B-V colours of CCSN hosts are similar to those of GRBs with a probability $P_{KS} = 0.29$.

However, though the stellar masses and star formation rates are also broadly comparable ($P_{KS} = 0.48$ and $P_{KS} = 0.15$), when weighting the star formation by the galactic mass this suggest, with a moderate statistical significance ($P_{KS} = 0.07$), that GRB hosts have less star formation per unit mass then those of CCSNe. Nevertheless the median specific star formation rates are both very similar at $\sim 1 Gyr^{-1}$.

A comparison of the radii of the two galaxy samples suggests, at a high significance, that GRB hosts are smaller than those of CCSN ($P_{KS} = 0.003$), which is consistent with the majority of GRB hosts having an irregular morphology. The most significant evidence for the difference between the progenitors of CCSN and GRBs comes from their locations. Despite a relatively small sample of GRBs with highly accurate positions on their hosts it is clear that they typically occur in regions of much higher surface brightness than CCSN (e.g. Figure 2.8), with the median difference between GRB and CCSN hosting sites being a factor of 4 in surface brightness ($P_{KS} = 0.01$), and $P_{KS} = 5 \times 10^{-3}$ when comparing the relative brightness (F_{light}) of the explosion site.

Although some of these results are surprising, in particular the broad agreement between the masses, star formation rates, and absolute magnitudes of the two

populations, there are a number of selection effects which are important to acknowledge in order to fully understand the results. In the following section these effects, and how they may have effected the sample distributions, will be discussed.

2.8 Selection effects

It is clear from the above results that there are differences between the two samples in several comparative properties (e.g. r_{80}, surface brightness), while others (e.g. absolute magnitudes) appear broadly similar. A key question is therefore what selection effects could plausibly operate within the sample, and how these might impact comparisons. I.e., could they force the two disparate distributions to look rather similar? Or alternatively, might they create apparent differences in similar underlying distributions? Below, I describe the motivation for the sample definition, and consider several selection effects, and their impact on the observed distributions of different parameters.

In the selection of the sample I have attempted to be as inclusive as possible, that is, including essentially all of the GRB hosts with $z < 1.2$ (and any available photometry) and all of the candidate CCSN hosts found within the GOODS fields. It is however necessary to explore how a number of selection effects could impact the bias of the samples, and how these would be affected if further (more restrictive) criteria were imposed. Below I discuss the effects of redshift, SN type and extinction on the samples.

2.8.1 Dust obscuration

Perhaps the most serious bias affecting GRB/CCSN selected galaxies is that incurred by dust obscuration along the line of sight. The brightest GRB opti-

Table 2.6: Name of the associated core-collapse event, the redshift and quantities derived from the Spectral energy distribution fits; Absolute magnitude in the V- and B-bands, star formation rate and stellar mass content. Hosts with only photometric redshift determination are marked in italic. Note that F_{light} and surface luminosity for bursts 2002fz to 2003N are calculated in the F606W filter, while the rest are in the F850LP filter.

SN name	z	r^{80} [kpc]	M_V AB mag	M_B AB mag	SFR [$M_\odot$/yr]	$\log M_\star$ [$M_\odot$]	12+ log(O/H)	Surface Lum [$\log(L_\odot kpc^{-2})$]	F_{light}
2002fv	0.7	0.86	-15.9	-15.47	0.18	8.04	7.9	7.83	0.46
2002fz	0.84	11.7	-22.08	-21.64	45.01	10.61	9.14	8.2	0.59
2002hs	0.39	8.43	-17.24	-16.89	1.3	9.11	8.42	7.67	0.09
2002hq	0.67	16.6	-22.66	-22.22	76.78	10.88	9.26	8.16	0.37
2002kb	0.58	15.82	-22.4	-22.21	30.64	10.42	9.04	8.7	0.84
2002ke	0.58	18.17	-21.61	-21.27	22.1	10.25	8.96	7.67	0.44
2002kl	0.41	5.91	-19.07	-18.9	0.6	8.86	8.3	7.35	0.14
2003ba	0.29	8.18	-20.93	-20.42	18.5	10.16	8.92	8.48	0.82
2003bb	0.96	20.37	-23.3	-22.77	173.35	11.3	9.46	7.97	0.18
2003bc	0.51	4.45	-20.65	-20.43	6.27	9.52	8.61	7.85	0.2
2003dx	0.51	2.17	-19.19	-18.94	1.59	9.15	8.43	8.34	0.45
2003dz	0.48	2.47	-16.88	-16.73	0.53	8.65	8.2	7.64	0.61
2003ea	0.98	4.38	-20.36	-20.21	4.81	9.47	8.59	8.74	0.57
2003en	0.54	1.64	-17.39	-17.19	0.14	8.03	7.9	8.61	0.91
2003er	0.63	7.16	-22.11	-21.68	32.74	10.73	9.19	8.02	0.08
2003et	1.3	4.97	-21.63	-21.51	48.3	10.56	9.11	8.62	0.86
2003ew	0.58	15.21	-20.58	-20.18	10.15	9.86	8.77	8.48	0.71
2003N	0.43	3.73	-17.51	-17.15	1.66	9.23	8.48	7.89	0.69
K0404-005	0.79	8.34	-22.29	-21.66	21.52	10.94	9.29	8.81	0.61
K0404-003	0.55	1.13	-15.54	-15.37	0.16	8.06	7.91	7.65	0.56
K0404-006	0.41	2.4	-18.31	-18.02	2.94	9.52	8.61	8.48	0.79
K0404-008	0.28	9.45	-21.16	-20.59	27.12	10.54	9.1	9.0	0.7
K0404-010	0.61	2.31	-18.83	-18.08	0.17	9.09	8.41	8.4	0.59
K0405-001	1.01	11.0	-22.7	-22.48	196.31	10.35	9.01	8.19	0.28
K0405-002	0.56	8.43	-21.18	-20.9	5.63	9.92	8.8	8.46	0.8

Table 2.7: Table 2.6 continued.

SN name	z	r^{80} [kpc]	M_V AB mag	M_B AB mag	SFR [$M_\odot$/yr]	$\log M_\star$ [$M_\odot$]	12+ log(O/H)	Surface Lum [$\log(L_\odot kpc^{-2})$]	F_{light}
K0405-005	0.68	2.55	-18.17	-18.05	0.4	8.48	8.12	7.93	0.3
K0405-007	0.5	4.78	-19.73	-19.28	1.72	9.46	8.58	9.32	0.98
K0405-008	0.88	3.32	-18.21	-17.72	1.85	9.17	8.45	8.03	0.6
HST04Pata	0.41	9.53	-21.87	-21.47	33.12	10.46	9.06	8.6	0.53
HST04Cli	0.75	1.52	-17.45	-17.33	0.85	8.89	8.31	8.23	0.72
HST04Wil	0.42	8.3	-20.2	-19.9	2.41	9.49	8.6	8.27	0.69
HST04Pol	0.56	7.9	-21.47	-21.14	14.89	10.3	8.99	7.87	0.14
HST04Jef	0.96	2.26	-18.37	-18.31	0.41	8.48	8.12	8.12	0.69
HST04Ken	0.52	5.28	-20.53	-20.13	2.34	9.75	8.72	8.38	0.7
HST04Cum	0.97	3.44	-18.78	-18.72	2.93	9.14	8.43	8.3	0.69
HST04Cay	0.8	1.15	-17.61	-17.41	1.5	8.8	8.27	7.9	0.2
HST04Bon	0.66	8.49	-22.15	-21.57	71.59	10.85	9.25	8.09	0.19
HST04Sos	0.55	4.41	-20.13	-19.83	4.13	9.66	8.68	8.46	0.8
HST04Fox	0.69	2.33	-18.59	-18.49	0.56	8.64	8.19	8.07	0.35
HST04Con	0.84	7.62	-21.27	-20.97	9.99	10.13	8.91	8.23	0.5
HST04Hei	0.58	14.92	-22.29	-22.06	31.05	10.43	9.05	7.4	0.14
HST04Riv	0.61	2.42	-17.43	-17.27	0.35	8.38	8.07	7.99	0.58
HST04Geo	0.94	5.13	-20.09	-19.97	3.34	9.28	8.5	8.62	0.85
HST04Gua	1.26	4.19	-22.9	-22.06	117.58	11.49	9.55	8.48	0.43
HST04Ida	0.91	1.59	-17.14	-17.1	0.51	8.63	8.19	8.38	0.77
HST05Kirk	0.45	2.65	-17.49	-17.36	2.37	7.7	7.74	8.13	0.74
HST05Pic	0.91	6.0	-20.49	-20.42	4.31	9.41	8.56	8.3	0.62
HST05Sev	0.96	7.61	-19.87	-19.87	1.67	8.94	8.34	7.6	0.07
HST05Sco	0.93	3.5	-18.96	-18.79	3.79	9.65	8.68	7.56	0.0
HST05Boy	0.66	2.28	-17.45	-17.47	0.26	8.0	7.89	8.24	0.69
HST05Den	0.97	3.09	-19.82	-19.67	2.97	9.46	8.59	8.53	0.87
HST05Bra	0.48	2.85	-20.18	-19.8	4.59	9.74	8.72	9.01	0.94
HST05Str	1.03	4.05	-20.56	-20.37	9.52	9.72	8.71	7.31	0.0
HST05Cas	0.73	1.47	-17.68	-17.61	0.33	7.96	7.87	8.09	0.77
HST05Mob	0.68	4.25	-19.79	-19.47	4.86	9.71	8.7	8.1	0.32
HST05Ton	0.78	6.75	-21.73	-21.31	25.92	10.56	9.11	8.6	0.76
HST05Fil	1.21	2.73	-19.37	-19.38	4.28	9.33	8.52	7.66	0.0
HST05Ste	0.47	7.1	-18.37	-18.27	0.6	8.41	8.08	7.7	0.88

Table 2.8: As table 2.6 but for GRB host galaxies. Surface luminosity and F_{light} depend on accurate positional information, hence, they are only calculated for hosts with *HST* imaging and positional errors < 0.1 arcsec and < 0.15 arcsec respectively.

GRB name	z	r^{80} [kpc]	M_V AB mag	M_B AB mag	SFR [$M_\odot$/yr]	$\log M_\star$ [$M_\odot$]	12 $+\log$(O/H)	Surface Lum [$L_\odot kpc^{-2}$]	F_{light}
GRB970228	0.695	3.2	-18.13	-18.04	0.25	8.21	7.99		
GRB970508	0.835	1.48	-18.37	-18.22	3.08	8.24	8.0	8.48	1.0
GRB970828	0.958	2.8	-19.43	-18.8	2.17	9.57	8.64		
GRB980326	1.0		-14.87	-14.59	0.01	6.93	7.38		1.0
GRB980425	0.0085		-18.34	-18.09	0.34	8.53	8.14		
GRB980613	1.1	3.75	-20.77	-20.42	6.34	9.83	8.76		0.42
GRB980703	0.97	2.42	-21.49	-21.23	53.79	10.15	8.92		0.56
GRB990705	0.86	9.38	-21.36	-21.11	5.5	9.94	8.81		
GRB990712	0.43	2.25	-19.57	-19.43	1.07	8.94	8.33	8.39	0.97
GRB991208	0.71	1.16	-18.8	-18.68	0.55	8.59	8.17		0.94
GRB991216	1.02	2.25	-17.86	-17.58	0.23	8.33	8.04		
GRB000210	0.846		-20.01	-19.85	1.89	9.21	8.47		
GRB000418	1.12	1.7	-20.55	-20.48	18.16	9.14	8.43		0.45
GRB000911	1.06		-19.37	-19.2	1.36	9.09	8.41		
GRB010921	0.45	2.76	-20.17	-19.87	1.74	9.38	8.54	8.62	0.44
GRB011121	0.36	5.89	-20.14	-19.75	1.4	9.55	8.63	8.36	0.51
GRB020405	0.69		-21.06	-20.75	4.96	9.89	8.79	8.31	0.59
GRB020819	0.41		-22.06	-21.53	14.5	10.52	9.09		
GRB020903	0.25	1.43	-19.33	-19.34	1.02	8.69	8.22	8.44	0.96
GRB021211	1.006	1.63	-19.95	-19.12	6.95	10.26	8.97	8.67	0.76
GRB030329	0.17	1.03	-16.67	-16.52	0.87	7.47	7.63	8.16	0.99
GRB031203	0.1055		-19.07	-18.52	0.44	9.24	8.48		
GRB040924	0.859	3.23	-19.55	-19.1	4.54	9.36	8.54		
GRB041006	0.716	5.19	-18.73	-18.29	1.17	9.69	8.69	8.23	
GRB050223	0.5915		-20.77	-20.51	4.3	9.81	8.75		
GRB050416A	0.6535	2.12	-19.48	-19.23	0.98	9.06	8.39	8.98	0.97
GRB050525A	0.606	1.76	-16.48	-16.22	0.06	7.66	7.72	8.19	0.95
GRB050824	0.83		-18.62	-19.02	1.37	7.45	7.62		
GRB050826	0.296		-20.97	-20.28	1.39	9.93	8.81		
GRB051016B	0.9364		-21.42	-21.16	5.78	9.96	8.82		
GRB051022	0.807		-21.55	-21.23	23.85	10.49	9.07		
GRB060218	0.0331	0.55	-15.92	-15.92	0.05	7.44	7.62		
GRB061126	1.1588		-22.36	-21.61	51.34	11.16	9.4		
GRB080319B	0.937		-17.49	-17.23	0.13	8.07	7.92	8.58	

	P_{KS}
$M_\star$	0.48
M_V	0.43
M_B	0.43
Σ	0.30
$B-V$	0.28
SFR	0.15
Φ	0.07
$L_{surface}$	0.01
r_{80}	0.003
F_{light}	5×10^{-3}

Table 2.9: KS probabilities for comparison of physical properties between GRB and CCSN host galaxies. Showing the probabilities that the distributions of each parameter are drawn from the same population. The parameters compared are the global star formation rates (SFR), the absolute B and V band luminosities (M_V and M_B), the B-V colour, the luminosity of the pixel underlying each GRB/SN $L_{surface}$, the 80% light radii r_{80}, the specific star formation rate Φ, the surface star formation rate Σ and the location of the GRB/SN on their cumulative host galaxy light.

cal afterglow observed is roughly 20 magnitudes brighter than a typical CCSN (Bloom et al., 2008; Racusin et al., 2008), and GRB afterglows typically remain brighter than their associated SN for several days. Although a deeply buried burst could be expected to suffer from large extinctions and with correspondingly faint optical afterglows, (so called 'dark' bursts, see e.g. Fynbo et al., 2001; Lazzati et al., 2002; Jakobsson et al., 2004; Levan et al., 2006a; Rol et al., 2007; Perley et al., 2009a, and Chapter 4) dust destruction by X-rays could still be effective enough to allow UV/Optical observations of the afterglow according to Fruchter et al. (2001). However, Fynbo et al. (2009) suggests very convincingly that dark bursts *may not* be representative of the general GRB population, and trace different environmental properties than bursts with detected optical afterglows. Either way, even in the absence of any transient optical emission it is possible to identify a redshift for a GRB from its X-ray identified host galaxy, (e.g. GRBs 970828 or 051022 Groot

et al., 1998; Rol et al., 2007). This relative insensitivity to dust obscuration is one of the key advantages of GRBs over many other techniques for high redshift exploration. Indeed, while it is interesting to note that both spiral host galaxies in the GRB sample (GRB 990705 (Masetti et al., 2000)) and GRB 020819 (Jakobsson et al., 2004)) are from bursts which were plausibly dust obscured, in general the GRB afterglow is much brighter than any SN, and hence if the low spiral fraction in GRBs were due to dust obscuring many optical afterglows, I would expect to see an even stronger bias against spiral galaxies in the CCSN sample, which is not the case.

Indeed, SN are likely much more strongly affected by dust that GRBs; studies of local starburst galaxies in the IR suggest that a reasonable fraction of CCSN may occur in deeply enshrouded regions of their hosts (Mannucci et al., 2003), essentially invisible to optical observations. This problem becomes even more extreme at moderate redshift, where optical observations probe rest-frame UV light, thus one may then suspect that the CCSN sample may be incomplete due to SN being lost to dust extinction. Since the dustiest galaxies tend to be those which are most massive it is likely that any dust obscuration would remove the brightest hosts in the sample, and would imply that any impact on a CCSN selected galaxy population from dust, would most likely act to decrease its mass distribution.

Indeed, while MIPS observations of the GOODS fields (Chary et al., 2005) suggest that $\sim$60% of SN hosts are detected, this is not true for GRB host observations; Le Floc'h et al. (2006) find a detection rate of only $\sim$ 20% implying that dust may well have a larger impact on CCSN detection than GRBs. In contradiction to this I note that the deeper observations of the CCSN host may be a factor in the higher detection rate, and that comparing

the detection rate above a uniform depth results in more similar rates.

2.8.2 Evolution of global properties

Although both CCSN and GRBs originate from young systems, this does not necessarily indicate that the relations between broad band properties and underlying physical conditions should be the same for each sample. Since it is explicitly assumed that there is a direct proportionality between the K band and stellar mass, or U-band and star formation rate, any systematic differences in these proportionalities between the two sample could create a bias in the observed populations. The morphological properties of the CCSN hosts, combined with their redder colours suggest that there is a significant older population already in place. In a sense these galaxies should therefore be reasonably representative of the samples of local star forming galaxies from which the stellar-mass and star formation rate indicators are derived. In contrast, GRB hosts are apparently irregular (e.g. Section 2.9), and several studies indicate they are extremely young, with ages for the *dominant* stellar populations of under 10^7 years (e.g. Christensen et al., 2004; Levesque et al., 2009). For very young systems the K-band luminosity is dominated by young stars (e.g. Berta et al., 2004), and therefore may well be enhanced per unit stellar mass, such an effect would cause a significant *overestimate* of the GRB host galaxy masses. Secondly, in very young stellar systems ($t < 10^8$ years) the relation between U-band luminosity and SFR is not constant, but *underestimates* the SFR for a given U-band luminosity (Verma et al., 2007). In other words, the very young stellar ages derived from detailed studies of individual GRB host systems (e.g. Levesque et al., 2009) suggest that the derived properties for the GRB hosts may be systematically too massive, with too low a star formation

rate. Were this corrected for, it is likely that the GRB and CCSN sample would seem more disparate than observed. To partly quantify this effect, it is relevant to note that not only is there a relationship between K-band luminosity and stellar mass, but also between effective radius and stellar mass (Bernardi et al., 2003; Damjanov et al., 2009). Since the median sizes of the GRB and SN hosts differ by a factor a ~ 2, this would also suggest that the median mass of a CCSN host would be a factor ~ 4 larger. In essence, it is not possible for both the GRB and SN hosts to satisfy both of these relations, given the very young stellar ages of GRB hosts, and their likely impact on the broadband properties. I hence suggest that it is the morphological (and size) difference which defines the GRB and SN populations, and that CCSN hosts are indeed typically more massive than those of GRBs. It can however not be discounted that some fraction of CCSN are missed in small, compact galaxies – i.e. similar to the typical GRB hosts observed. Due to the relative faintness of CCSNe, the efficiency with which they are detected drops when the surface brightness of the host galaxy is of comparable magnitude as the SN itself.

2.8.3 Redshift

A further selection effect to consider is the origin of the redshifts for any given CCSN or GRB. For CCSN the broad-band photometric data available enables the derivation of a photometric redshift (although see below). In contrast most GRB hosts do not have this coverage and therefore redshifts come primarily from either emission redshifts of the hosts or via absorption redshifts derived via observations of their afterglows. Although emission line flux is not directly proportional to host continuum magnitude there is a broad dependence which means that emission line redshifts can normally only be derived for brighter

hosts. In contrast, absorption redshifts can be determined *independently* of host magnitude (e.g. Berger et al., 2002; Hjorth et al., 2003a; Vreeswijk et al., 2004), although this is not necessarily straightforward for low redshift bursts where the UV metal lines are not redshifted into the optical band. The consequence of this is that the requirement of a measured redshift biases the GRB sample toward intrinsically brighter hosts. Indeed, if I perform a KS test between the hosts with absorption line spectra and those with emission line redshifts I find that the sample with absorption redshifts is fainter than those with redshifts derived from emission lines; KS-probability of being drawn from the same distributions is only $P_{KS} = 0.001$. In other words, it is plausible (though not certain) that a population of intrinsically faint, low to moderate redshift GRB hosts, are missing.

In part because of the above discussion, I have included photometric redshifts for the CCSN sample where possible. Since, if the photometry is sufficiently well sampled, they do provide a necessary handle on the faint hosts not observed with TKRS or GOODS/FORS2. Though exclusion of hosts without spectroscopic redshift would narrow down the sources of random errors, it would also bias the sample towards observationally bright, and thus on average more luminous, host galaxies. I note that the mean apparent magnitudes and absolute magnitudes are 23.54 and -19.8 for the complete sample, and 22.79 and -20.5 for hosts with spectroscopic redshifts, hence I include all CCSN hosts in the sample, independently of how the redshift was determined.

2.8.4 SN typing

Approximately half of the CCSN are typed with low confidence (Bronze medal), hence there is a probability that there is a fraction of SN Ia hosts in the sample. SN Ia can appear in both old stellar population due to long delay times between star formation and explosion, as well as exploding rapidly after the formation of the progenitor system. Since they are more likely than CCSN to occur in latent stellar populations, this could clearly affect the colours, star formation rates and specific star formation rates of the CCSN sample analysed. It is, however more difficult to determine how the mass distribution will be affected. Performing SED-fitting and estimating the host stellar masses of the GOODS-detected SN Ia's gives a ~ 0.2 dex higher mass distribution, though the KS-probability conclude they are consistent with a single distribution.

As a further test to rule out that the results have been disturbed by mistyped SN, I perform the KS-test also on the sample containing only securely typed CCSN (Gold and Silver medal). I find that the G+S sample are brighter in the V band absolute magnitudes, but not significantly more massive than the complete sample. Using this subsample the absolute magnitudes are still broadly consistent, although with a somewhat decreased probability: $P_{KS} \sim 0.17$. The same trend is echoed by the mass distributions which are also consistent with $P_{KS} = 0.27$.

However, I also note that this in part may well be due to the reduced numbers of hosts in the sample (G+S:23 , B:35) when culling by SN confidence level, as well as due the fact that this sample is also brighter in apparent magnitudes. Though some influence cannot be ruled out, the conclusions are overall not changed by including or excluding parts of the sample based on SN typing.

There is some evidence that SN Ib/c host galaxies are typically more luminous (Prantzos and Boissier, 2003) and more metal enriched (Prieto et al., 2007) than hosts of SN II, and Kelly et al. (2007) gives a strong indication that they typically lie on the brighter parts of the host. Nevertheless, it should be noted that such a bias introduced by an unusually large SN Ib/c fraction in the sample would act to decrease the separation between the CCSN and GRB populations when considering the F_{light} and surface luminosity distributions, and act in the opposite direction when considering absolute magnitudes. However, few SNe in the sample have their subtypes resolved, and this effect would most likely be much smaller than that of dust obscuration and redshift selection discussed above.

2.8.5 The overall impact of selection effects on the observed sample

Above I have considered various biases which are likely to be operating within the samples of GRB and CCSN host galaxies. These include selection effects which are inevitably introduced into any magnitude/flux limited sample and also intrinsic systematic errors which propagate through the sample due to incomplete knowledge of the detailed physical states of the galaxies that are studied. Overall, I considered the apparent differences in size and morphology to be compelling. Although dust extinction will impact both SN and GRB hosts it should impact SN more, and hence the different morphologies observed are inconsistent with it being a dominant selection effect. Similarly, the lack of GRB hosts with photometric redshifts biases them to the brighter hosts, where emission line redshifts can be obtained. The difference between apparent host luminosities of bursts with host emission, or afterglow absorption redshifts is indicative that there may be a faint population of GRB hosts (currently GRBs

without redshift measurements) omitted from the sample. Finally, the extreme properties of the GRB stellar populations based on detailed population modelling (e.g. Levesque et al., 2008) imply that using empirically determined relationships between monochromatic luminosities and physical properties is not necessarily optimal. Hence I conclude that the environments of CCSN and GRBs are indeed different, and consider explanations for this below.

2.9 Discussion

Although supernovae and GRBs are closely related phenomena, one question of interest is the characteristic environments – both local and galactic – in which they form. By contrasting the environments of the two transient events, clues can be obtained concerning their stellar progenitors. This in turn provides observational constraints to the pathways which can create GRBs and is central to understanding any biases in using GRBs as cosmological probes (e.g. as probes of star formation) as opposed to galaxy samples selected in flux limited surveys. For example, the comparison with the MUSIC sample suggests that roughly a few percent of the starformation tracked by CCSN and GRB is too faint to be included in the flux limited sample. Finally, the fraction of stars which may create GRBs as a function of environmental properties can feed into predictions of high redshift (and hence low metallicity) GRB rates, as an input for potential future GRB missions targeting high redshift GRBs (e.g. EXIST [6] and JANUS).

The conclusion of F06 is echoed by the results presented here, suggesting that GRB hosts are consistently less massive and have more irregular morphology than their SN counterparts. Given the well calibrated relation between

[6] http://exist.gsfc.nasa.gov/

luminosity and metallicity, e.g. Tremonti et al. (2004), this is most clearly explained by a preference for GRBs in low metallicity environments. F06 also compared how CCSN and GRBs trace blue light in the hosts. The findings are in this thesis are broadly consistent with those of previous works. In the larger sample presented here, CCSN are tracing the blue light, and therefore broadly the global star-formation. The GRB population on the other hand appears to be significantly more concentrated on the brightest regions of the galaxies. This could naturally be interpreted as GRBs being due to the collapse of more massive stars, probably with initial masses >20 $M_{\odot}$ (Larsson et al., 2007). These stars form in large OB-associations, and, since stellar luminosity traces a high power of stellar mass (crudely $L_{\star} \propto M_{\star}^{3}$), produce much more light than stars of lower mass, even those which produce supernovae.

This is further reflected in an analysis of the surface brightnesses measured *directly* under the transient position, which accepts the possibility that they are being drawn from the same population with a KS-probability of only 0.01. Furthermore a comparison of locations within the hosts following the method of F06 is even more compelling, suggesting that the two distributions cannot be reconciled with a probability higher than $P_{KS} = 5 \times 10^{-3}$. These results are naturally explained by the origin of GRBs in very young, and subsequently very massive stellar progenitors.

The so far most successful progenitor model for long GRBs is the collapsar model (Woosley, 1993), predicting that the bursts are the result of the collapse of rapidly rotating cores from massive stars. The metallicity to a large extent determines the rate of mass loss that is due to stellar wind in the progenitor star, and hence also the angular momentum loss. Core collapse progenitors arising in low metallicity environments support only weak winds

and may be able to retain a large fraction of the initial rotation. As rapid rotation is thought to be one of the key discriminators between GRB and CCSN explosions, it is natural to expect that GRB progenitors may therefore form in lower metallicity environments. However, all SN so far associated with GRBs are of the Ic variety, suggesting that the hydrogen envelope has been lost, and indicating that low metallicity may not be sufficient to create GRBs and that in single stars more exotic processes such as complete mixing on the main sequence (e.g. Yoon and Langer, 2005) may be necessary.

Introducing the option of a binary star evolution (e.g. Levan et al., 2006b; van den Heuvel and Yoon, 2007; Podsiadlowski et al., 2004) can potentially create GRBs across a wider range of metallicity. A binary scenario is suggested where two massive ($M > 8M_{\odot}$) stars after main sequence evolution and separation tightening through a common envelope phase end up as a neutron star or black hole and helium core binary. Tidal locking of the helium core's rotation enables enough angular momentum to create a torus, and the accretion of this onto the central compact object at core collapse powers the GRB. Although this scenario remains possible at all metallicities, magnetic braking by a strong stellar wind could bias also binary progenitors towards low metallicity environments.

The discrimination between the different progenitor routes can potentially be made via metallicity measurements for the host galaxies. While binary channels will operate at all metallicities (albeit with an increased rate toward the lower end), single star evolution may produce a sharp cutoff in the metallicity at which GRBs can be created. The two possibilities can potentially be tested via metallicities for a large sample of GRB hosts.

The task of host galaxy metallicity measurement is made difficult owing

to the large redshift of many bursts. Therefore, many studies of long burst host galaxy metallicities have used a luminosity-metallicity relation for the estimate, as I will attempt in the next chapter. Other possibilities to measure the local metallicity are by using the GRBs optical or X-ray afterglow as a probe, and study the absorption lines when it shines through the immediate environment, see for example Starling et al. (2005); Vreeswijk et al. (2004); Chen et al. (2005).

Wolf and Podsiadlowski (2007) studied the host metallicities using largely the same sample as F06, but with a more conservative redshift constraint. Their modelling of metallicity dependent efficiency for producing GRBs suggests that progenitor metallicity is of importance, their favoured model being one with constant efficiency up to nearly solar composition and with a sharp cutoff, although they make the implicit assumption that the shape of the mass metallicity relation for GRB hosts is the same as for field galaxies. While this may be the case, it is far from clear (Modjaz et al. 2008). The authors also comment on the global versus local metallicity *within* the galaxy. Importantly, without spatially resolved spectroscopy, the variations between metallicity in different parts of the galaxy can be almost as large as the scatter in the M-Z relationship. Thus spectroscopy without spatial resolution may not yield better results (for the progenitors metallicity) than using mass or K-band luminosity as proxy.

The new sample of GRB and CCSN hosts used here is a factor of 2-4 larger than previously available samples, and with broadband coverage allowing estimates of physical parameters to be made. It is interesting to investigate how these results may be interpreted in terms of the above discussion.

In contrast to previous studies, I do not find highly significant (consid-

ering the KS-test) differences between the M_V or M_B distributions for GRB and CCSN hosts, although the median GRB hosts is roughly a factor of ~ 1.5 fainter than the median of CCSN (see Figure 2.10 where I show the cumulative distribution function of M_V). Considered alone, this is inconsistent with previous studies, although it should be noted that the distinction in absolute magnitude is previous samples was the least significant of a number of parameters compared. The origin of the apparent discrepancy between these results and those of F06 is down to the combination of two factors. Firstly, I attempt to derive absolute magnitudes based on spectral templates, rather than assuming flat spectrum sources. Secondly, the larger sample of CCSN used here is apparently fainter than the sample considered in F06. Indeed, the mean apparent magnitude of the new CCSN sample is ~ 1 magnitude fainter, despite a similar redshift distribution. Although the new larger sample of CCSN does not suggest a globally different luminosity function it is particularly interesting to note that the sample of GRB hosts contain no galaxies brighter than $M_V \sim -22.4$, while the CCSN host population continues to $M_V \sim -23.3$. Given the luminosity – metallicity relations discussed above this may be consistent with a sharp cutoff in the metallicity at which a GRB can be created. Comparison of these two distributions with models for GRB efficiency in binary and single star models as a function of metallicity may help to elucidate this further, although in practise a still larger sample of GRB and CCSN hosts may be necessary to place strong constraints. The main bias effects on the distributions of B and V absolute magnitudes are redshift method, and dust obscured hosts. Both emission line redshifts and dust will bias the GRB sample towards brighter hosts, while dust in CCSN hosts will give a fainter sample - although a quantitative estimation of how large these effects are is

difficult, they are acting in opposite directions, suggesting a fainter true GRB host population and a brighter true CCSN population.

Since the absolute magnitude distributions of the two populations show only modest differences, it is unsurprising that the global distributions of other parameters which depend directly on the magnitude in a given band (principally mass and star formation rate) are also similar. Further, since GRB hosts are on average bluer and of lower mass (even though the difference between each distribution are not significant in their own right) the distinction in the specific star formation rate is much stronger (this is also in part since the order of individual galaxies is obviously not identical in the mass and SFR cumulative distributions).

While the estimated stellar masses and starformation rates are compatible with a common distribution, it should be noted that galaxy and stellar population age can have an effect on the measurements and derived restframe properties,it causes one to overestimate the mass, and underestimate the SFR for young starbursts as discussed previously, while also dust obscuration will narrow the mass distributions of the samples. Hence, it is *possible* that the mass and SFR distributions are more diverse than a direct interpretation of the results would indicate. This suggestion is further supported by simple morphological analysis of the host galaxy samples, which show striking differences. In the sample of CCSN hosts the spiral fraction is approximately $\frac{27}{58} \sim 0.45$ with a Poisson counting error ~ 5. If the GRB host sample has identical spiral fraction, the expected number of spirals is $\sim 15 \pm 4$, whereas only two can be recognised as spirals in the GRB host sample (GRBs 990705 and 020819)[7]. The Poisson probability of two or less spiral galaxies to be found in a sample

[7]This count ignores the unusual GRB 980425, but its inclusion only slightly affects the results

with an expected spiral fraction of 0.45, is $\sim 4 \times 10^{-5}$.

Performing a more quantitative analysis on the physical sizes of the hosts reveals that GRB hosts are also significantly smaller than CCSN hosts. A comparison of the 80% light radii using the KS-test results in $P_{KS} = 0.003$ that the sizes are drawn from the same parent distribution. In Figure 2.6 I plot r_{80} versus M_V. Visual inspection confirms that the GRB host population is smaller than the CCSN host population, which is accepted by the KS-test, and is in excellent agreement with the morphological distribution - small irregulars versus large grand design spirals.

As an alternative to estimating mass from the K-band luminosity, I note that there is also a strong trend in the size-stellar mass relation (e.g. Shankar and Bernardi, 2009). Since the luminosity based mass estimates suggest consistent distributions for the CCSN and GRB samples, but the size distributions are inconsistent, *both* of these relations cannot be correct. Due to the uncertainties in stellar population ages, and their contributions to the K-band luminosities, I suggest that size is a more stable proxy for mass when comparing samples of potentially different ages. Inserting the size distributions into any size-to-mass relation would hence yield a significantly lower mass distribution than estimated by the K-band luminosity and result in a KS-probability for the mass identical to that of r_{80}. However, if this argument is wrong, and the K-band mass estimates are indeed correct, this would suggest that the host masses are more similar than previously though, and implications on global environments and metallicities would put constraints on the collapsar model.

The low probability of the size and morphological distributions being compatible is obviously in conflict with the apparently similar mass (K band

luminosity) distributions discussed above, and does suggest markedly different large scale environments. Assuming that GRB hosts have *similar mass* distributions but *smaller size* distribution than the CCSN host sample, I look at size - metallicity relations at constant mass. A positive correlation between size and metallicity is found by Hoopes et al. (2007) for UV selected galaxies and by Ellison et al. (2008b) for galaxies in close pairs. On the opposite side, Ellison et al. (2008a) indicate that the mass-metallicity relation in $\sim$ 44000 SDSS galaxies is offset to higher metallicities for galaxies with decreasing size.

The ambiguity of these results can be interpreted in two ways: If the estimates mirror the true distributions, then it can be deduced that GRB hosts, and progenitor stars, have similar mass and metallicity distributions, but have significantly higher stellar densities. Alternatively, if the estimated mass distributions are dominated by galaxy-evolutionary or dust obscuration bias effects, then the GRB hosting population could be significantly less massive than it appears from the K-band estimates. Instead, if the mass-to-light ratio is violated, galaxy size will be a more stable indicator of galaxy mass; This notion is supported by strong trends in the size-stellar mass relation (e.g. Shankar and Bernardi, 2009), which also notes the age-dependency of this relation establishes smaller sizer for old galaxies at a given mass - hence galaxy evolution is not likely a major concern for galactic size distributions derived here.

2.10 Summary

I have used multiwavelength photometry to investigate the physical properties of long gamma ray bursts and core-collapse supernovae hosting galaxies at

low to intermediate redshifts. I fit spectral energy distributions, and estimate restframe absolute magnitudes, stellar masses and star formation rates. From the stellar masses I have also attempted to estimate host metallicities. Galaxy sizes and morphologies are studied. The results show that within the sample the derived masses and absolute magnitudes are not significantly different between the two populations, although the majority of likely selection effects act to make any differences in the underlying distributions smalled when analysed as done here. Indeed, while not statistically significant in terms of a KS test, the cutoff in the luminosity function of GRB hosts about 1 magnitude fainter than the CCSN hosts, is suggestive of a metallicity cutoff. Further, the physical sizes and morphologies within the two samples are different with high statistical significance, and this lends further support to models in which GRBs form only in certain environmental conditions, most likely related to low mass and metallicity.

Finally, the locations of the bursts and CCSN on their hosts, measured both in absolute terms, and relative to their cumulative light distributions shows GRBs to be more highly concentrated on their host light, and to be occurring in regions of high absolute surface brightness.

To summarise my interpretation in terms of current models for GRB production I suggest the following

- GRB hosts have consistently smaller physical sizes than CCSN hosts, and they are consistently of irregular morphology as opposed to CCSN hosts.

- The high surface brightness of the immediate burst location and their concentration on the host light, suggest that GRBs are originating in a

younger stellar population than CCSNE, with more massive stars.

- This and other lines of evidence suggest that the dominant stellar populations in GRB hosts are very young. This may introduce systematic errors which overestimate stellar mass and underestimate star formation rates.

Chapter 3

The masses and metal abundances of GRB hosts

3.1 Introduction

Galaxy selection by the presence of GRBs has been suggested to offer significant advantages over other methods for sampling the galaxy luminosity function of star forming galaxies down to faint luminosities even at high redshifts. This relies on the uniquely high luminosities of the transient event itself, having proved to be observable at least to redshift $z = 8.2$ (e.g. Tanvir et al., 2009; Salvaterra et al., 2009) and due to the fact that selection is, at least to first order, independent of the galaxy luminosity. In addition, the GRB itself is a transient event, and after the afterglow has faded the underlying host galaxy can be studied without interference. This is mainly what prefers GRB selection over e.g. AGN or Quasars to study high redshift galaxy populations.

The luminosity distribution of GRB hosts is well studied at low redshift and at optical wavelengths, e.g. (Savaglio et al., 2009; Niino et al., 2010)

and in Chapter 2. The galaxy mass function can be studied by the proxy of the nIR restframe luminosity. The calibration from nIR luminosity, typically K-band to mass is relatively straight-forward and varies less with age and star formation history than optical bands since it traces the older stellar population. Typically GRB host galaxies are blue and sub-luminous, or in terms of fundamental properties; star forming and low mass. Since the presence of the GRB implies that the galaxy is actively forming massive stars – it is not surprising that studies of low redshift host SED properties confirm their star forming nature (e.g. Chapter 2). Whilst this is comparable to that observed in SN hosts, it is also found that GRB hosts have comparatively small physical sizes, and are on average less massive than their SN producing counterparts, suggesting that GRB selection is not directly proportional to SFR. While these studies have focused on hosts at low to intermediate redshifts, up to $z \sim 1$, it is also interesting to study the growing sample of GRB hosts beyond the low redshift regime that have been followed up with deep imaging observations. These high redshift events offer unique opportunities to study the metal abundances of the early Universe from GRB afterglows, and constrain the luminosity function and galaxy stellar mass function even at the faint end where flux limited samples struggle. At high redshift where possible selection effect due to metallicity are small or non-existent, this allows the evolution of the mass-metallicity relation to be constrained, i.e. to study the Universal build-up of mass and chemical elements beyond the capabilities of other techniques (e.g. Chary et al., 2007). Above redshift $z \sim 2$ Lyman-α is redshifted into observed frame optical, and it becomes possible to measure the hydrogen column as well as metal line column densities from their absorption of the afterglow light (e.g. Savaglio et al., 2003; Prochaska

et al., 2007). Indeed, since this method is independent of the host luminosity, metal abundances can be determined even when the host remains undetected in deep observations. However, at low redshifts, metallicities instead have to be measured from host emission, which requires that the host is bright enough for spectroscopy, possibly biasing the sample to high mass, high metallicity systems.

Here I present a study of 92 GRB hosts galaxies at $0 < z < 8.2$ with host observations. I study the mass distribution of the GRB selected galaxy population by means of their spectral energy distributions (SEDs). As in the previous chapter, I fit model templates and host extinction in order to extract physical properties (e.g. $M_\star$ and absolute magnitudes) of the hosts. I present a mass versus redshift plot of the host galaxies and discuss the observations in the context of the evolving galaxy mass function and Universal chemical enrichment. For this purpose, I consider measured metal abundances for a subset (34 in number) of the hosts in our sample published in the literature. I use these spectroscopically determined metallicities in conjuncture with our mass estimates to study the mass-metallicity relation as it is traced by the GRB host population to $z \sim 6$.

3.2 Data sample

I make use of the low redshift host sample discussed in Chapter 2, which is appended with an additional 42 detected host galaxies at $z > 1.2$ and 9 hosts for which only upper limits are available (See table 3.1 for a summary and sources). As in the low-z sample, I have chosen to include also hosts with only a single detection, or even only limits in order to avoid biasing the sam-

ple towards higher luminosities. The additional photometry is sourced from the GHost online database[1] and references within, see (Savaglio et al., 2006), or obtained from observations at Gemini Observatory and *HST*. The Gemini observations are reduced with standard techniques in IRAF and zeropoints are calibrated against USNO standard stars in the field. The magnitudes are listed in Table 3.2. The *HST* observations (Levan et al. in prep) are obtained with ACS in the F775W or F814W filters, WFC3 in the F110W filter, or with NICMOS in either F160W or F125W. These *HST* observations include limiting magnitudes for the three highest redshift bursts – GRBs 050904, 080913 and 090423, all above redshift 6. All *HST* magnitudes and observations are summarised in Table 3.3 The full host sample covers the redshift range from 0.01 to 8.2. In Figure 3.1 I plot the redshift distributions of both the host sample and the full burst sample with known redshift. I note that the median redshift of the host sample is $\sim$ 1 in contrast to $\sim$ 2.5 for the full sample of GRBs with determined redshifts. While the fraction of bursts that have reported host measurements is relatively high in the lowest and highest redshift bins, I also note that at the mean GRB redshift ~ 2.5, only $\sim 1/3$ have received host followup resulting in reported detections or upper limits on the flux. Metal abundances measured by either host emission lines or afterglow absorption are adopted from the literature, see Table 3.4 for details.

I note that this set of measured metal abundances is far from homogeneous. The majority at low redshift are oxygen abundances from host emission, based on the R_{23} calibration (e.g. Pagel et al., 1979; Tremonti et al., 2004). Above redshift $z \sim 2$ restframe Lyman-α moves into observed frame UV or optical, allowing hydrogen columns and metallicities to be measured

[1] http://www.grbhosts.org/

Table 3.1: Summary of GRB and CCSN data sources.

GRB host Sample	
Sample size	92
Number of hosts detected in only a single band	13 (GRBs 980326, 990705, 991216, 050416A, 050525A, 050824, 051016B, 060206, 060605, 050824, 000301C, 030429 and 030323)
Number of hosts with only photometric limit	9 (GRBs 080928, 070721B, 060607, 060522, 060223, 050922, 050730, 030226 and 020124)
Redshift sources	Savaglio et al. (2009) and sources within.
Public photometry sources	Savaglio et al. (2009) and sources within.
Public metallicity sources	See 3.4 for details.
New photometry in this thesis	Tables 3.2 and 3.3. Also Levan et al. (in prep)
Selection Criterion	Long GRB with host detection or limit.

Gemini observations		
GRB	z	mag
050814	5.3	> 26.23
060105	~ 4	> 24.87
060108	2.03	23.91 ± 0.04
060124	2.296	> 25.42
060204B	~ 3.1	24.15 ± 0.04
060210	3.91	24.96 ± 0.08
060502A	1.51	25.45 ± 0.07
061222A	2.088	24.64 ± 0.07
071112C	0.823	25.48 ± 0.07

Table 3.2: Photometry for GRB hosts observed at Gemini Observatory. The host of GRB 050814 is observed in the i-band, all other in the r-band. Quoted errors are $1-\sigma$ sky variance and limiting magnitudes are estimated from the $3-\sigma$ sky variance. Zeropoints errors are a further ~ 0.1. All magnitudes are in the AB system.

HST observations

GRB	z	filter	mag
050730	3.97	F775W	> 28.8
050904	6.29	F850LP	> 27.50
050908	3.34	F775W	27.88 ± 0.19
060115	3.53	F814W	> 28.6
060223	4.41	F110W	27.85 ± 0.15
060522	5.11	F110W	> 27.9
060526	3.22	F775W	> 28.3
060605	3.71	F775W	27.98 ± 0.20
060607	3.08	F775W	> 30.1
060927	5.47	F110W	> 28.3
061110B	3.44	F775W	27.78 ± 0.17
070721	3.63	F775W	28.53 ± 0.33
080913	6.73	F160W	> 28.50
090423	8.2	F160W	> 28.36
		F125W	> 30.29

Table 3.3: Photometry for GRB hosts observed with *HST*.
Quoted errors are $1 - \sigma$ sky variance and limiting magnitudes are estimated from the $3 - \sigma$ sky variance. All magnitudes are in the AB system.

from the afterglow absorption spectrum. In this redshift range, a mixture of sulphur, silicon, iron, and zinc abundances is seen. It should also be noted that metallicities from host emission will be averaged over the host galaxy, while afterglow absorption metallicities probe only the line of sight. The variety of elements measured by absorption spectroscopy poses further challenges to a direct comparison. Here I have assumed a solar abundance pattern in order to estimate $12 + \log O/H$. I.e. assuming that in the general case, the metallicity $[O/H]$ can be expressed as $[O/H] = [X/H] + C_X$ for any element X, where the conversion term C_X depends on the usually unknown abundance ratio. Since by definition, $[X/H] \equiv \log\left(\frac{N(X)}{N(H)}\right) - \log\left(\frac{N(X)}{N(H)}\right)_{\odot}$, the term C_X is reduced to $C_X = 0$ under the assumption of solar abundance ratios because $\log\left(\frac{N(O)}{N(X)}\right) + \log\left(\frac{N(X)}{N(O)}\right)_{\odot} = 0$.

Though the assumption of a solar number ratio between elemental species is not an ideal solution, the abundance patterns of GRB host galaxies, or indeed any high redshift stellar population, are too poorly understood to improve on the conversions. However, the abundance patterns observed in Calura et al. (2009) for a sample of four bursts do not appear to be systematically offset from solar, and Prochaska et al. (2004) find abundance patterns broadly consistent with solar in the host galaxy of GRB 031203, making the assumption a reasonable approximation. This is also further strengthened by studies of local group dwarf galaxies where solar-like abundance ratios have been observed (e.g. Hunter et al., 2007; Trundle et al., 2007; Venn et al., 2001, 2003).

I fit the photometry with galaxy template SEDs using the same methods presented in Chapter 2. Hosts with only a single filter measured are handled the same way, i.e. by fitting the template that is most common amongst hosts

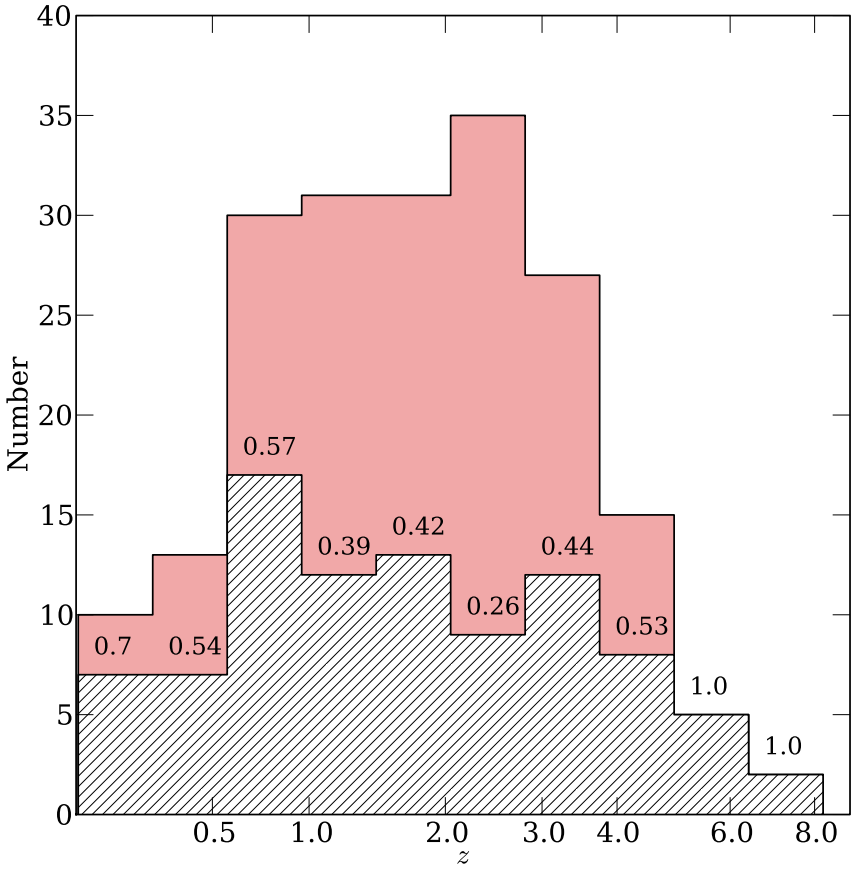

Figure 3.1: The redshift distribution of all GRBs with measured redshift and low Galactic extinction ($A_V < 0.5$) between 1997 and 2010 is shown by the shaded red histogram. The redshift distribution for bursts with host observations, i.e. either host detection or measured upper limit is shown by the hashed histogram. Labels on top of the histogram indicate the fraction of bursts that have host observation, that is, the ratio of the number counts in each bin.

with good SED coverage. In addition, I also fit hosts with only upper limits on the flux in the same way to estimate limits on their restframe properties. As previously, a ΛCDM cosmology with $\Omega_M = 0.27$, $\Omega_\Lambda = 0.73$ and $H_0 = 71$ kms^{-1}Mpc^{-1} is adopted.

3.3 The high-z M-Z relation

The mass metallicity (M-Z) relation is well constrained in the local universe, as discussed in Chapter 2 (e.g. Tremonti et al., 2004), but is more difficult to sample at early cosmic times. However, Maiolino et al. (2008) estimate the evolution of the mass-metallicity relation with nIR spectroscopy of a sample of Lyman-break galaxies near $z \sim 3$. At lower redshift the M-Z relation is estimated from Tremonti et al. (2004) and Savaglio et al. (2005), giving in total the relation in four redshift bins:

$$12 + \log\left(\frac{O}{H}\right) = -0.0864(\log(M_\star) - M_0))^2 + K_0, \tag{3.1}$$

where

$$M_0 = \begin{cases} 11.18 \\ 11.57 \\ 12.38 \\ 12.76 \end{cases} \text{ and } K_0 = \begin{cases} 9.04 \\ 9.04 \\ 8.99 \\ 8.79 \end{cases} \text{ for } z = \begin{cases} \sim 0.07 \\ 0.07 \text{ to } 0.7 \\ 0.7 \text{ to } 2.2 \\ 2.2 \text{ to } 3.5 \end{cases} \tag{3.2}$$

assuming units of solar masses for the total galaxy stellar mass, $M_\star$. Recalling that the solar oxygen abundance, $12 + \log\left(\frac{O}{H}\right) \sim 8.69$ (Asplund et al., 2009),

the mean stellar mass of a galaxy with solar abundance becomes approximately

$$\log\left(\frac{M_\star(Z_\odot)}{M_\odot}\right) = M_0 - \left(\frac{8.69 - K_0}{-0.0864}\right)^{1/2}, \tag{3.3}$$

which can be interpolated for redshift up to $z = 3.5$. As many GRBs are observed substantially above this redshift, evaluation of the M-Z relation above $z = 3.5$ requires extrapolation which is uncertain, or only provide an upper limit of the M-Z relation, i.e. assuming that the metal enrichment is monotonically increasing with cosmic age. Where necessary, a second order polynomial extrapolation of the M-Z relation parameters was used. Although it should be noted that the difference between zeroth, first or second order polynomial are small compared to the intrinsic uncertainty in $M_\star$.

3.4 Results and discussion

Selection of high redshift galaxies is often strongly affected by luminosity biases, i.e. any magnitude limited sample would be challenged to detect the faint end of the luminosity function. One of the goals of GRB selection is to counter this effect, but what are the limitations of current observations? In Table 3.4 I present the estimated restframe properties (M_B and $M_\star$) of the sample along with their redshifts and metal abundances. In Figure 3.2 I show the mass versus redshift distribution of all 92 GRB hosts in our sample. An estimate of the detection limit, assuming a maximum depth of $K = 28$(AB) is shown as a function of redshift. At redshifts $z \lesssim 1$ even very faint (low mass) systems can, and have been detected, but at increasingly higher redshift the minimum detectable mass is increasing. However it should be noted that this is an oversimplification of a very complex situation involving both

the SED shape and the magnitude limit of individual observations, and as a result several upper limits are significantly above this idealised detection limit.

The mass distribution suggests that at redshifts $\lesssim 2$ a significant fraction of hosts have supersolar metallicities as estimated from the M-Z relation, in contrast to only two host for which this has been spectroscopically confirmed (GRBs 050826 (Levesque et al., 2010a) and 020819 (Levesque et al., 2010c)). Indeed only half of these have measured metal abundances, and mass estimates can be sensitive to the spectral range covered by photometry. Still a a number of hosts (e.g. GRBs 020405, 051022 and 980703) have good photometry in the nIR range, but nevertheless overestimate the metallicity from the M-Z relation compared to their spectroscopic metallicities. This would seem to indicate that relatively local GRB hosts are offset from the mass-metallicity relation inferred from the field galaxy population.

Over the complete redshift range where GRBs and their host galaxies have been studied, they appear to be consistently sub-luminous. With a few exceptions, GRB hosts around $z \sim 2-3$, when the Universal star formation density peaked, are typically 2-3 orders of magnitude less massive than seen in the fIR and sub-mm bright galaxies that drive the increase in star formation density (e.g. Chary and Elbaz, 2001). This is suggesting that GRBs selected by optically bright afterglows only trace star formation at the faint end of the galaxy mass function, and implies that at these redshifts, GRBs only probe galaxy environments that are comparatively unevolved in terms of mass assembly and chemical enrichment. However, the exceptions may be crucial to complete this view – GRBs 020117 and 030115 both showed evidence of significant excess extinction in their afterglows (Berger et al., 2007; Levan et al., 2006a), and were shown to be hosted by massive dust rich galaxies

around the characteristic mass of the galaxy mass function, M^*. This could indicate that the lack, in current samples, of GRBs that trace star formation in massive and chemically evolved galaxies, does not reflect intrinsic properties of the GRB progenitors, but is more likely to be due to selection of GRBs by the presence of bright optical afterglows (i.e. not dust obscured). As this may have far-reaching implications on how GRBs can be utilised as cosmic probes, I will return to the problem of these so called *dark* bursts in Chapter 4.

Since GRBs trace star formation even at the faint end of the galaxy luminosity function, they are in principle ideal tools for studying the build-up of chemical elements and probing the M-Z relation of faint star forming galaxies. However, due to the enrichment of metal abundances with cosmic time and the evolution of the galaxy luminosity function, the M-Z relation displays evolution with redshift. Thus, although constructing an M-Z relation purely from GRB selected galaxies is an interesting prospect (e.g. Levesque et al., 2010b), small sample sizes still makes this difficult at redshifts $z \gtrsim 1$. Even though it is still difficult to constrain the evolution of the Universal metal abundances from GRBs, it is possible to check whether the metallicities of GRB hosts are consistent with their luminosities and masses as they are estimated from the nIR fluxes. By comparing with the evolution of the M-Z relation described in Section 3.3, we can test whether GRB hosts are consistent with other star forming galaxy populations at similar redshifts. From these results we can infer if low redshift bursts appear biased to low metallicity environments, and if high redshift GRB host environments are consistent with same Universal chemical history as probed by LBGs.

As a preference for sub-luminous and low metallicity hosts has been noted by several authors (e.g. Sollerman et al., 2005; Fruchter et al., 2006),

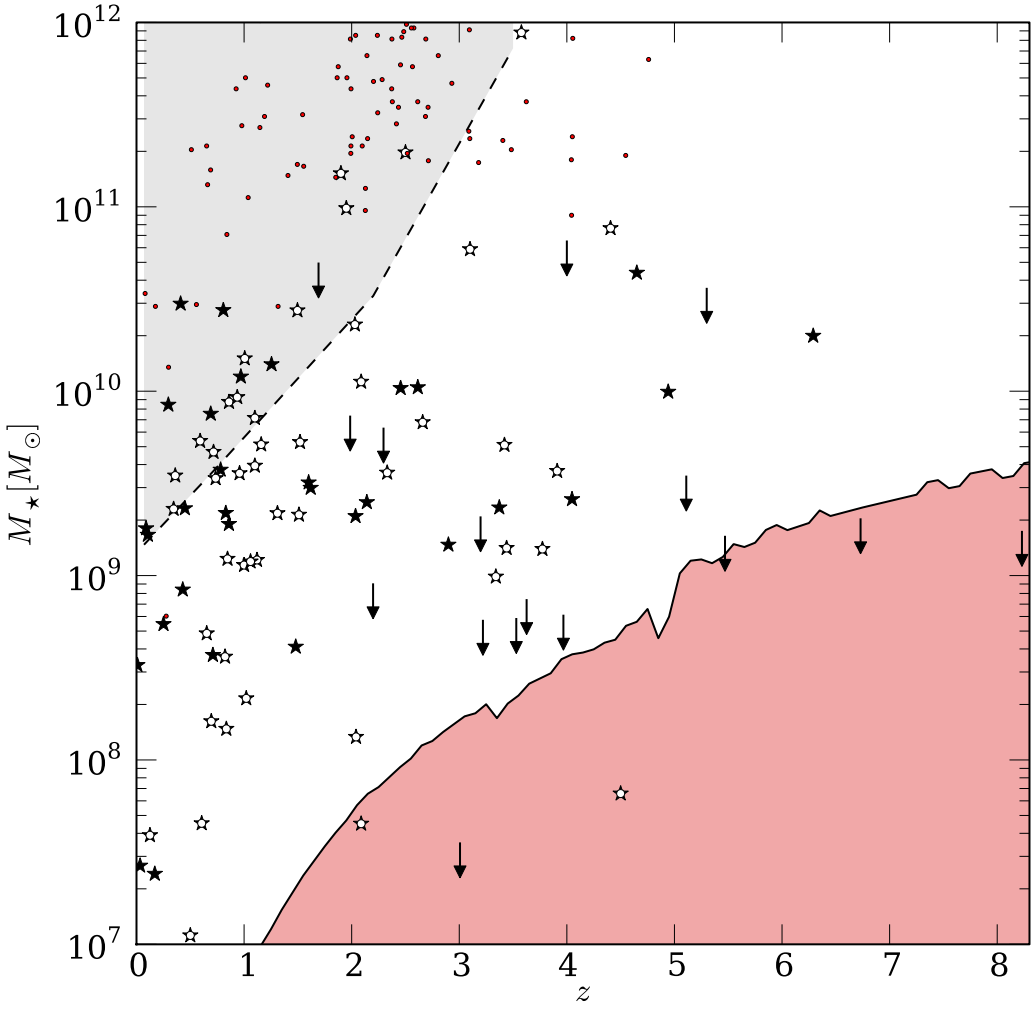

Figure 3.2: GRB host galaxies in the $M_\star - z$ plane. Filled and unfilled stars are hosts with measured/not measured metallicity respectively. The dashed line and grey area show the approximate mass of a solar metallicity galaxy and above, assuming a redshift evolution of the M-Z relation. Small red points are sub-mm selected galaxies for a comparison. The shaded red area covers stellar masses of an $K > 28$ source with a typical GRB host SED.

there is a keen interest in understanding the nature of metallicity effects on the GRB selection method. Although single progenitors may only be able to retain sufficient angular momentum for a rapidly rotating collapsar if it is relatively metal poor, this necessity for low metallicity can be relaxed if angular momentum is transferred in a binary progenitor system. Perhaps most likely, the bulk of the observed GRB population comes from a mix of both single and binary progenitors, similar to core-collapse supernovae progenitors, which are known to evolve in both single and binary systems (e.g. Aldering et al., 1994; Maund et al., 2004; Ryder et al., 2004; Crockett et al., 2008). It has been suggested that low metallicity galaxies are more star forming than equally massive, but more metal rich galaxies (Mannucci et al., 2010a), and that this could explain the fact that most GRB hosts studied have been metal poor (e.g. Kocevski and West, 2010; Mannucci et al., 2010b). Even though, the preference for GRBs to occur in lower metallicity environments compared to broad lined SNe Ic (Modjaz et al., 2008), would be difficult to explain, and is compelling in favour of a true metallicity threshold to produce GRBs from massive progenitors.

The luminosity-metallicity relation for 34 GRB hosts with $0.01 \lesssim z \lesssim 6.3$ is shown in Figure 3.3 where absolute B-band magnitude is plotted against the oxygen abundance. The restframe B-band is better sampled by the photometry, meaning that M_B requires less or no extrapolation of the templates, compared to mass estimates where the restframe K-band is not observed. For a comparison, the L-Z relation for low metallicity galaxies at redshift $z \sim 0.8$ (Jabran Zahid et al., 2010) is also shown. Although the local host sample with emission line metallicities (red points in the figure) appear broadly consistent with a linear relation, this falls consistently below that estimated for field

galaxies. At high redshift hosts should furthermore be less chemically evolved than present day galaxies, placing them at low metallicity compared to this relation. While this is indeed seen in Figure 3.3 it should also be pointed out that for many afterglows of high redshift events only lower limits on the metal abundance are measured due to saturated metal lines, it is therefore difficult with the current data to estimate the L-Z relation for GRB hosts above $z \gtrsim 3$.

Figure 3.4 shows the mass versus oxygen abundance. While the large redshift range obscures any clear view of any M-Z relation, I also plot the evolving M-Z estimated from Equation 3.1. The Left inset figure shows the difference between the M-Z expected and measured metallicities, indicating that, although some hosts are comparatively massive, at low redshift the majority fall below the expected M-Z relation of field galaxies. This view changes at higher redshifts, $z \gtrsim 2-3$ where the host galaxies appear to follow more closely the mass-metallicity relation of high redshift galaxies. Although these are still few events, prohibiting any firm statistical conclusions, it should be noted that this is coincident with the redshift where the M^* metallicity becomes subsolar. This suggests that, as the universal metallicity drops at high redshift, GRB selection will probe star formation across the galaxy mass function without bias towards low metallicity hosts. However, it should also be noted that all the hosts below $z = 1$ are measured from host emission, and that the transition to metallicities from afterglow spectroscopy makes a direct comparison difficult. Further, since the majority of the emission line metallicities are measured from oxygen, the comparison to a variety of other elements is made even more complicated if the abundance patterns vary significantly from solar.

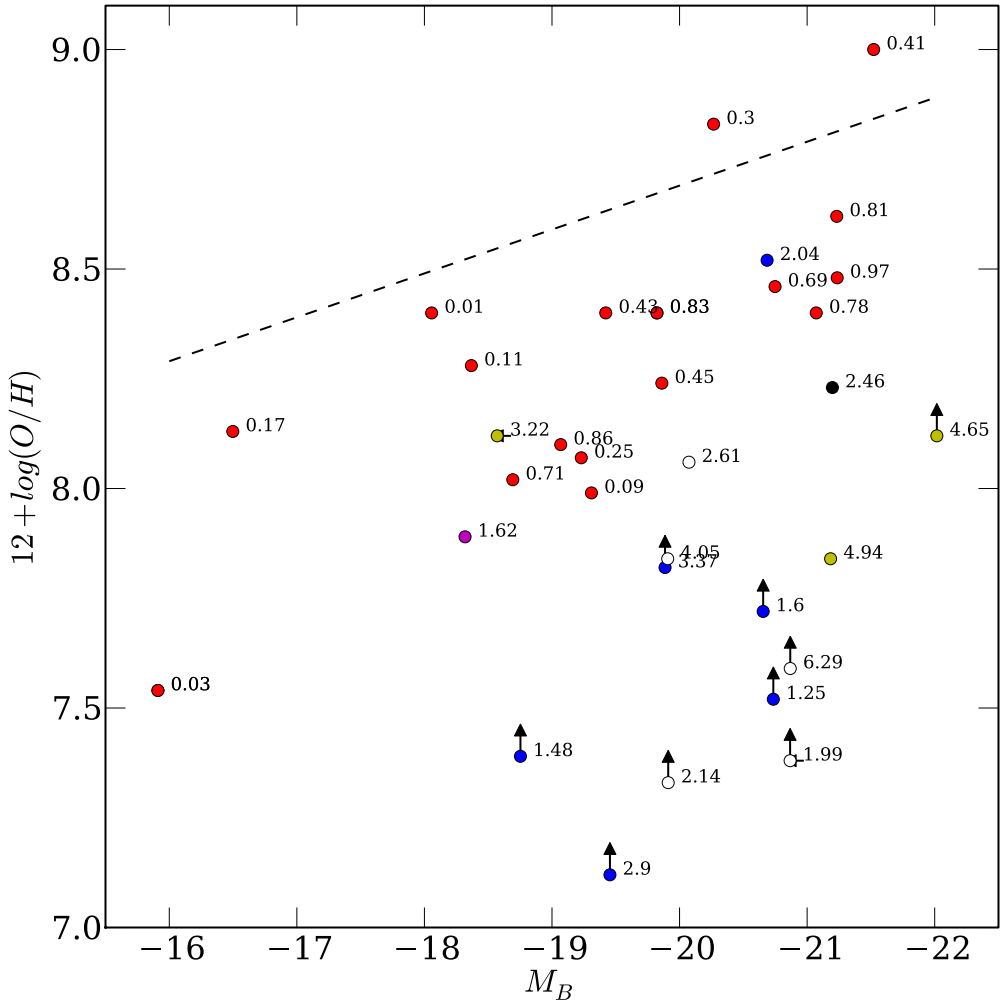

Figure 3.3: The L-Z relation for 33 host galaxies up to redshift $z = 6.3$. Colours indicate the source of the metal abundances (red: oxygen, white: α elements, blue: zinc, black: silicon, yellow: sulphur and magenta: iron.) which are re-normalised to $12 + \log(O/H)$ assuming a solar abundance pattern, and the points are labelled with the redshifts of the bursts. The dashed line shows L-Z relation calibrated to M_B at redshift $z \sim 0.8$ (Jabran Zahid et al., 2010).

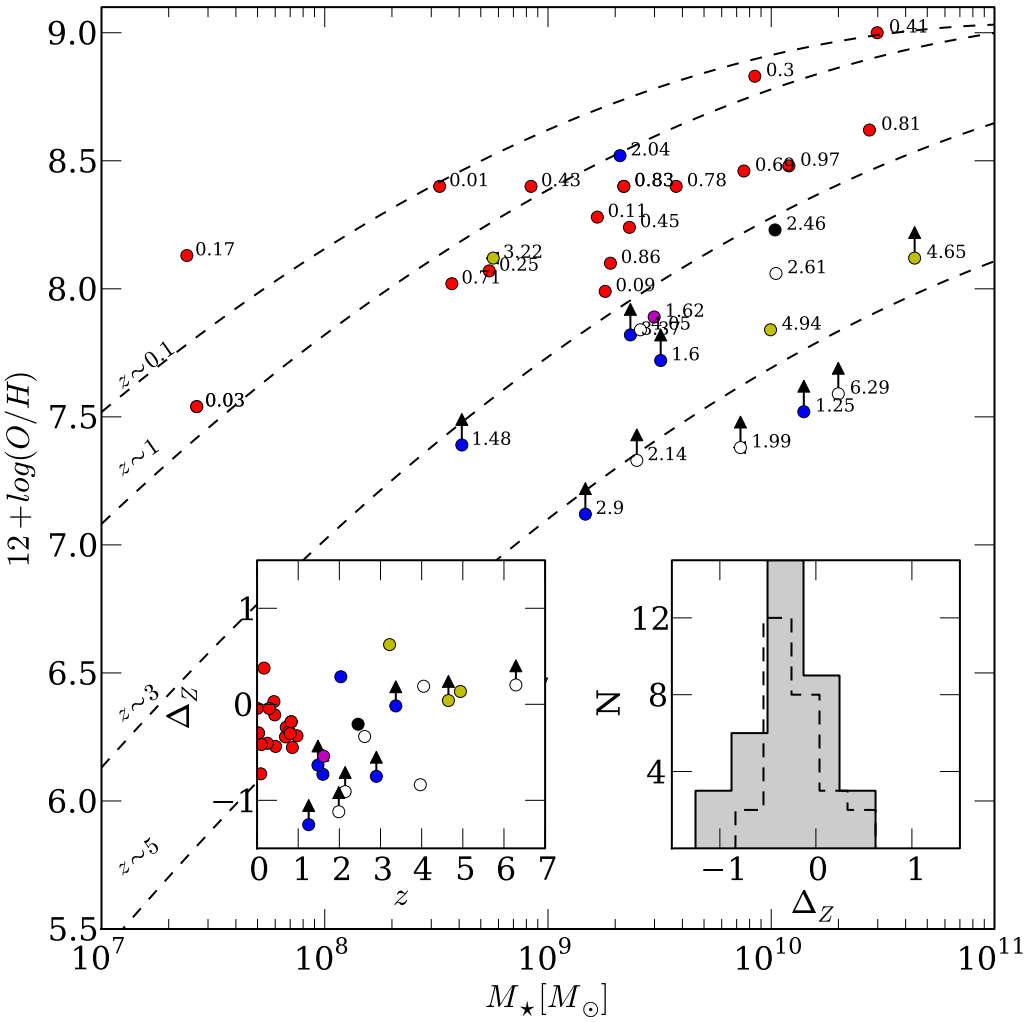

Figure 3.4: The mass-metallicity relation for 33 host galaxies up to redshift $z = 6.3$. Colours indicate the source of the metal abundance, red: oxygen, white: α elements, blue: zinc, black: silicon, yellow: sulphur and magenta: iron. All metallicities are re-normalised to $12 + \log(O/H)$ assuming a solar abundance pattern. The points are labelled with the redshifts of the bursts. Dashed lines represent the evolving mass-metallicity relation as estimated by Maiolino et al. (2008) at redshifts $z = 0.1, 1, 3$ and 5 from top to bottom. Note that the parameters of the M-Z relation at $z = 5$ are extrapolated from the lower redshift bins. The right inset figure shows the difference Δ_Z between the measured metallicity and that predicted from the model (Solid grey histogram: includes metallicities taken at the limit, dashed histogram: not including metallicity limits). The left inset figure shows the metallicity differences versus redshift.

Although afterglow spectroscopy, and hence metallicities, are measured independently of host luminosity at redshifts where this is possible, a bias towards high luminosity hosts is possible at low redshift where host emission spectroscopy can only obtain meaningful signal to noise for brighter hosts. Hence, untangling the physical meaning behind the low metallicity nature of hosts at low redshift is non-trivial. Two distinct hypothesis can be recognised: Either there is an intrinsic preference for low metallicity, i.e. single progenitors for the collapsar, or low metallicity is a secondary effect of selecting the most star forming galaxies, i.e. the anti-correlation between metallicity and star formation rate. Both of these cases could be expected to offset the L-Z and M-Z relations in consistency with the distribution seen at low redshift in Figures 3.3 and 3.4, although the fact that GRB selected galaxies appear to follow the M-Z relation above redshift $z \gtrsim 3$ would suggest that low metallicity is selected due to increased GRB efficiency rather than increased star formation. However, a distinct metallicity threshold for the progenitors is not evident at any redshift, though if progenitors could follow from either single or binary evolution, this effect would indeed be smeared out.

Assuming that high redshift bursts trace star formation across the galaxy mass function, the mass-metallicity relation of their host galaxies can give an indication of the evolution of the global metal enrichment. In Figure 3.5 the metal abundances of hosts are plotted versus redshift, showing the general trend of decline of metals with increasing redshift. Above $z \gtrsim 2-3$, the GRB hosts M-Z relation is broadly consistent with that of LBGs extrapolated from Maiolino et al. (2008), suggesting that both metal abundances and the luminosity function of host galaxies has evolved on par with the star forming field galaxy population. GRB hosts are then consistent with a cosmologi-

cal history where galaxy mass build up faster than the chemical enrichment. Maiolino et al. (2008) suggest this is an indication that massive galaxies are assembled by the merger of low mass (low metallicity) systems before the star formation efficiency increase and chemicals build up more rapidly. Chary et al. (2007) also find evidence from GRB selected galaxies of a strong evolution in the M-Z relation. Their interpretation of the results suggest that low mass star forming galaxies appear less chemically evolved due to the loss of metals to the intergalactic medium. Hence, larger samples of metallicities from high redshift GRB afterglows coupled with broad-band observations of their hosts to estimate luminosities and masses, are needed to constrain a more detailed view of how the metal enrichment has evolved. Importantly, due to the brightness of GRB afterglows, this will be made possible also at redshifts beyond the limits of QSO absorption systems and flux limited samples.

This chapter has suggested that GRB selection can indeed be a powerful tool for studying the evolution of both mass assembly (i.e. the luminosity function and galaxy mass function) and chemical enrichment. To gain a better view of this at high redshift, the number of detected burst and measured redshifts need to increase, in particular above $z \sim 4$. While this may not be possible until next generation instruments become available, improved host sample selection also at lower redshift are promising in order to understand how GRBs progenitors depend on their environments, and ultimately to fully use them as cosmological probes. The next chapter will continue to follow the hints that dark bursts trace also a more massive, dustier and possibly more metal rich galaxy population, and how current host samples may be biased due to their omission.

GRB host properties

GRB	z	M_B	$M_\star$	$12 + \log(O/H)$
GRB971214	3.42	-21.468	9.709	
GRB980425	0.0085	-18.05	8.51	8.4 (1)
GRB980703	0.97	-21.23	10.09	8.48 (1)
GRB990123	1.6	-20.65	9.50	>7.72 (2)
GRB990506	1.31	-20.08	9.33	
GRB990510	1.619	-18.31	9.47	7.54 (3)
GRB990712	0.43	-19.42	8.92	8.4 (1)
GRB991208	0.71	-18.69	8.56	8.02 (1)
GRB000131	4.5	-19.69	7.81	
GRB000301C	2.0404	-17.14	8.12	
GRB000926	2.036	-20.68	9.32	8.52 (4)
GRB010222	1.48	-18.75	8.61	>7.39 (4)
GRB010921	0.45	-19.86	9.36	8.24 (1)
GRB011211	2.141	-19.91	9.39	>7.33 (4)
GRB020124	3.198	> -19.69	< 9.31	
GRB020127	1.9	-23.51	11.18	
GRB020405	0.69	-20.74	9.87	8.46(1)
GRB020813	1.255	-20.73	10.14	>7.52 (4)
GRB020819	0.41	-21.52	10.47	9.0 (5)
XRF020903	0.251	-19.23	8.73	8.07 (1)
GRB021004	2.33	-20.96	9.55	
GRB030115A	2.5	-22.45	11.29	
GRB030226	1.986	> -20.86	< 9.86	>7.38 (4)
GRB030323	3.372	-19.88	9.36	>7.82 (4)
GRB030328	1.52	-20.64	9.72	
GRB030329	0.17	-16.49	7.38	8.13 (1)
XRF030429	2.66	-20.80	9.83	
XRF030528	0.782	-21.07	9.57	8.4 (1)
GRB031203	0.1055	-18.36	9.22	8.28 (1)
GRB040924	0.859	-19.06	9.28	8.1 (6)
GRB050401	2.899	-19.45	9.16	>7.12 (4)
GRB050730	3.968	> -18.63	< 8.78	6.43 (4)
GRB050814	5.3	> -22.42	< 10.55	
GRB050820	2.6147	-20.07	10.02	8.06 (4)
XRF050824	0.83	-19.82	9.34	8.4(7)
GRB050826	0.296	-20.26	9.92	8.83 (1)
GRB050904	6.29	-20.86	10.3	>7.59 (4)
GRB050908	3.34	-19.08	8.99	
GRB050922	2.199	> -18.99	< 8.95	
GRB051022	0.807	-21.23	10.44	8.62 (1)
GRB060105	4.0	> -22.97	< 10.81	

GRB060108	2.03	-22.01	10.36	
GRB060115	3.53	$>$ -18.51	$<$ 8.76	
GRB060124	2.296	$>$ -20.80	$<$ 9.79	
GRB060204B	3.1	-22.88	10.77	
GRB060206	4.048	-19.90	9.41	7.84 (4)
GRB060210	3.91	-22.22	9.56	
XRF060218	0.0335	-15.91	7.42	7.54 (8)
GRB060223	4.406	-20.56	10.88	
GRB060502A	1.51	-19.80	9.33	
GRB060505	0.0889	-19.30	9.25	7.99 (9)
GRB060510B	4.942	-21.18	9.99	7.84 (10)
GRB060522	5.11	$>$ -20.17	$<$ 9.53	
GRB060526	3.22	$>$ -18.57	$<$ 8.75	8.12 (11)
GRB060605	3.773	-19.40	9.14	
GRB060607	3.007	$>$ -15.91	$<$ 7.54	
GRB060927	5.47	$>$ -19.54	$<$ 9.21	
GRB061110B	3.44	-19.34	9.15	
GRB061126	1.1588	-20.54	9.71	
GRB061222	2.088	-19.63	7.65	
GRB061222A	2.088	-21.34	10.05	
GRB070306	1.4959	-22.23	10.43	
GRB070721B	3.626	$>$ -18.73	$<$ 8.86	
GRB070802	2.455	-21.19	10.01	8.23 (12)
GRB080319C	1.95	-23.28	10.99	
GRB080913	6.73	$>$ -19.74	$<$ 9.30	
GRB080928	1.692	$>$ -22.64	$<$ 10.69	
GRB090205	4.6503	-22.01	10.64	$>$8.12 (13)
GRB090323	3.5774	-23.55	11.94	
GRB090423	8.23	$>$ -19.52	$<$ 9.23	

Table 3.4: Restframe properties of high redshift GRB hosts. Hosts at $z < 1.2$ are duplicated from Chapter 2 if a spectroscopic metallicity is available. Quoted metallicities above have been converted to the oxygen abundance $12 + \log(O/H)$ where necessary. References for metal abundances are as following: 1: Levesque et al. (2010a) 2: Prochaska et al. (2007) 3: Vreeswijk et al. (2001) 4: Prochaska et al. (2007) 5: Levesque et al. (2010c) 6: Wiersema et al. (2008) 7: Sollerman et al. (2007) 8: Wiersema et al. (2007) 9: Han et al. (2010) 10: Chary et al. (2007) 11: Thöne et al. (2008b) 12: Elíasdóttir et al. (2009) 13: D'Avanzo et al. (2010)

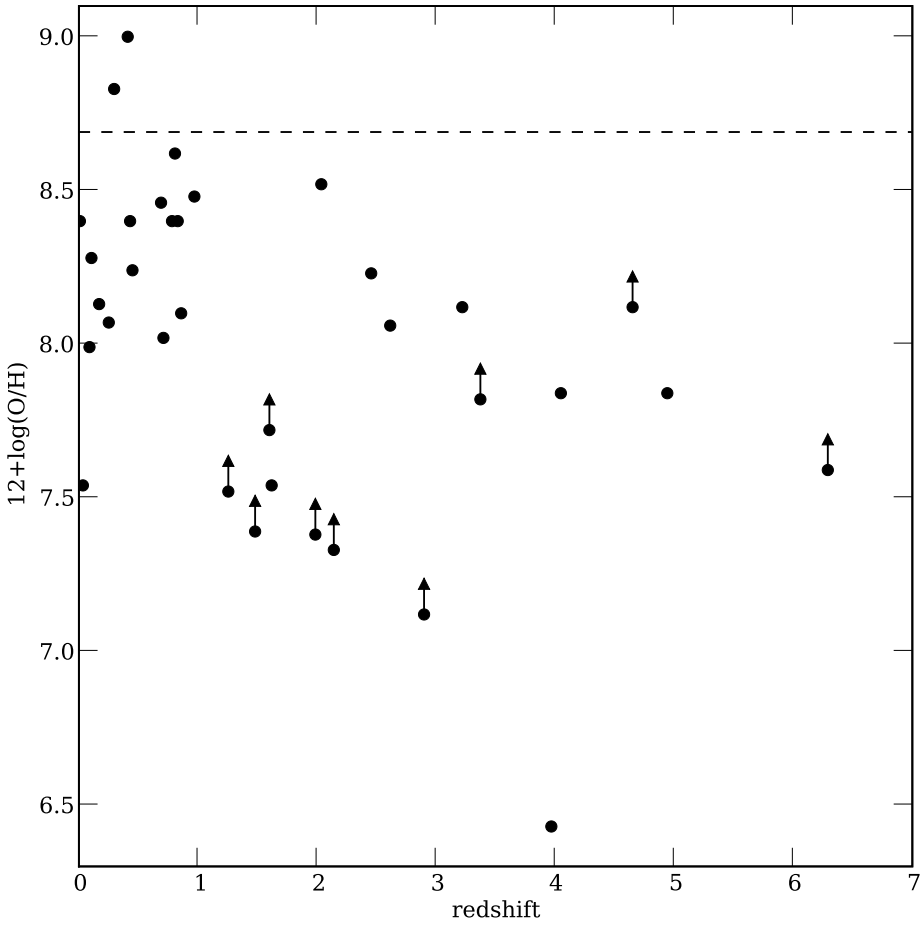

Figure 3.5: The metallicity vs. redshift distribution of 34 GRB host galaxies. The horizontal dashed line marks solar oxygen abundance, $12 + log(O/H) = 8.69$. The majority redshift $z \lesssim 2 - 3$ hosts are offset from the M-Z relation probed by field galaxies at these redshifts, while the higher redshift hosts don't appear to be preferentially metal poor at a given mass. This suggests that high redshift events trace star formation across the luminosity function – and that the decline of metallicity seen at high redshift seen in this figure reflects the global chemical enrichment with cosmic age.

Chapter 4

The dark GRB 080207 in an extremely red host and the implications for GRBs in highly obscured environments

4.1 Introduction

A fraction of gamma-ray burst afterglows are undetected or have suppressed flux in the optical and even in the nIR (e.g. Groot et al., 1998). These bursts may include high-redshift events or where there is significant absorption in the host galaxy. Alternatively, observational selection effects may result in a non-detection due to unfavourable location, poor weather etc. for ground based observatories . These observational selection effects can largely be avoided by selecting bursts based on some quantitative criteria, in particular by comparing the optical limits on the afterglow emission to the expected values based

on the observed X-ray flux and spectral slope. Approximately 60% of *Swift* bursts are have both X-ray observations and optical follow-up, allowing at least a rudimentary estimate or limit the X-ray to optical spectral slope. However the fraction of bursts that have simultaneous X-ray and optical observation, and where the optical observations are deep enough to provide detection or a meaningful limit, is more difficult to quantify. By the above criterion, Jakobsson et al. (2004) (see also Rol et al., 2005) define dark bursts as those with an X-ray-to-optical spectral slope, $\beta_{OX} < 0.5$, where $F_\nu \propto \nu^{-\beta}$ and

$$\beta_{OX} = \frac{\log_{10}(F_{\nu,X}/F_{\nu,Opt})}{\log_{10}(\nu_X/\nu_{Opt})}. \tag{4.1}$$

In the range $0.5 < \beta_{OX} 1.25 <$ which is suggested by the standard fireball model, the distribution of β_{OX} is approximately flat (e.g. Figure 1 in Jakobsson et al., 2004), with a tail of $\beta_{OX} < 0.5$ outliers. van der Horst et al. (2009) suggest a more sophisticated approach and define dark bursts by $\beta_{OX} < \beta_X - 0.5$. Selecting bursts which are dark by these requirements, ensures the sample studied appears genuinely physically distinct from the optically bright GRBs, in contrast to simple requirement of an optical non-detection, which is often not constraining in terms of physical models of the afterglow (Rol et al., 2005). Understanding these dark bursts, and the physical causes of darkness is important, not only for understanding the diversity of GRBs themselves, but also for characterising their utility as cosmological probes, and in particular as tracers of the star formation rate.

As we have discussed earlier, long GRBs are known to be associated with massive stars (e.g. Stanek et al., 2003; Hjorth et al., 2003b, as well as Chapter 2), and hence an ideal scenario would be one in which there was di-

rect proportionality between GRB rate and star formation rate, allowing the GRB rate to be an immediate proxy for the star formation rate across cosmic history. Two particular advantages of GRBs in this role come from their brightness, allowing them to be seen at the most extreme redshifts (Tanvir et al., 2009; Salvaterra et al., 2009) and their high energy emission, enabling them to be seen through high dust columns. Coupled with this, they select galaxies across the luminosity function (rather than just at the bright end). Hence, GRBs have the potential to infer the star formation rate, largely free from the order of magnitude corrections that other techniques must apply to allow for contributions from the faint end of the luminosity function, and dust obscuration (e.g. as discussed in Chapters 2 and 3). In practise however, this promise remains to be fulfilled. This is largely due to a combination of incompleteness in the available samples (e.g. Jakobsson et al., 2006; Fynbo et al., 2009) for example because of the difficulty in locating dust obscured GRBs, and because of poorly known environmental effects (such as metallicity, e.g. Wolf and Podsiadlowski, 2007; Modjaz et al., 2008) on the GRB progenitors which impact any direct proportionality between GRB rate and star formation rate. An understanding of dark bursts offers a route through both of these problems; by increasing the completeness of GRB samples, the ability to obtain an accurate redshift distribution for the whole of the GRB population currently detected by *Swift* is gained. In tandem, studies of the environments of dark bursts, in comparison with those of bright examples can be extremely valuable in elucidating the impact of environment on GRB production.

It is therefore reasonable to ask how studies of dark bursts can be achieved. GRBs are located in the gamma-rays and subsequently pinpointed by their X-ray afterglows. Although X-ray afterglows in the *Swift* era are

ubiquitous, they frequently do not allow detailed study of the burst due to the inability to obtain either absorption spectroscopy of the afterglow, or the unambiguous detection of the host galaxy. Although *Swift* X-ray positioning has been greatly improved by more refined algorithms that determine the satellite's pointing using UVOT, The median XRT error circle is still ~ 1.5 arcsec, with 90% of bursts being positioned to less than 2 arcsec (Evans et al., 2009). This suggests that the bulk of GRB host galaxies still can't be unambiguously determined using only X-ray. Purely by chance (e.g. considering the galaxy number counts by Hogg et al., 1997), they have $\sim 15\%$ probability of *randomly* containing a galaxy with $R < 25$ – roughly the median magnitude of GRB hosts (Hogg and Fruchter, 1999), and may contain more than one galaxy comparable to the faintest known GRB hosts – $R < 29$ (Fruchter et al., 2006). Hence, even the now well refined X-ray positions from the *Swift* X-ray Telescope (Evans et al., 2007) cannot unambiguously locate a host. Although absorption in the X-ray afterglows can provide a clue to the GRB environment via the measurement of hydrogen column (N_H), this is one of few constraints that can be obtained from the X-ray afterglow alone. Indeed, in the absence of a redshift, even the rest frame X-ray column cannot be accurately constrained. Although the definition of dark bursts doesn't require an optical afterglow non-detection, (and indeed in many cases the afterglow has been detected), selecting an unbiased sample of dark burst hosting galaxies calls for accurate identification of the host even in cases where the optical afterglow remains undetected. A possible solution to the problem of identifying the hosts is to obtain sub-arcsec astrometric positions, reducing the chance alignment by a factor of ~ 10, for dark GRBs via their X-ray afterglows. Currently, this is only enabled by the *Chandra* X-ray Observatory, and this is the approach

employed here.

A consequence of the relative dearth of dark bursts (per the $\beta_{OX} < 0.5$ definition rather than simply optical non-detection, also throughout this work) in the pre-*Swift* era and relatively weak constraints which can be obtained from X-ray afterglows alone means that the origins and hosts of dark GRBs remain relatively poorly understood, despite the relatively large number uncovered by *Swift*. It is therefore not entirely clear how the environments of dark GRBs (both local and galactic) differ from those of the optically bright population. From the sample of Cenko et al. (2009) the fraction of dark bursts appears to be ~ 0.5 with the majority of these being consistent with low to medium redshift events suffering from dust extinction in the host (Perley et al., 2009b). This agrees with the fraction of dark bursts reported by Melandri et al. (2008) (~ 0.5) and Fynbo et al. (2009) ($0.25 - 0.4$), and could significantly bias samples based on optical detection of the afterglow as discussed in the latter work. Studying the host population of dark GRBs is therefore a priority in order to understand how they differ from normal bursts and what impact the difference will have on statistical host samples (e.g. the ones seen in Chapters 2 and 3) – either by inclusion of dark hosts, or by their exclusion. Although the number of dark GRBs with securely identified hosts is still relatively small (~ 12, see e.g. section 4.5.2) it is noteworthy that several of other heavily extinguished bursts hitherto have been associated with galactic environments that are *atypical* of the overall host population: The hosts of GRB 020127 and GRB 030115 are massive extremely red objects (EROs) (Berger et al., 2007; Levan et al., 2006a), although the β_{OX} values are poorly or unconstrained due to the lack of follow-up observations (e.g. Fox and Frail, 2002; Smith et al., 2005). GRB 051022 has a massive host (Chapter 2, Svensson et al. 2010)

with large average extinction as well as a red afterglow (e.g. Rol et al., 2007; Castro-Tirado et al., 2007) and GRB 080325 also has a massive host with evidence of significant extinction (Hashimoto et al., 2010). Although this is not an exhaustive list of all dark bursts, in these cases the evidence seems to suggest either unusually red hosts, unusually massive hosts or hosts with very high extinction. It is also interesting to note that, the 5 hosts of dark burst contained in the sample discussed in Chapter 2, all have estimated galaxy masses above the sample median.

Here I will present observations of GRB 080207: the X-ray afterglow by *Swift* XRT, and the subsequent *Chandra* observations that allowed a sub-arcsec position of the afterglow to be determined. The small errorbox of the X-ray afterglow determined by *Chandra* subsequently enabled the host galaxy to be determined, and I will present the 19 band observations of the host, ranging from optical to sub-mm wavelengths. I estimate a photometric redshift and restframe properties from the host SED, and show that it is an extremely red galaxy, which likely contains significant amounts of dust. This implies that GRB 080207 was heavily extinguished, with sufficient local extinction to render even its nIR afterglow invisible to deep observations. Furthermore, I will discuss the general properties of the dark burst hosting galaxy sample and its implications for dark bursts.

4.2 Observations

GRB 080207 was discovered by *Swift* at 21:30:21 UT on 7 February 2008. A prompt slew enabled the location of an X-ray afterglow, however no optical afterglow was found in UVOT observations. The burst was long duration with

$t_{90} > 300$s (at which point the source moved out of the BAT field of view (Stamatikos et al., 2008)). *Chandra* X-ray observations of the afterglow were obtained, which enabled the determination of a sub-arcsec position for the dark GRB 080207 and the identification of its host galaxy, followed by observations of the host galaxy in 19 bands ranging from optical g-band observations with Keck, to sub-mm observations with SCUBA2.

4.2.1 Afterglow

X-ray

Observations with the *Swift* X-ray Telescope (XRT) began 124 seconds after the burst, and continued for 30 hours post burst. For spectral analysis the XRT observations were processed through `xrtpipeline` to create cleaned event lists in both Windowed Timing (WT) and Photon Counting (PC) mode. I separately fit spectra to the WT and PC mode data using XSPEC (Arnaud, 1996). The WT data are best fit by an absorbed power-law model with spectral slope $\beta = 0.34 \pm 0.1$ ($F_\nu \propto \nu^{-\beta}$), and $N_H = (96 \pm 11) \times 10^{20}$ cm^{-2} (assuming zero redshift for the absorption), significantly in excess of the galactic value of 1.94×10^{20} cm^{-2}. The PC mode observations yield a similar excess column density, $N_H = (75 \pm 16) \times 10^{20}$ cm^{-2} , but a much softer spectral slope of $\beta = 1.4 \pm 0.1$. It is also worth noting that a consistently high N_H for the zero redshift case was also found by Racusin (2008).

The WT mode observations took place during the period 130 to 194 seconds post burst. Throughout this time the BAT was also detecting higher energy emission, and the harder spectral index measured in the WT data is most likely a representation of the prompt emission in the X-ray band. I therefore adopt the spectral slope of the afterglow as $\beta = 1.3 \pm 0.1$, as measured

in the PC mode observations.

The adopted X-ray lightcurve comes from the *Swift* repository (Evans et al., 2007, 2009), with the addition of the Chandra observation at $t \sim 7{\times}10^5 s$. The lightcurve is broadly flat during the WT mode observations. The period between the end of WT and the beginning of PC mode observations is broadly consistent with a single power law decay ($F(t) \propto t^{-\alpha}$) of index $\alpha \sim 1.0$. There is no sign of, or requirement for steep initial decays, or a later time plateau as seen in many X-ray afterglows (Nousek et al., 2006). The PC mode late time (between 1000 and 10^6 s) (Figure 4.1) is fitted with a single power law with a decay index $\alpha = 1.7 \pm 0.1$ and $\chi^2/dof = 65.36/65 \sim 1.005$.

Chandra observed the afterglow of GRB 080207 on the 16th of February 2008. The afterglow was placed on the ACIS S-3 (back illuminated) chip and Very Faint (VF) mode employed to enable better rejection of background events. The standard cleaned event files are utilised, but filtered to the energy range of 0.5-7 keV (largely to reduce background events and better isolate the afterglow). The afterglow is detected at a position of RA=$13^h\ 50^m\ 02.98^s$, Dec = $07^\circ\ 30'\ 07.4''$ (J2000) with a 0.4 arcsec error circle. The background subtracted count rate of the afterglow in this band is found to be 5.3×10^{-4} cps. There are insufficient counts in the image to obtain a spectrum directly, however, by assuming the same spectral index as measured in the *Swift* PC mode data this implies a flux of 3.8×10^{-15} ergs s^{-1} cm^{-2} in the 0.3-10 keV band equivalent to *Swift* XRT, and is consistent to $\sim 1\sigma$ with the extrapolation of the earlier X-ray lightcurve – indicating that any jet-break has jet to occur 8 days post burst. Alternatively the jet break could have occurred earlier than the onset of the PC mode observations ($\lesssim 5000s$), although this is unusual.

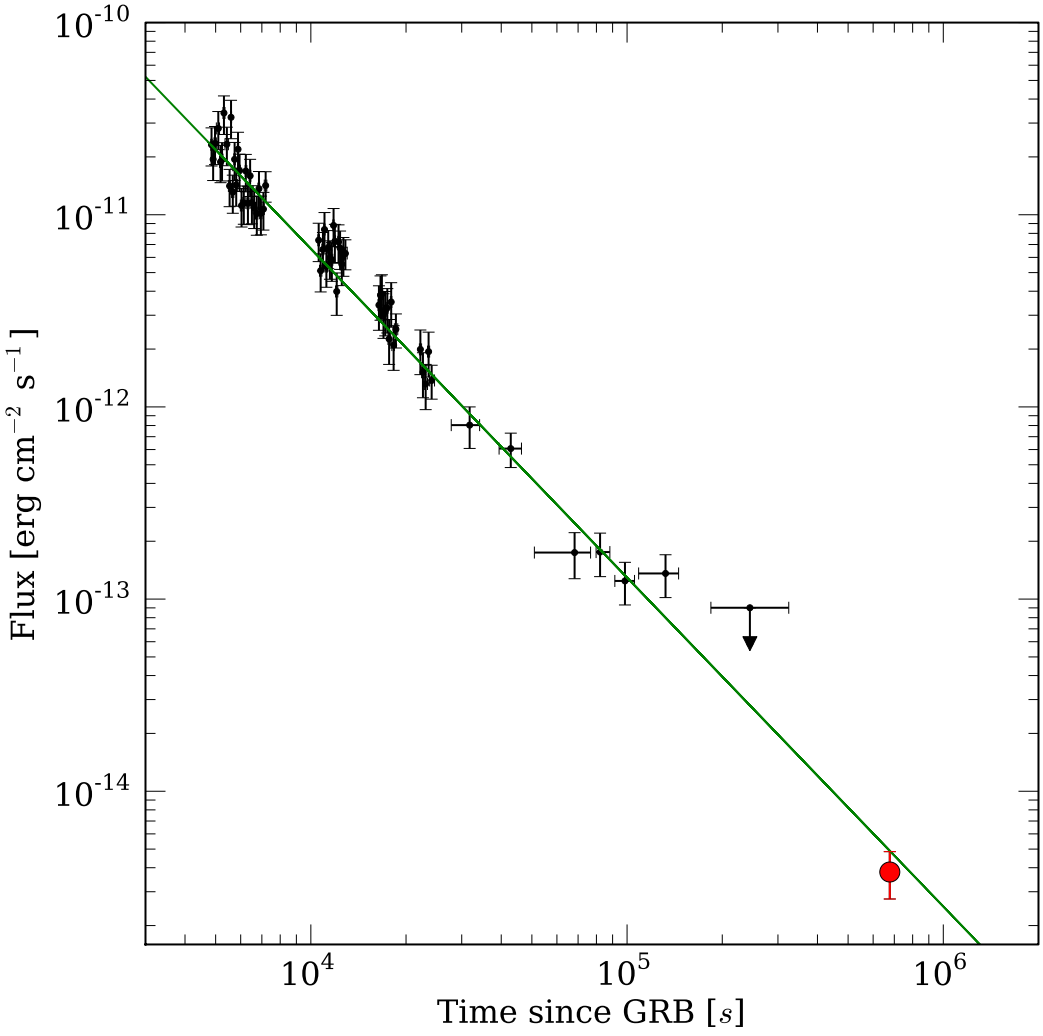

Figure 4.1: The X-ray lightcurve of GRB 080207 from *Swift* XRT PC mode (small black points) and *Chandra* (large filled circle). The *Chandra* flux is rescaled from its observed ACIS bandwidth to equivalent of the *Swift* XRT in this figure. The solid green line shows a single power law fit with a decay slope $\alpha = 1.7$.

Optical

Deep optical observations of GRB 080207 were pursued by several groups roughly 12 hours after the GRB and include observations by 2 to 8 metre class telescopes in both the optical and nIR. None of these observations yielded any afterglow candidates to deep limits. Kuepcue Yoldas et al. (2008) report deep optical limits from GROND: g'>23.9 r'>23.8 i'>23.5 and z'>22.8, nIR limits from VLT are reported by Fugazza et al. (2008) as J>23.5, H>22.8 and K>21.5.

These limits are amongst the deepest obtained for emission from any GRB at moderate times after the burst ($\sim$ 12 hours). The deep limits in both the optical and the IR rule out colours similar to that of high-z GRBs like 050814 (Jakobsson et al., 2006), 050904 (Kawai et al., 2006; Haislip et al., 2006), 080913 (Greiner et al., 2009), 090423 (Tanvir et al., 2009; Salvaterra et al., 2009), and also very red colours due to extinction as have been observed in a handful of bursts (e.g. Levan et al., 2006a; Rol et al., 2007; Jaunsen et al., 2008; Tanvir et al., 2008).

4.2.2 Astrometry

To locate the X-ray afterglow precisely on the deep host galaxy images, relative astrometry is performed between the *Chandra* frames and those obtained at the VLT (see Section 4.2.3). Sources located in the *Chandra* frame were centroided by fitting Gaussian profiles to their point spread function. These were then compared with the *VLT* FORS2[1] frame (see section 4.2.3), giving a total of 6 optical counterparts to X-ray sources in the optical image. An astrometric

[1] Although using the *HST* images would have been preferable, this is unfeasible due to the small field of view

solution was computed with the IRAF task `geomap`, which places the afterglow on the FORS2 frame with an accuracy of 0.45 arcsec. Subsequent relative astrometry between the FORS2 and *HST* WFPC2 and NICMOS frames was performed using 10 (WFPC2) and 7 (NICMOS) sources in common to each frame. The total error in the placement of the X-ray afterglow on the *HST* images is ~ 0.5 arcsec.

4.2.3 Host galaxy

In addition to the prompt afterglow observations reported above deep observations of the host galaxy in 19 bands ranging from observed frame optical B-band to sub-mm 850μm have been obtained. The host galaxy is faint or undetected in the optical and bright at longer wavelengths, indicating very red colours not usually associated with GRB hosts. The host galaxy is displayed in Figure 4.2. The XRT position (large green circle) is unable to uniquely determine the host, while the improved Chandra position (small red circle) intersects three small knots with similar colours, which will be assumed to belong to the host galaxy system.

Hubble Space Telescope

The X-ray position of GRB 080207 was observed by the Hubble Space Telescope using both WFPC2 in the F606W, F702W and F814W filters, NICMOS with the NIC3 camera and F160W filter (H-band) and WFC3 with the F110W filter. Details of the individual observations and photometry are reported in Table 4.2. All photometry presented in this table is performed as part of this thesis.

The WFPC2 data was retrieved from the archive with "On-The-Fly"

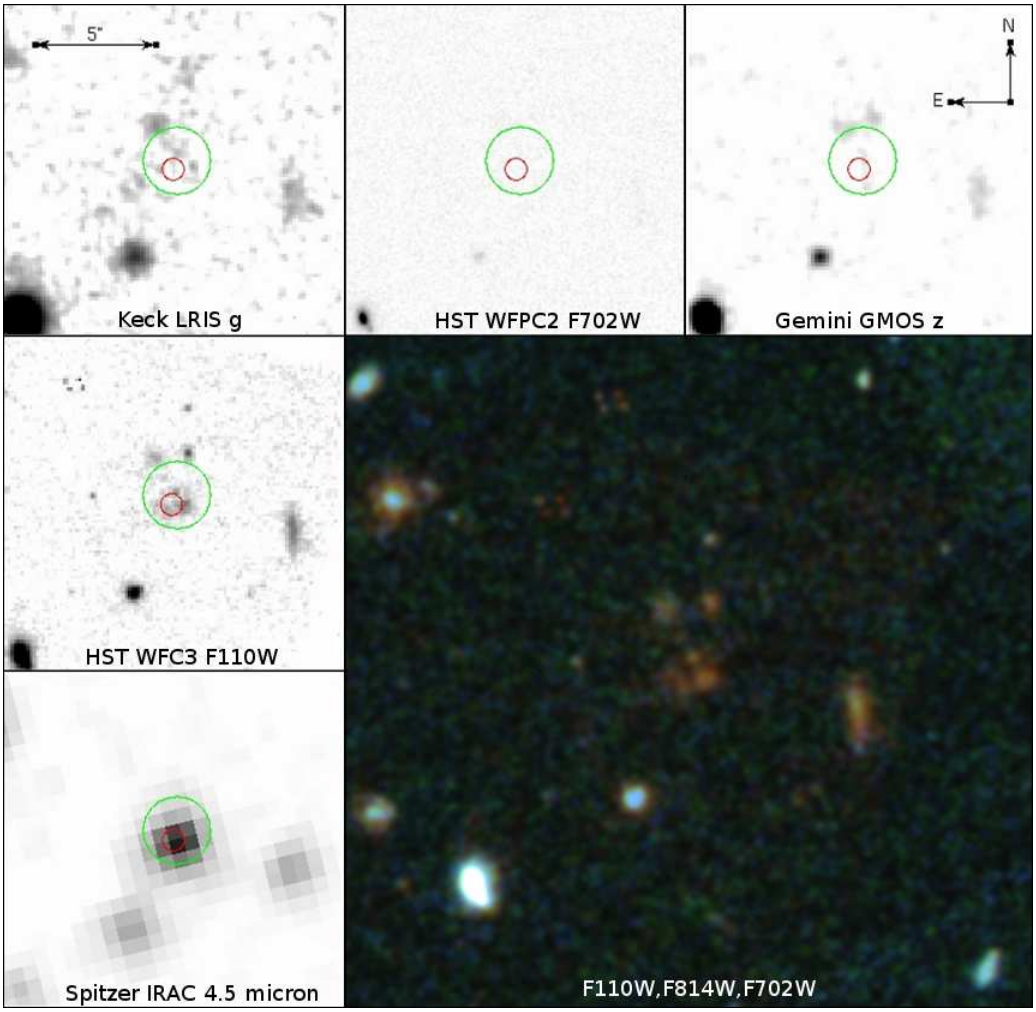

Figure 4.2: Five band mosaic image of the field of GRB080207 including its host galaxy (top and left panels). The red circle marks the Chandra X-ray position and errorbox, the green circle show the *Swift* XRT position and errorbox. The host is faint or undetected in the optical but shows strong emission in nIR and longer wavelengths. The large lower-left panel shows a 3 filter false colour image showing the extremely red host galaxy in the centre and a number of other red galaxies also in the field.

processing. The individual images were then cosmic ray rejected, shifted and combined via `multidrizzle` to produce a final image with a scale of 0.06 arcsec per pixel (roughly 2/3 of the native pixel size).

NICMOS images were cleaned for quadrant dependent residual bias levels (pedestal effect) using `pedsky` and subsequently processed through `multidrizzle` onto an output grid with pixel size 0.1 arcsec. WFC3 observations were obtained with a standard 4-point box dither pattern, and also combined via `multidrizzle`, with the native pixel size unchanged (0.13 arcsec).

There is no evidence for host galaxy emission in any of the WFPC2 observations. However, the F160W observations clearly show evidence for a host galaxy at the location of the X-ray afterglow of GRB 080207. Point source limits for objects at the location of GRB 080207 in the WFPC2 images are F606W = 26.8, F702W=27.2, F814W=27.0 (all 3σ AB magnitude limits). However, the galaxy is clearly extended in the NICMOS F160W observations, hence I have derived more realistic limits using apertures equal to the half light radius of the galaxy as measured in the F160W observations (0.4 arcsec), and then assumed this aperture correction to the total flux of the host. This is also broadly in agreement with the magnitude limits obtained by populating the images with fake sources of half light radii equal to that of the host, and subsequently attempting to recover them via SExtractor (Bertin and Arnouts, 1996). The resulting limits are F606W=25.4, F702W=25.65, F814W=25.02 (See also Table 4.2).

Ground based host observations

In addition to the optical and nIR observation with *HST*, deep observations of the host galaxy with the VLT, Gemini and Keck observatories are obtained.

The VLT R-band observation were carried out on the 1st of April 2008, using FORS2. These observations obtained 4×500 s exposure time, but the host galaxy remains undetected to a limit $R > 25.65$. Although the R-band limit is affected by blending with a neighbouring source, the limiting magnitude is broadly consistent with those from *HST*.

The Gemini observations utilising z (GMOS), J and K (NIRI) obtained exposure times of 720s (in z) and 2880s (in J and K). The seeing in the z band observations was very good (~ 0.5 arcsec), but was poorer for the J and K band (~ 0.9 arcsec). These observations were reduced in the standard fashion under IRAF. The host is detected in each of these observations, although only with marginal significance in the J-band observations. Photometric calibration of the host galaxy was performed relative to SDSS observations of the field for the z-band observations, and in comparison to 2MASS for the J and K.

The Keck observations were performed in the g and I bands (LRIS) with exposure times of $4 \times 330 + 1 \times 320$ s and 5×300 s exposure respectively. The data were reduced with standard IRAF techniques and zero magnitudes were calibrated relative to SDSS stars in the field. I note that both the g and I bands are deeper than the *HST* and Gemini optical observations, resulting in a detection of the host at short wavelength indicating redshift $z \lesssim 2.8$. The Keck K-band observations obtained 25×60 s exposure time enabling a factor ~ 2 better signal-to-noise than the Gemini observations in the K band, and flux consistent within $1 - \sigma$. The Ks band is calibrated using sources in the field common with the Gemini frame. See Table 4.2 for a full summary of all observation details and results.

Spitzer

The host of GRB 080207 was also observed by the *Spitzer Space Telescope*, utilising both IRAC in all 4 bands (3.6, 4.5, 5.8 and 8.0 micron) and with MIPS at 24 microns. The host is clearly detected in all IRAC and MIPS bands, indicating significant nIR and mIR emission, possibly suggesting a massive and dusty host. The clear detections in these bands are in contrast to the majority of GRB hosts which are undetected (or very weakly detected) in similar observations (e.g. Le Floc'h et al., 2006; Castro Cerón et al., 2008). As the host is unresolved at the resolution of *Spitzer*, photometry of the host was performed on the standard post-BCD mosaics, utilising small apertures (2.4 and 7.4 arcsec for IRAC and MIPS respectively) and applying tabulated aperture corrections and zeropoints. The resulting magnitudes are shown in Table 4.2.

SCUBA2

As a part of early observations with SCUBA2 (Holland et al., 2006; Economou et al., 2008) on the JCMT, $\sim$ 43 minutes of observations in the 450μm and 850μm bands during the nights 2010-02-25,2010-02-26 and 2010-03-12 were obtained. The observations were carried out in the SCAN mode with a DAISY scanning pattern. The data is reduced using the STARLINK module SMURF, running makemap in the iterative mode [2] to map the SCAN data into a sky image with a pixel scale of 3 arcsec (e.g. Jenness et al., 2010). The sky maps are flux calibrated relative to the sub-mm flux of CRL618 which is observed during the same nights as the science observations (e.g. Dempsey et al., 2010). Before the maps for all nights are co-added, astrometric corrections are ap-

[2] i.e. iteratively fitting detector signal and background noise.

plied as determined by separate observations of pointing sources also observed during each night. I perform aperture photometry in the 450μm and 850μm bands respectively - measuring fluxes of $23037 \pm 17740\mu$Jy and $2529 \pm 4374\mu$Jy respectively, although the host is undetected. Using blank apertures on the map I estimate $3-\sigma$ limiting magnitudes of 12.1 and 13.6 (AB magnitudes) in the 450μm 850μm bands respectively.

4.3 Afterglow properties

The X-ray spectrum exhibits apparent absorption significantly in excess of the Galactic value. The zero redshift model results in $N_H \sim 75 \times 10^{20}\mathrm{cm}^{-2}$ (c.f. total Galactic N_H column $\sim 1.94 \times 10^{20}\mathrm{cm}^{-2}$) with $\chi^2/dof = 125/153$. Attempting to fit a broken power law with fixed $\Delta\beta = 0.5$, e.g. assuming the spectral turn-over to be influenced by a cooling break in the X-ray band, results in significantly worse fits with $\chi^2/dof = 168/152$, and 36/29 respectively for PC and WT mode data, suggesting that excess N_H is the most likely explanation for the observed spectrum.

Grupe et al. (2007) suggest that the X-ray measured N_H column can be used to limit the redshift by

$$\log(1+z) < 1.3 - 0.5[\log(1+\Delta N_H)], \tag{4.2}$$

where ΔN_H is the difference between Galactic and observed N_H values in units of $10^{20}cm{-}2$, fitted at zero redshift. This would suggest that GRB 080207 originates from $z < 1.3$. Interestingly the only GRB in the sample of Grupe et al. (2007) to be found with a higher N_H than GRB 080207 is GRB 051022, whose optical afterglow was also markedly suppressed (Rol et al., 2007). Indeed, al-

though it is commonly very difficult to assess the redshifts for dark GRBs it is occasionally possible to pinpoint redshifts for bursts whose optical afterglows are somewhat suppressed, and are invisible to UVOT, but are still visible to deep ground based optical observations. In these cases the measured (rest frame) column densities are apparently higher than those for the GRBs with very bright optical afterglows (Schady et al., 2007).

Assuming that GRB 080207 is *not* limited to $z < 1.3$, I fit the X-ray spectrum with single power law model absorbed by the Galactic N_H column *and* an absorber redshifted to $z = 1.74$ as suggested by the photometric redshift solutions for the host (see section 4.1). This model suggests an X-ray spectral slope $\beta = 1.34^{+0.17}_{-0.16}$ and a significantly higher N_H column than the zero redshift case with $N_H = 679^{+125}_{-114} \times 10^{20}\mathrm{cm}^{-2}$. This makes this the highest measured restframe N_H column of any GRB host yet, to my knowledge.

Extrapolating the X-ray power law to optical/nIR frequencies and re-normalising the integrated flux to be consistent with the 11 hour post burst flux as suggested by the lightcurve, reveals the optical/nIR flux limits are fainter than expected. The X-ray-to-optical spectral slope is estimated to be $\beta_{OX} < 0.3$ and thus this burst fulfils the criteria for dark bursts of Jakobsson et al. (2004) (and also fulfils the dark criterion by van der Horst et al. (2009) since $0.3 < \beta_X - 0.5$). To evaluate an optical extinction that explains the optical darkness of this burst, I adopt extinction curves fitted to Galactic (MW) conditions (Seaton, 1979) with $R_V = 3.1$, SMC conditions (Prevot et al., 1984) with $R_V = 2.72$, a starburst (SB) law (Calzetti et al., 2000) with R_V=4.05 and the extinction curve fitted the afterglow of the dark GRB 080607 (Perley et al., 2010b).

The afterglow is reddened after extrapolating the X-ray into the optical-

Afterglow properties	
Ra, Dec(J2000)	13:50:02.98, +07:30:07.4
Errorbox	0.5 arcsec
χ^2/dof (spectral fit)	$48.49/48 \sim 1.01$
β	$1.34^{+0.17}_{-0.16}$
N_H	$679^{+125}_{-114} \times 10^{20}\mathrm{cm}^{-2}$
A_V (MW law)	≥ 2.6
A_V (GRB 080607 law)	≥ 3.4
A_V (SMC law)	≥ 3.7
A_V (SB law)	≥ 4.1
χ^2/dof (lightcurve)	$65.78/66 \sim 1.00$
α	1.7 ± 0.1

Table 4.1: *Chandra* X-ray position and fitted parameters for the afterglows analysis. The quoted hydrogen column and extinction are calculated in the restframe of the hosts photometric redshift ($z_{phot} = 1.74$).

nIR regime, and after introducing a cooling break with $\Delta\beta = 0.5$ short-wards of the XRT band (Figure 4.3). By requiring that the absorbed extrapolation falls below the detection limits, at the redshift $z = 1.74$ a restframe line of sight extinction in excess of $A_V \sim 2.6$ (MW), 3.7 (SMC), 4.1 (SB) and 3.4 (GRB 080607) magnitudes is found. These all suggest that the optical extinction is indeed also very high compared to the bulk GRB population, but that the dust-to-gas ratio is comparable to that found in other hosts (e.g. Schady et al., 2010; Perley et al., 2009b). A summary of derived afterglow properties can be found in Table 4.1.

4.4 Host galaxy properties

The g-band detection of the host galaxy suggests that it lies below $z \sim 4$. Coupled with the relatively bright magnitudes in the nIR to mIR, and the red colours across the whole of the wavelength range, rather than a sharp break

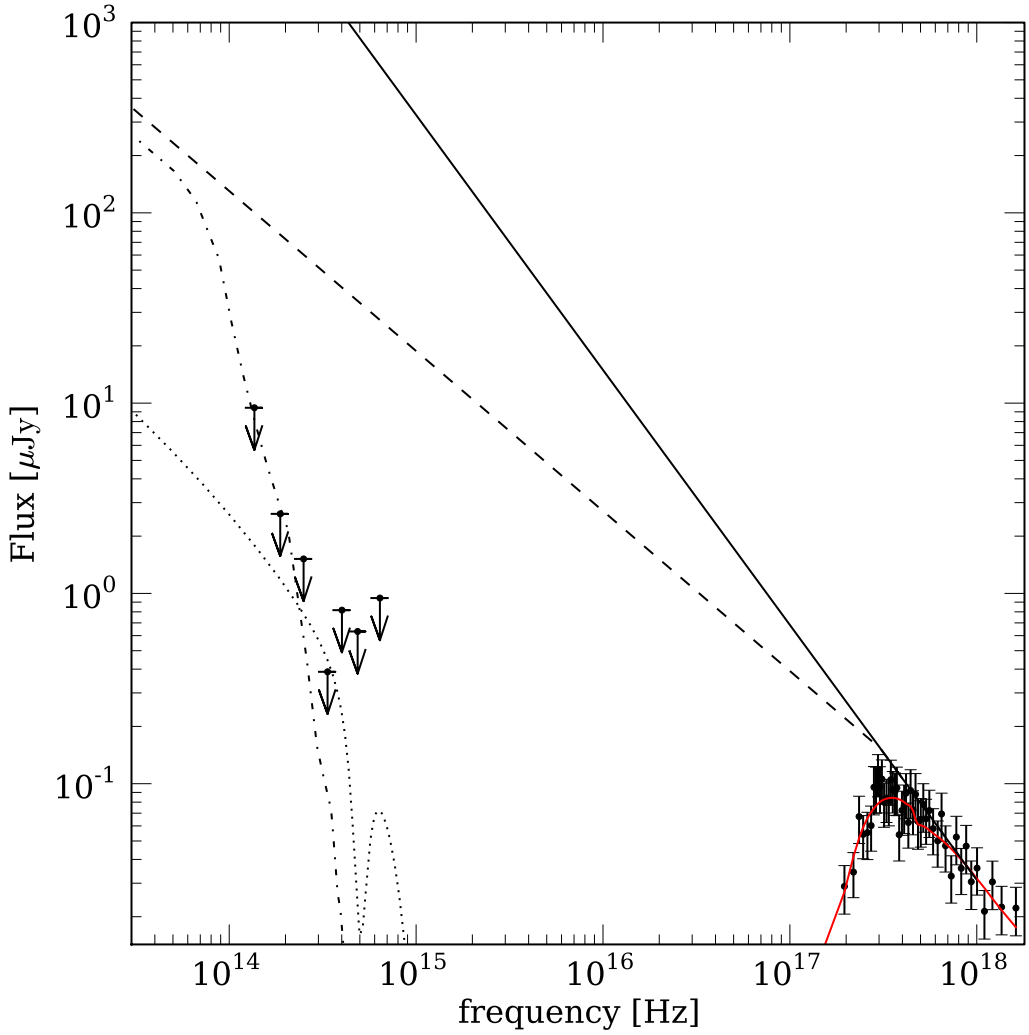

Figure 4.3: The afterglow spectral energy distribution ~ 11 hours post burst, ranging from nIR to X-ray frequencies. The solid red line shows the X-ray model fitted with redshift $z = 1.74$, the solid black line is the X-ray power law extrapolated without a spectral break and the dashed line with a $\Delta\beta = 0.5$ cooling break. The power law and spectral break model is shown absorbed in the restframe by a Milky Way reddening law with $A_V = 2.6$ (dotted line), and by a SMC law with $A_V = 3.7$ (dash-dotted line).

in the optical and a flat SED in the optical - nIR, the favoured interpretation is that of a dusty sight-line. This is also strongly supported by the detection of the host galaxy at 24 microns, and although the SCUBA2 limits are not deep enough to offer any significant constraints, they are fully consistent with sub-mm dust emission at the photometric redshift $z \sim 1.7$ I derive in Section 4.4.1.

The observed R-K colour of $R-K > 5.4$ (equivalent to $R-K > 3.7$ in AB magnitudes) is one of the reddest GRB hosts yet discovered, and indicates that, at least in the case of GRB 080207, the environment is markedly different to that of optically bright bursts. The high resolution imaging acquired by the WFC3 on *HST* resolves the large scale structure of the host, which is displaying an irregular morphology, tentatively suggesting a merging or disturbed system.

In the following section I will discuss the photometric redshift solutions and the restframe properties implied. The 19 bands covered by photometry are presented in Table 4.2 and a four band mosaic image in Figure 4.2 shows the host going from non-detected in the visual, to faint in z-band to strong detections in nIR J-band and IR 4.5μm. In the following I have assumed a ΛCDM cosmology with $\Omega_M = 0.27$, $\Omega_\Lambda = 0.73$ and $H_0 = 71 \mathrm{kms}^{-1}\mathrm{Mpc}^{-1}$.

4.4.1 Photometric redshift

The 19-band observations cover a broad wavelength range from optical to sub-mm, and should allow a well constrained photometric redshift to be determined, and estimates of the physical properties (e.g. mass and star formation rate) of the host galaxy to be made without relying on extrapolating an assumed spectral shape. To enable detailed and accurate modelling of a system that could possibly contain both a young and starbursting stellar population

Host observation log

Date	Instrument	Filter	Exp.Time (s)	Magnitude (AB)	flux (μJy)
2009-02-19	Keck/LRIS	g	1640	27.41 $\pm$ 0.3	0.04 $\pm$0.01
2008-03-18	*HST*/WFPC2	F606W	1600	$>$ 25.4	0.16 $\pm$0.10
2008-04-01	VLT/FORS2	R	2000	$>$ 25.65[1]	0.14 $\pm$0.07
2009-03-21	*HST*/WFPC2	F702W	3600	$>$ 25.65	0.2 $\pm$0.08
2009-02-19	Keck/LRIS	I	1500	25.84$\pm$ 0.29	0.17 $\pm$ 0.05
2009-03-20	*HST*/WFPC2	F814W	3300	$>$ 25.03	0.38 $\pm$0.13
2009-02-24	Gemini/GMOS	z	1260	25.02 $\pm$ 0.25	0.18 $\pm$0.05
2009-02-19	Gemini/NIRI	J	2880	23.87 $\pm$ 0.31	1.06 $\pm$0.35
2009-12-10	*HST*/WFC3	F110W	2400	23.32 $\pm$ 0.09	1.75 $\pm$0.17
2008-04-05	*HST*/NICMOS	F160W	2560	23.04 $\pm$ 0.14	2.27 $\pm$ 0.34
2009-02-19	Gemini/NIRI	K-prime	2880	21.94 $\pm$ 0.24	6.25 $\pm$1.62
2009-05-31	Keck/NIRC	K-short	1500	21.74 $\pm$ 0.13	7.52 $\pm$0.93
2009-03-20	*Spitzer*/IRAC	3.6 μm	1600	20.81 $\pm$ 0.04	17.7 $\pm$ 0.76
2009-03-20	*Spitzer*/IRAC	4.5 μm	1600	20.67 $\pm$ 0.03	20.14 $\pm$ 0.65
2009-03-20	*Spitzer*/IRAC	5.8 μm	1600	20.21 $\pm$ 0.13	30.76 $\pm$ 4.32
2009-03-20	*Spitzer*/IRAC	8.0 μm	1600	20.63 $\pm$ 0.19	20.89 $\pm$ 4.29
2008-07-31	*Spitzer*/MIPS	24 μm	5407	18.50 $\pm$ 0.20	148.59 $\pm$ 32.1
2010-02-25,26,03-12	JCMT/SCUBA2	450 μm	2616	$>$ 12.1	23040 $\pm$ 17740
2010-02-25,26,03-12	JCMT/SCUBA2	850 μm	2616	$>$ 13.6	2530 $\pm$ 4370

Table 4.2: Photometric observations of the GRB 080207 host galaxy. Magnitude are in the AB system. [1] indicates blending with a nearby source affects the limiting magnitude. Limits in the magnitude column are 3-sigma estimated from half-light radius apertures (WFPC2) or point source limits (SCUBA2). In the flux column, the actual flux measured in the aperture also in the cases of non-detections, are reported.

and an older, redder component I find that allowing for a linear combination of two templates provide a significantly better fit than only using a single template. Hence, to simultaneously fix the photometric redshift and the full restframe spectral energy distribution, I fit a linear combination of two templates, one coming from a set of detailed optical templates including models described in Coleman et al. (1980) and Bruzual A. and Charlot (1993). The second set of templates (described by Siebenmorgen and Krügel, 2007) contain galaxies with significant amounts of dust increasing their IR and sub-mm luminosities by reprocessing the UV and optical light. Furthermore, I fit the reddening of the first set of models by assuming a Calzetti et al. (2000) reddening law. The dusty templates in the second set already include a dust screen model, and are not reddened any further. In total this includes 6 free parameters (redshift, A_V, two templates and two normalisation constants.), and for 19 photometry data points, this gives $dof = 19 - 6 = 13$ degrees of freedom.

Fitting the available photometry, including measured fluxes for the non detections, and allowing both redshift and host absorption to vary as free parameters (e.g. Chapter 2) yields a primary photometric redshift solution of $z = 1.74^{0.06}_{0.05}$ with $\chi^2/dof = 19.37/13 \sim 1.49$, shown in Figure 4.4. The redshift error is the central $1 - \sigma$ interval, i.e the integrated probabilities above and below the interval are both $(1 - 0.683)/2$. This result is broadly consistent with an independently derived solution with *HyperZ* (Bolzonella et al., 2000) using only the optical and nIR photometry. It is also worth noting that a higher redshift than provided by the best fit would further increase the restframe hydrogen column derived from the X-ray spectrum, e.g. $\sim$ 10% higher at z=2.2. A significantly higher solution, e.g. above 4-5, also seems

highly unlikely in the perspective of the extremely high luminosities this would imply, e.g. a secondary local χ^2 minimum around $z \sim 5.8$ has $M_V < -25$.

4.4.2 Restframe properties of the host

The restframe properties of the host galaxy as derived from these fits are shown in Table 4.3. I estimate physical galactic properties from the restframe k-corrected and extinction corrected spectral energy distribution. Stellar mass content is estimated from the restframe K band absolute magnitude (Savaglio et al., 2009), corresponding to between IRAC 5.8 and 8μm at $z = 1.74$. For the star formation rate I make two estimates, one based on the U-band luminosity (Cram et al., 1998) and one based on the far-IR luminosity (Kennicutt, 1998). The host is massive and highly star forming - assuming that the fIR traces the true SFR more accurately than the U band. Placing it on the $\frac{SFR}{M_*}$ vs M_* plane compared to the bulk GRB hosting galaxy population (e.g. Castro Cerón et al., 2006, 2008; Savaglio et al., 2009) suggests that it is one of the most massive and most actively star forming GRB hosts to date. From the SED model I estimate a restframe far-IR luminosity $L_{fIR} \sim 3 \times 10^{12}$Ł$_\odot$ suggesting that GRB 080207 is one of few bursts with a ULIRG host (Michałowski et al., 2008). However it should be noted that the ULIRG classification rests mainly on the 24 μm MIPS detection, and while the SCUBA2 limits are consistent, they are also too faint to offer significant constraints on the fIR nature of the SED.

Comparing the host with the luminosity function at $z \sim 2$ (e.g. Dahlen et al., 2005, 2007) suggests that it is comparable to the characteristic luminosity in the B-band; $L_B \sim 1.3L_B^*$, in contrast to the typically under-luminous properties of optically bright selected samples.

In particular it is clear that the host extinction in this case is high in comparison to the bulk GRB population - the dominant model in the optical has an $A_V \sim 1.9$ while the second component has a total of ~ 100 magnitudes of extinction from core to surface (see Siebenmorgen and Krügel (2007) for a description of their dust model) - suggestive of a major dust content within the host. Although a $3-\sigma$ detection is lacking from SCUBA2, I estimate a $3-\sigma$ upper limit of the dust mass as $\sim 1.2 - 1.4 \times 10^9 M_\odot$ assuming a dust temperature of 45K (e.g. Michałowski et al., 2008), and also note that a lower temperature would increase the necessary dust mass. The possibility of significant dust content is in contrast to the majority of GRB host galaxies, whose photometry suggests relatively little dust (e.g. Savaglio et al., 2009; Tanvir et al., 2004), indeed it is more similar to that commonly found in sub-mm selected galaxies (e.g. Michałowski et al., 2010a). However, it should be noted that these studies have mainly concerned optically selected host samples, and *may not* be representative of the true population.

4.5 Discussion

4.5.1 Implications for dark GRBs

The host galaxy of GRB 080207 is one of very few GRB hosts which can be classified as an ERO. The other examples GRBs 030115 (Levan et al., 2006a) and 020127 (Berger et al., 2007) also host bursts which were dark, or showed significant extinction in their afterglow lightcurve. Several other bursts also show very red colours in their afterglows, indicating significant extinction along the line of sight (e.g. Tanvir et al., 2008), however at least in some cases where the afterglow is unusually red, observations of the host galaxies do not reveal

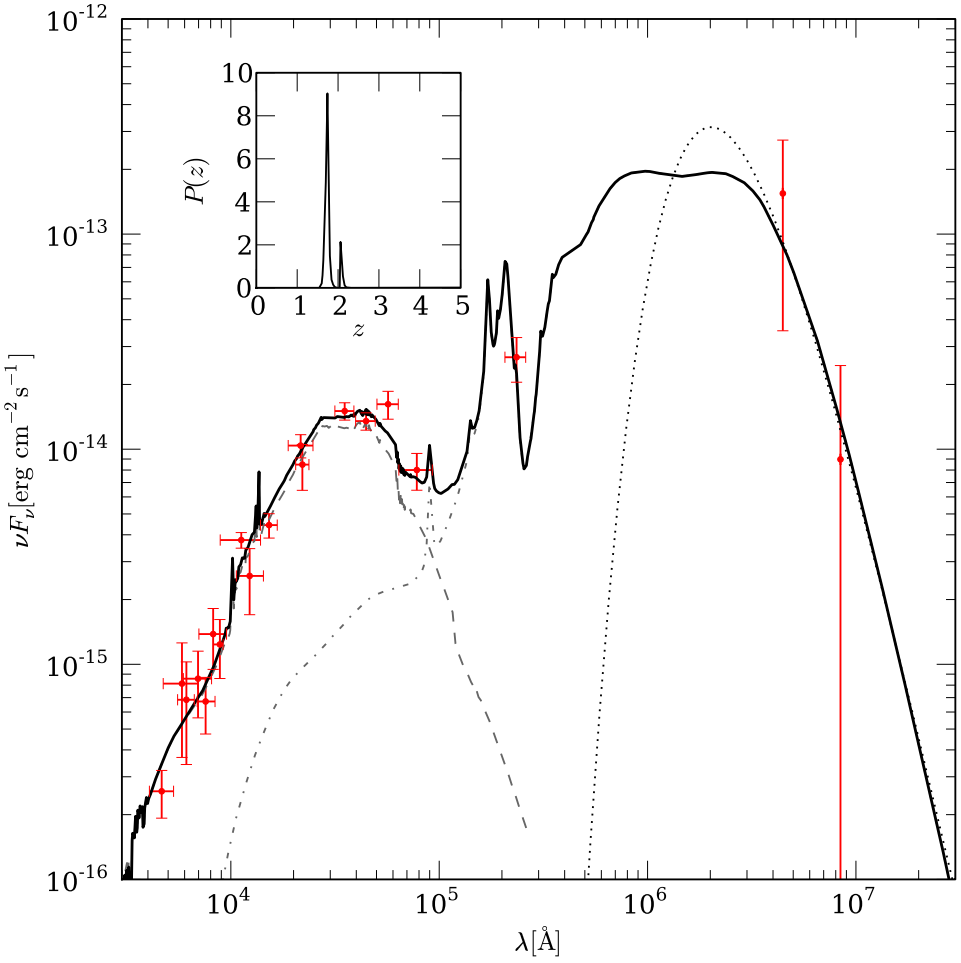

Figure 4.4: The host galaxy spectral energy distribution and photometric redshift solutions at $z_{phot} = 1.74^{0.06}_{0.05}$. The wavelength scale is in the observer frame. The thick solid line shows the composite template model with the dashed, and dash-dotted lines showing the individual components. The dotted line is purely thermal emission from $\sim 7 \times 10^8 M_\odot$ dust at $\sim$ 45K. The inset figure shows the probability distribution as a function of redshift.

Host restframe properties	
z_{phot}	$1.74^{0.06}_{0.05}$
χ^2/dof	$19.37/13 \sim 1.49$
A_V	~ 1.9
M_U	-20.29 ± 0.04
M_B	-20.99 ± 0.04
M_V	-21.86 ± 0.04
M_K	-23.89 ± 0.04
L_{fIR}	$2.4 \pm 0.0910^{12} L_\odot$
$\log(M_\star/M_\odot)$	11.05 ± 0.02
SFR_U	$40.7 \pm 1.6 M_\odot$/yr
SFR_{fIR}	$416 \pm 17.0\ M_\odot$/yr

Table 4.3: Restframe properties of the hosts SED template fit. Absolute magnitudes are not corrected for host extinction. Stellar mass and star formation rates are corrected extinction corrected for $A_V = 1.9$. The quoted errors are 1σ statistical errors on the best fit template.

exclusively red colours (e.g. Gorosabel et al., 2003a,b; Rol et al., 2007; Jaunsen et al., 2008; Perley et al., 2009b; Djorgovski et al., 2001), although there is an apparent trend for the dark GRB host population to include much redder galaxies than that of the optically bright population (e.g. Hashimoto et al., 2010; Küpcü Yoldaş et al., 2010). Indeed, GRB hosts in general are very blue and typically sub-luminous (Le Floc'h et al., 2003; Christensen et al., 2004), suggesting that only a relatively small fraction of GRB selected star formation is obscured - at least so far as the bulk GRB hosting population is represented by burst with optically bright afterglows. Further the blue colours of the GRB hosts, and the relatively low detection rate at long wavelength (e.g. Berger et al., 2003; Tanvir et al., 2004) in the pre-*Swift* sample suggest that few GRB hosts are dusty systems, in contrast to sub-mm observations operating in a similar redshift range, which suggest that the bulk of star formation is obscured, with a good fraction occurring in ULIRG-like galaxies (Chapman

et al., 2005; Michałowski et al., 2010a).

At first sight then it would appear that the complete set of galaxies hosting GRBs are very different from those of sub-mm galaxies, although the direct comparison is far from trivial (e.g. Watson et al., 2004). Indeed, when comparing the rate of sub-mm detections with that expected under simple models of paucity, sub-mm bright GRB hosts are only marginally ($\sim 2\sigma$) below the expected values (Tanvir et al., 2004; Le Floc'h et al., 2006). Though it should be noted that the sample of sub-mm observations of hosts is relatively small, and that this host sample had a median redshift ~ 1.2 compared to the median redshift of sub-mm galaxies of $z \sim 2.2$ (Chapman et al., 2005).

An alternative approach is to study the optical/IR properties of both GRB hosts and sub-mm galaxies. The median I-K colour of sub-mm selected galaxies is I-K = 4.1 $\pm$ 0.2 (Smail et al., 2004), much redder than the general field population which has median I-K = 2.8 $\pm$ 0.1 (Smail et al., 2004). In contrast the GRB population is typically very blue (if somewhat heterogeneously selected to date), with mean colours for optically bright bursts of I-K = 1.6 $\pm$ 0.3, based on the sample of Savaglio et al. (2009), although a significant fraction of GRB hosts are undetected in deep K-band observations, implying at times even bluer colours.

The mean ratio of [N II] / Hα in sub-mm galaxies at $z \sim 2$ is of order 0.5 based on deep IR spectroscopy (Swinbank et al., 2004), in contrast to the (relatively local) GRB hosts with the same measure which yield [N II] / Hα ~ 0.1 (Savaglio et al., 2009; Levesque et al., 2010b). This suggests that even at $z \sim 2$, where the universal metallicity may have dropped significantly, sub-mm bright galaxies may not be the most promising locations for GRBs. Indeed, the highest [N II]/Hα ratio in the optically bright GRB sample of ~ 0.2 would

only include approximately $\sim 20\%$ of the sub-mm sample of Swinbank et al. (2004) as shown in Figure 4.5. Although few hosts of dark bursts have direct measurements of their metallicities, making a direct comparison difficult, I note that the dark GRB 020819 has the highest measured [N II] / Hα so far (Levesque et al., 2010c), making the corresponding distribution for dark bursts to include metallicities at least $\sim \times 2$ higher. Future observations of the [N II]/Hα ratio in GRB hosts at higher-z (for example in the IR with X-shooter), should enable firm statistical statements to be made. In the meantime, I discuss the mass distributions which also commonly act as a proxy for a direct metallicity.

4.5.2 The mass distribution of dark burst hosts

In order to further understand the relations between the dark burst hosting galaxy population and ULIRG / sub-mm like galaxies, I compare the stellar mass distributions of sub-mm galaxies calculated by Michałowski et al. (2010a,b) with the stellar masses of dark burst hosts (see Table 4.4) and the optically bright bursts from Chapter 3 to redshift $z \lesssim 4$. I also estimate the sub-mm galaxy masses with my own SED fitting code, and note that the results are consistent with the adopted values. The cumulative mass distributions are shown in Figure 4.6. While it is important to note that the host sample of dark GRBs consists of only 11 galaxies, the results clearly show that dark bursts are systematically hosted by the most massive systems compared the optically bright GRBs. The formal probability that the samples of optically dark and optically bright bursts are drawn from the same population is given by the Kolmogorov-Smirnov (KS) test, where $P_{KS} = 0.009$. The contrasting host masses between optically bright and dark bursts is particularly

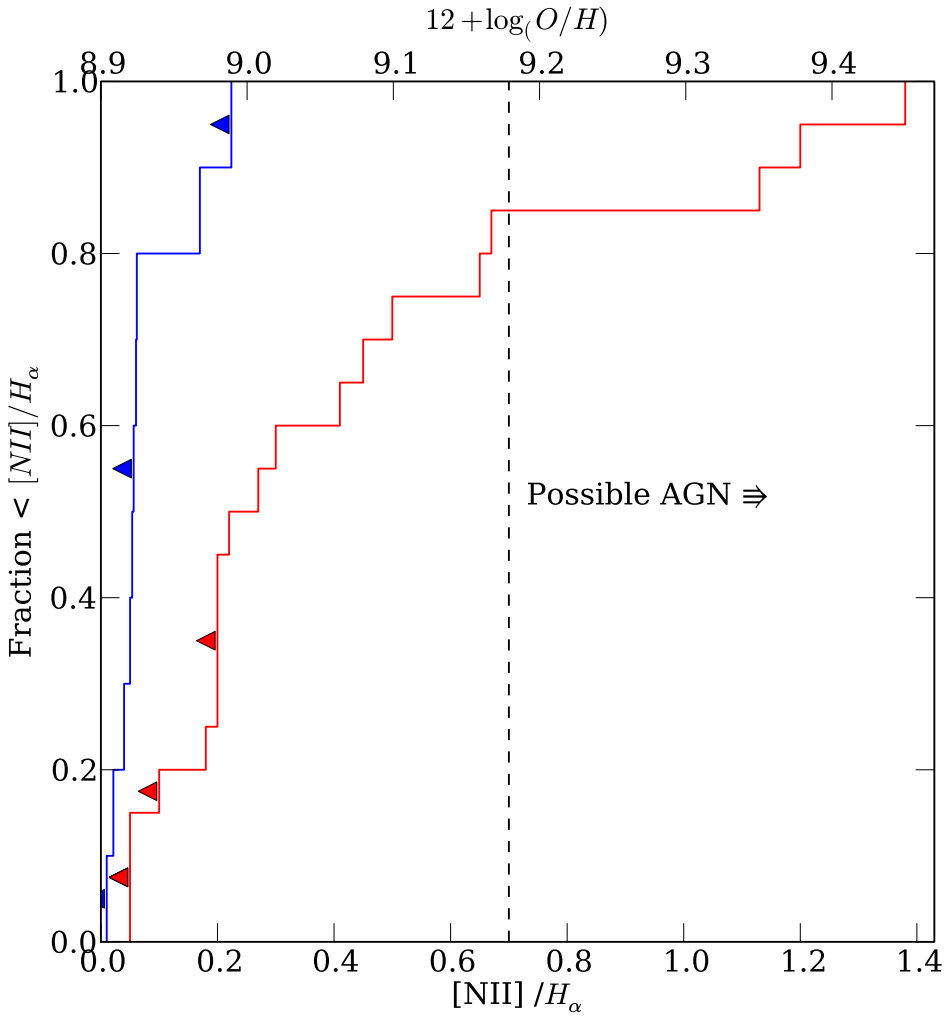

Figure 4.5: Cumulative distributions of the $[NII]/H\alpha$ ratio for low redshift ($z < 0.7$), optically bright GRB hosts (blue) in comparison to $z \sim 2$ sub-mm galaxies (red). Triangles indicate upper limit measurements. Sub-mm galaxies with $[NII]/H\alpha > 0.7$ may have AGN contribution. All galaxies with Hα restframe $FWHM < 1000 kms^{-1}$ from Swinbank et al. (2004) have been included.

GRB	z	$\log_{10}(M_*/M_\odot)$	Ref. (mass or photometry)
970828	0.958	9.57	Chapter 2
000210	0.846	9.21	Chapter 2
020819	0.41	10.52	Chapter 2
050223	0.59	9.81	Chapter 2
051022	0.807	10.49	Chapter 2
060210	3.9	10.56	Perley et al. (2009b)
061126	1.16	11.16	Chapter 2
061222	2.08	7.65	Perley et al. (2009b)
080207	1.74	11.05	this chapter
080325	2	10.85	Hashimoto et al. (2010)
080607	3.036	11.88	Chen et al. (2010)
090417B	0.3	9.25	Holland et al. (2010)

Table 4.4: Stellar masses of all host galaxies of dark bursts available to date. Note that in the case of GRB 090417B I have supplemented the existing data with additional photometry and derived new stellar mass estimates.

interesting as it lends further credibility to claims that samples based primarily on bursts with optically detected afterglows could be severely inhibited by selection effects (e.g. Fynbo et al., 2009).

Although I have not been able to reach a detection of the host sub-mm flux by SCUBA2, the number of GRB hosts with significant dust content be can roughly estimated. Assuming that some fraction of dark bursts occur in obscured systems, and also have similar dust to mass ratios – I compare their stellar mass distributions in Figure 4.6. Roughly estimated, $\sim$ 90% of the dark burst hosts are more massive than the least massive sub-mm galaxy – and hence under this simple argument one could expect a similar detection rate of dark GRB hosts in the sub-mm at SCUBA sensitivity. Depending on the intrinsic mass function of the sub-mm population, even greater detection rates could be plausible with SCUBA2 when considering that the sub-mm galaxy sample in this comparison is flux-limited (Chapman et al., 2005). In

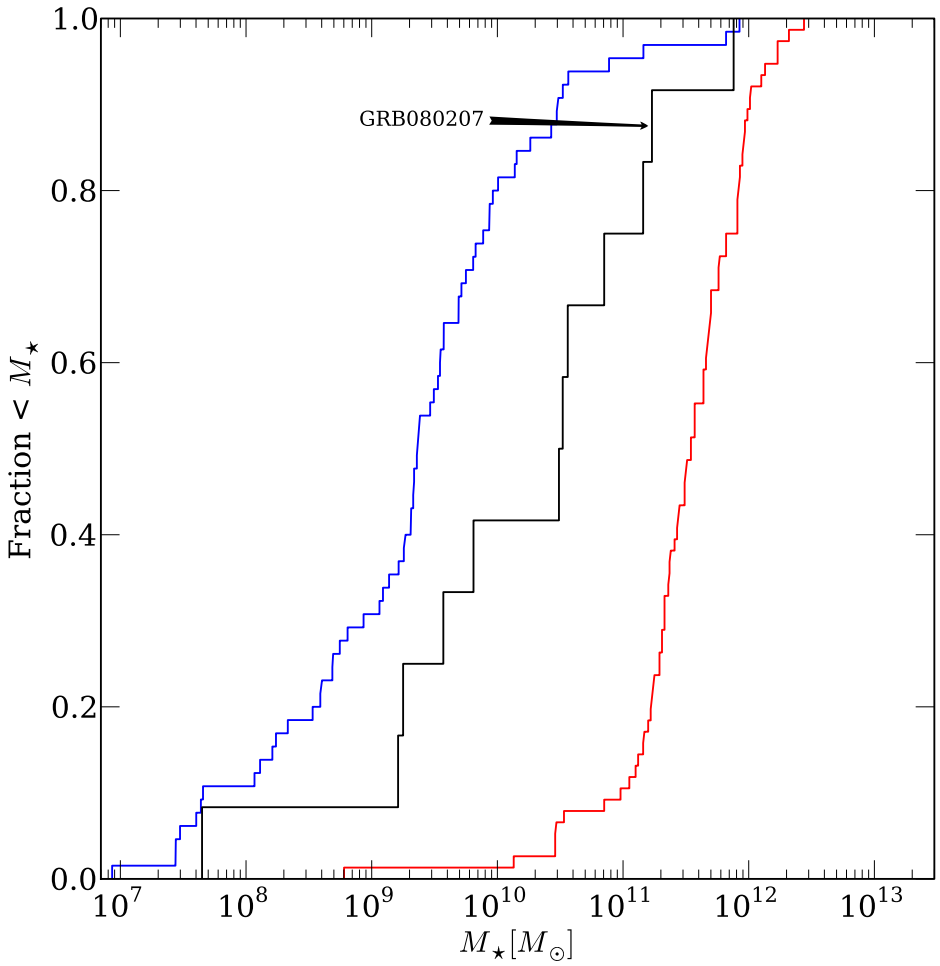

Figure 4.6: Cumulative distribution of stellar mass in optically bright GRB host galaxies (blue line) and hosts of dark bursts (black line). For a comparison I also show the distribution of stellar masses of the sub-mm galaxies (red line) calculated by (Michałowski et al., 2010a,b)

terms of physical properties of the dark burst hosts, this suggests that dark bursts are hosted predominantly by a very dust rich galaxy population.

Given that GRBs trace (at best) a fraction of star formation, potentially even at moderately large redshift, it is surprising that attempts to transfer directly between GRB rate and star formation rate produce even moderately consistent results (e.g Price and Schmidt, 2004; Yüksel et al., 2008; Kistler et al., 2009). Although the sample of dark bursts to date with detected and studied host galaxies is still small, the emerging picture suggests that they indeed trace a different galaxy population than the optically bright sample, certainly the host of GRB080207 is more akin to sub-mm or ULIRG galaxies than to the typical GRB hosts, suggesting that it is part of a subset of the GRB hosting galaxy population that trace star formation in more massive, dusty and metal rich environments. In the face of the growing evidence that dark bursts can be hosted at higher metallicity than the bulk GRB population studied today, it should be considered likely that GRBs can offer significant advantage over other methods to study the evolution of the cosmic star formation history – but only by paying due attention to sample selection effects and understanding the dark burst host population to avoid bias effects.

Although there is no direct measurement of the metallicity of the host of GRB 080207, the high stellar mass is suggestive of a metal enriched environment – again raising the question of what is the nature and metallicity dependence of GRB progenitors? Considering the low metallicities typically associated with the bulk of the GRB hosts, I note that several authors (e.g. Levan et al., 2006b; Davies et al., 2007) have discussed tight binary systems as possible progenitors to GRBs in high metallicity environments. While this would still require ongoing star formation and high mass stars, Habergham

et al. (2010) report evidence for top-heavy IMFs in merging systems, increasing the likelihood of a GRB progenitor.

If the galaxy hosting GRB 080207 is undergoing a merger that further increased its rate of forming massive stars, and if a binary progenitor is indeed possible at high metallicity - maybe massive and dust-rich galaxies are hosting a non-negligible fraction of bursts. Although to which extent these conclusions can be generalised to other dark bursts is far from certain.

4.6 Summary

I have studied the afterglow of the dark GRB080207 from X-ray to nIR wavelengths and presented evidence of significant extinction in excess of at least 2.6 magnitudes (MW law) in the restframe visual as the cause of its optical-nIR darkness. The high optical extinction is also echoed by the restframe hydrogen column which is the highest measured in any GRB environment to date. Lacking optical detection of the afterglow I have used observations of the X-ray afterglow at late time with *Chandra*, enabling an X-ray position to accurately identify the host galaxy. The ERO host spectral energy distribution has been studied in 19 bands from optical to sub-mm allowing me to estimate a photometric redshift ~ 1.74 and an average optical extinction of $A_V \sim 1.9$ in a massive galaxy. Furthermore, the host appears to be a ULIRG from its far-IR SED, with a high star formation rate as traced by the far-IR light. With a significant fraction of all bursts being classified as dark, and an increasing desire to utilise GRBs as high redshift probes of the star formation evolution, the understanding of the nature of dark bursts should be highlighted. This, and a number of other dark bursts in similar hosts should further encourage

the study of dark bursts, their host environments and how they relate to the evolving rate of star formation.

Chapter 5

Conclusions

In conclusion, I have studied the star forming and GRB hosting galaxy population from low to high redshifts, and discovered the highly varied nature of the environments in which these events occur. In this chapter, I will summarise the most important results and conclusions from the Chapters 2, 3 and 4, and then briefly discuss the future strategies for improving our understanding of how GRB progenitors depend on their environments, and how this impacts on GRB selected galaxy samples.

5.1 Summary of results

In Chapter 2, I presented a comprehensive study of the galactic and small scale environments of gamma-ray bursts and core collapse supernovae in order to compare and contrast the environments their respective progenitors evolve in. This study included a sample of 34 GRB hosts at $z < 1.2$, and a comparison sample of 58 supernova hosts located within the Great Observatories Origins Deep Survey footprint. The properties of the hosts were studied by means of their spectral energy distributions, morphologies and the surface luminosities

under the transient positions. Physical properties of the hosts were estimated by fitting template spectra to the available photometric data, ranging from HST optical (0.45 μm) to *Spitzer* infrared (24μm), and extracting absolute magnitudes, stellar masses and star formation rates from the resulting fits. The local environments of the progenitors were studied performing relative astrometry between the GRB or SNe discovery images and images taken either before or after the transient has faded, and thereafter calculating surface luminosities and the fraction of light statistic. The morphologies are divided into Spiral or Irregular galaxies, and the restframe 80% light radius is calculated as an estimate of the physical size.

The results for the low redshift GRB host population presented in this thesis broadly corroborate previous findings, but offer significant enhancements in spectral coverage and a factor 2-3 increase in sample size. Specifically, it is found that CCSN occur frequently in large galaxies, which is consistent with the spiral fraction, which is $\sim$ 50%. In contrast to this, GRBs typically occur in small and morphologically irregular galaxies, where the spiral fraction is only $\sim$ 10%. Although these results are statistically significant at a high level, the comparison between the rest frame absolute magnitudes of the GRB and CCSN sample is less conclusive than found in previous work, suggesting that while GRB hosts are typically smaller than those of CCSN, their total blue light luminosities are only slightly lower. I suggest this is likely due to rapid periods of intensified star formation activity, which both create the GRB progenitors and briefly but significantly enhance the host galaxy luminosity across the spectrum. Finally, the analysis of local environments of GRBs and CCSN showed that GRBs are highly concentrated on their host light, and further occur in regions of higher absolute surface luminosity than

CCSN. This suggests that their progenitors are more massive than those that explode as CCSNe, and as a result they never reach far from the clusters or OB associations where they formed.

In Chapter 3 I studied the masses, mass-metallicity and luminosity-metallicity relation for 92 GRB hosts at $z \lesssim 8.2$. Metallicities from either afterglow absorption or host emission were compiled from literature for a subset of roughly one third of the hosts. Host galaxy masses and absolute magnitudes were estimated from their spectral energy distributions by fitting model templates. I show that at low redshift a significant fraction of GRB hosts lie below the M-Z and L-Z relations of the general star forming galaxy population. Though sample sizes are still small, these results suggest that low redshift hosts are selected by a preference of low metallicity, although this is currently being challenged by other lines of evidence. Though a low metallicity nature of GRB progenitors is consistent with the collapsar model, some host are also found in metallicities at high as $12+\log(O/H) = 9.0$ or in very massive hosts, suggesting that at least a fraction of GRBs evolve through channels that are not affected by their metallicities, or that large scale metallicity gradient are in place. At higher redshift, $z \gtrsim 3$ the M-Z and L-Z relations are poorly sampled. I have used and estimated the high redshift M-Z relation and found that the metal abundances of high redshift bursts, $3 \lesssim z \lesssim 6$, are broadly consistent with that traced by Lyman-break galaxies at similar redshifts. This indicates that galaxies across the luminosity function are probed at higher redshift, and that the metal abundances traced by GRB hosts is consistent with a cosmological chemical enrichment that evolves slower than the mass assembly of galaxies.

In Chapter 4 I presented results on one of a small number of well ob-

served and studied dark bursts and its unusual host galaxy. Dark bursts often suffer from optically faint afterglows, making it difficult to achieve accurate positions only relying on the *Swift* XRT. To uniquely determine the host galaxy in this case, I used *Chandra* observations obtained 8 days post-burst to place the afterglow on the sky with sub-arcsec accuracy. The host is noticeably different from those of the optically bright GRB sample, being an extremely red galaxy, with observed R-K colour > 5.4.

The first evidence that GRB 080207 was a dark burst became apparent when the afterglow was undetected in both optical and nIR wavelengths. Extrapolating the spectral slope from the X-ray suggested an optical to X-ray slope of $\beta_{OX} < 0.3$, which is significantly shallower than that predicted by the standard model. I show that a likely explanation for this comes from the *Swift* X-ray observations, which suggest extreme absorption in the line of sight. By modelling the X-ray to nIR spectral energy distribution of the afterglow, I demonstrate that unusually high host extinction can explain the optical-nIR darkness. High extinction in the host galaxy is further supported by the restframe X-ray spectrum, which suggests one of the highest neutral hydrogen columns found in GRB hosts so far.

To study the host of GRB 080207 I used comprehensive follow up observations with *HST*, *Spitzer Space Telescope*, Gemini, Keck and SCUBA2 in optical, near- and mid-infrared and sub-mm filters to determine a photometric redshift of $z = 1.74$ and fundamental restframe properties.

Unlike most other GRB hosts in the same redshift range, which are typically blue in optical colours and sub-luminous, the host of GRB 080207 is massive, $M_\star \sim 1.1 \times 10^{11} M_\odot$, and extremely dust obscured as evident from both the ~ 1.9 magnitudes of extinction fitted to the host SED, and the

extreme absorption of the afterglow. The fIR to sub-mm properties of the host amounts to a best fit SED model with significant dust content in the host and a fIR luminosity in excess of $10^{12} L_{\odot}$, suggesting it is a ULIRG.

These results add further substance to the growing evidence that GRBs originating in very red hosts always show some evidence of dust extinction in their afterglows, although the converse is not true as some extinguished afterglows are also found in blue hosts. This indicates that a poorly constrained fraction of GRBs occur in very dusty environments. By comparing the inferred stellar masses, and estimates of gas phase metallicity in both GRB hosts and sub-mm galaxies, I showed evidence to suggest that many GRB hosts, even at $z \sim 2$ are at lower metallicity than the sub-mm galaxy population, offering a possible explanation for the dearth of sub-mm detected GRB hosts. However, I also showed that the dark burst hosts are systematically more massive than those hosting optically bright event, and by proxy of the mass-metallicity relation, this may also suggest that they have higher metal abundances. As the fraction of bursts that show signs of heavy extinction along the line of sight may be as large as $\sim 50\%$, these results are implying that previous host samples may be severely biased by the exclusion of dark events.

As a conclusion, in this thesis I have examined the environments of gamma-ray burst host galaxies and how GRBs probe star formation, the luminosity function and metal abundances. Thus I have been able show that low redshift hosts show evidence of an apparent metallicity bias in the evolution of GRB progenitors compared to those of CCSN. However, I have also shown that evidence is accumulating that GRBs selected by optically bright afterglows do not provide a complete census of the environments that can spawn GRBs. This evidence that bursts which have their optical fluxes suppressed relative

to their X-ray fluxes (dark) often are extinguished by dust or gas in the host galaxy, suggests that there is a poorly studied population of GRB hosts that include also massive, dusty and presumably metal rich systems. Though the fraction of dark bursts is poorly constrained, this implies that the metallicity bias on GRB progenitors could be weaker than previously though, or even non-existent. Although the question of a metallicity bias may have significant impact on what fraction of star formation is traced by GRBs at low and intermediate redshifts, I have also showed that at higher redshift, where the Universal metal enrichment is still low, GRB hosts don't contradict the mass-metallicity relations of the general galaxy populations, and hosts are selected across the luminosity function. Taken together, these points suggest that a selection of GRBs not biased to only events with optically bright afterglows, may provide a more complete census of star formation than has previously been assumed.

5.2 The future of GRB host studies

To effectively be able to use GRBs as cosmic probes we first need to understand what environments they evolve in and which fundamental properties they trace. In this thesis I have attempted to do just this, although the job is still incomplete. Future work will principally investigate one of two major themes by means of their host galaxies:

How does metallicity affect the GRB rate, and how are the hosts of dark bursts related to obscured star formation in ULIRGs and sub-mm galaxies? Although I have already been able to show that at least some dark bursts trace star formation in gas and dust rich massive galaxies, a more complete

understanding of the dark population is needed. This would include building a statistically significant sample of dark bursts with accurate X-ray positioning in order to locate their hosts. Studying their long wavelength emission properties, i.e. sampling the SEDs from IR to sub-mm will be a complement to optical photometry and enable measurement of extinction curves, stellar masses and dust masses. Indeed, observation to this goal are already ongoing, or will begin in the near future through observing proposals with space observatories such as *HST*, *Spitzer* and *Chandra*, as well as ground based observatories, e.g. Gemini and the VLT. As dark bursts are optically faint and indeed often undetected, afterglow spectroscopy is of little value to obtain redshifts. As I have demonstrated, estimating photometric redshifts from the SED fitting is a useful but challenging option and gives a self consistent solution to redshift and galaxy properties simultaneously.

Hopefully dark bursts could answer our questions of how host properties are sampled by GRB selection. If the current results persist, e.g. larger and statistically significant samples also show that dark bursts are are frequent in massive and heavily obscured galaxies with high star formation rates, this could end the debate of whether there is a metallicity bias for GRB production. If this becomes the case, the collapsar model may be up for a challenge unless it can be further substantiated that GRBs progenitors can evolve in binary systems. It is however far from certain that all GRB progenitors evolve the same way. It could well be the case that a fraction of single progenitor bursts trace a low metallicity environment, whereas bursts with binary progenitors give a complete view of star formation at all metallicities. Whether this is the case or not, further studies of the local an galactic scale environments will bring light to the stellar populations and progenitors of GRBs.

The second theme assumes that we have a workable knowledge of how GRBs relate to their host galaxy environments, in order to study the formation and evolution of early galaxies without being dominated by selection effects. Most directly, the characteristics and slope of the luminosity function at high redshift can be constrained by GRB selected galaxies, preventing the difficulties of reaching the faint end that are present in magnitude limited samples. Even when the hosts themselves are too faint to detect, their locations are pinpointed by their afterglows, allowing limits to be measured where otherwise nothing would be seen. Probing the faint end of the luminosity function is one way of studying the formation and evolution of galaxies, but also their chemical evolution can be traced by their absorption of the afterglows. Going even further back in time, to when the intergalactic medium was still partly neutral, GRB afterglows will have the potential to probe the fraction of neutral hydrogen as a function of redshift. By doing this, a better understanding of how the Universe was re-ionised will be gained. Thus, observations of GRBs is an extremely useful tool for understanding how the Universe has evolved from the formation of the very first stars until present day.

Bibliography

Aldering, G., Humphreys, R. M., and Richmond, M.: 1994, *AJ* **107**, 662

Arcavi, I., Gal-Yam, A., Kasliwal, M. M., Quimby, R. M., Ofek, E. O., Kulkarni, S. R., Nugent, P. E., Cenko, S. B., Bloom, J. S., Sullivan, M., Howell, D. A., Poznanski, D., Filippenko, A. V., Law, N., Hook, I., Jönsson, J., Blake, S., Cooke, J., Dekany, R., Rahmer, G., Hale, D., Smith, R., Zolkower, J., Velur, V., Walters, R., Henning, J., Bui, K., McKenna, D., and Jacobsen, J.: 2010, *ApJ* **721**, 777

Arnaud, K. A.: 1996, in G. H. Jacoby & J. Barnes (ed.), *Astronomical Data Analysis Software and Systems V*, Vol. 101 of *Astronomical Society of the Pacific Conference Series*, pp 17–+

Asplund, M., Grevesse, N., Sauval, A. J., and Scott, P.: 2009, *Annual Rev.* **47**, 481

Band, D. L.: 1997, *ApJ* **486**, 928

Barthelmy, S. D., Cannizzo, J. K., Gehrels, N., Cusumano, G., Mangano, V., O'Brien, P. T., Vaughan, S., Zhang, B., Burrows, D. N., Campana, S., Chincarini, G., Goad, M. R., Kouveliotou, C., Kumar, P., Mészáros, P., Nousek, J. A., Osborne, J. P., Panaitescu, A., Reeves, J. N., Sakamoto, T., Tagliaferri, G., and Wijers, R. A. M. J.: 2005, *ApJ* **635**, L133

Berger, E., Cowie, L. L., Kulkarni, S. R., Frail, D. A., Aussel, H., and Barger, A. J.: 2003, *ApJ* **588**, 99

Berger, E., Fox, D. B., Kulkarni, S. R., Frail, D. A., and Djorgovski, S. G.: 2007, *ApJ* **660**, 504

Berger, E., Kulkarni, S. R., Bloom, J. S., Price, P. A., Fox, D. W., Frail, D. A., Axelrod, T. S., Chevalier, R. A., Colbert, E., Costa, E., Djorgovski, S. G., Frontera, F., Galama, T. J., Halpern, J. P., Harrison, F. A., Holtzman, J., Hurley, K., Kimble, R. A., McCarthy, P. J., Piro, L., Reichart, D., Ricker, G. R., Sari, R., Schmidt, B. P., Wheeler, J. C., Vanderppek, R., and Yost, S. A.: 2002, *ApJ* **581**, 981

Bernardi, M., Sheth, R. K., Annis, J., Burles, S., Eisenstein, D. J., Finkbeiner, D. P., Hogg, D. W., Lupton, R. H., Schlegel, D. J., SubbaRao, M., Bahcall, N. A., Blakeslee, J. P., Brinkmann, J., Castander, F. J., Connolly, A. J., Csabai, I., Doi, M., Fukugita, M., Frieman, J., Heckman, T., Hennessy, G. S., Ivezić, Ž., Knapp, G. R., Lamb, D. Q., McKay, T., Munn, J. A., Nichol, R., Okamura, S., Schneider, D. P., Thakar, A. R., and York, D. G.: 2003, *AJ* **125**, 1849

Berta, S., Fritz, J., Franceschini, A., Bressan, A., and Lonsdale, C.: 2004, *A&A* **418**, 913

Bertin, E. and Arnouts, S.: 1996, *A&A Supp.* **117**, 393

Bethe, H. A.: 1939, *Physical Review* **55**, 434

Bloom, J. S., Djorgovski, S. G., and Kulkarni, S. R.: 2001, *ApJ* **554**, 678

Bloom, J. S., Perley, D. A., Chen, H., Butler, N., Prochaska, J. X., Kocevski, D., Blake, C. H., Szentgyorgyi, A., Falco, E. E., and Starr, D. L.: 2007, *ApJ* **654**, 878

Bloom, J. S., Perley, D. A., Li, W., Butler, N. R., Miller, A. A., Kocevski, D., Kann, D. A., Foley, R. J., Chen, H. ., Filippenko, A. V., Starr, D. L., Macomber, B., Prochaska, J. X., Chornock, R., Poznanski, D., and Klose, S.: 2008, *ArXiv e-prints* 803

Bloom, J. S., Perley, D. A., Li, W., Butler, N. R., Miller, A. A., Kocevski, D., Kann, D. A., Foley, R. J., Chen, H., Filippenko, A. V., Starr, D. L., Macomber, B., Prochaska, J. X., Chornock, R., Poznanski, D., Klose, S., Skrutskie, M. F., Lopez, S., Hall, P., Glazebrook, K., and Blake, C. H.: 2009, *ApJ* **691**, 723

Bloom, J. S., Prochaska, J. X., Pooley, D., Blake, C. H., Foley, R. J., Jha, S., Ramirez-Ruiz, E., Granot, J., Filippenko, A. V., Sigurdsson, S., Barth, A. J., Chen, H., Cooper, M. C., Falco, E. E., Gal, R. R., Gerke, B. F., Gladders, M. D., Greene, J. E., Hennanwi, J., Ho, L. C., Hurley, K., Koester, B. P., Li, W., Lubin, L., Newman, J., Perley, D. A., Squires, G. K., and Wood-Vasey, W. M.: 2006, *ApJ* **638**, 354

Bolzonella, M., Miralles, J.-M., and Pelló, R.: 2000, *A&A* **363**, 476

Botticella, M. T., Trundle, C., Pastorello, A., Rodney, S., Rest, A., Gezari, S., Smartt, S. J., Narayan, G., Huber, M. E., Tonry, J. L., Young, D., Smith, K., Bresolin, F., Valenti, S., Kotak, R., Mattila, S., Kankare, E., Wood-Vasey, W. M., Riess, A., Neill, J. D., Forster, K., Martin, D. C., Stubbs, C. W., Burgett, W. S., Chambers, K. C., Dombeck, T., Flewelling, H., Grav, T., Heasley, J. N., Hodapp, K. W., Kaiser, N., Kudritzki, R., Luppino, G., Lupton, R. H., Magnier, E. A., Monet, D. G., Morgan, J. S., Onaka, P. M.,

Price, P. A., Rhoads, P. H., Siegmund, W. A., Sweeney, W. E., Wainscoat, R. J., Waters, C., Waterson, M. F., and Wynn-Williams, C. G.: 2010, *ApJ* **717**, L52

Brahe, T.: 1573, *De nova stella*

Bruzual A., G. and Charlot, S.: 1993, *ApJ* **405**, 538

Bucciantini, N., Quataert, E., Metzger, B. D., Thompson, T. A., Arons, J., and Del Zanna, L.: 2009, *MNRAS* **396**, 2038

Calura, F., Dessauges-Zavadski, M., Prochaska, J. X., and Matteucci, F.: 2009, *ApJ* **693**, 1236

Calzetti, D., Armus, L., Bohlin, R. C., Kinney, A. L., Koornneef, J., and Storchi-Bergmann, T.: 2000, *ApJ* **533**, 682

Castro Cerón, J. M., Michałowski, M. J., Hjorth, J., Malesani, D., Gorosabel, J., Watson, D., and Fynbo, J. P. U.: 2008, *ArXiv e-prints*

Castro Cerón, J. M., Michałowski, M. J., Hjorth, J., Watson, D., Fynbo, J. P. U., and Gorosabel, J.: 2006, *ApJ* **653**, L85

Castro-Tirado, A. J., Bremer, M., McBreen, S., Gorosabel, J., Guziy, S., Fakthullin, T. A., Sokolov, V. V., González Delgado, R. M., Bihain, G., Pandey, S. B., Jelínek, M., de Ugarte Postigo, A., Misra, K., Sagar, R., Bama, P., Kamble, A. P., Anupama, G. C., Licandro, J., Pérez-Ramírez, D., Bhattacharya, D., Aceituno, F. J., and Neri, R.: 2007, *A&A* **475**, 101

Cenko, S. B., Kelemen, J., Harrison, F. A., Fox, D. B., Kulkarni, S. R., Kasliwal, M. M., Ofek, E. O., Rau, A., Gal-Yam, A., Frail, D. A., and Moon, D.: 2009, *ApJ* **693**, 1484

Chapman, S. C., Blain, A. W., Smail, I., and Ivison, R. J.: 2005, *ApJ* **622**, 772

Chary, R., Berger, E., and Cowie, L.: 2007, *ApJ* **671**, 272

Chary, R., Dickinson, M. E., Teplitz, H. I., Pope, A., and Ravindranath, S.: 2005, *ApJ* **635**, 1022

Chary, R. and Elbaz, D.: 2001, *ApJ* **556**, 562

Chen, H., Perley, D. A., Wilson, C. D., Cenko, S. B., Levan, A. J., Bloom, J. S., Prochaska, J. X., Tanvir, N. R., Dessauges-Zavadsky, M., and Pettini, M.: 2010, *ArXiv e-prints*

Chen, H.-W., Prochaska, J. X., Bloom, J. S., and Thompson, I. B.: 2005, *ApJ* **634**, L25

Chevalier, R. A. and Li, Z.: 2000, *ApJ* **536**, 195

Chornock, R., Berger, E., Levesque, E. M., Soderberg, A. M., Foley, R. J., Fox, D. B., Frebel, A., Simon, J. D., Bochanski, J. J., Challis, P. J., Kirshner, R. P., Podsiadlowski, P., Roth, K., Rutledge, R. E., Schmidt, B. P., Sheppard, S. S., and Simcoe, R. A.: 2010, *ArXiv e-prints*

Christensen, L., Hjorth, J., and Gorosabel, J.: 2004, *A&A* **425**, 913

Christensen, L., Vreeswijk, P. M., Sollerman, J., Thöne, C. C., Le Floc'h, E., and Wiersema, K.: 2008, *A&A* **490**, 45

Cobb, B. E., Bailyn, C. D., van Dokkum, P. G., and Natarajan, P.: 2006, *ApJ* **651**, L85

Cole, S., Norberg, P., Baugh, C. M., Frenk, C. S., Bland-Hawthorn, J., Bridges, T., Cannon, R., Colless, M., Collins, C., Couch, W., Cross, N., Dalton, G., De Propris, R., Driver, S. P., Efstathiou, G., Ellis, R. S., Glazebrook, K., Jackson, C., Lahav, O., Lewis, I., Lumsden, S., Maddox, S., Madgwick, D., Peacock, J. A., Peterson, B. A., Sutherland, W., and Taylor, K.: 2001, *MNRAS* **326**, 255

Coleman, G. D., Wu, C.-C., and Weedman, D. W.: 1980, *ApJS* **43**, 393

Cram, L., Hopkins, A., Mobasher, B., and Rowan-Robinson, M.: 1998, *ApJ* **507**, 155

Crockett, R. M., Eldridge, J. J., Smartt, S. J., Pastorello, A., Gal-Yam, A., Fox, D. B., Leonard, D. C., Kasliwal, M. M., Mattila, S., Maund, J. R., Stephens, A. W., and Danziger, I. J.: 2008, *MNRAS* **391**, L5

Crowther, P. A.: 2007, *Annual Rev.* **45**, 177

Crowther, P. A., Dessart, L., Hillier, D. J., Abbott, J. B., and Fullerton, A. W.: 2002, *A&A* **392**, 653

Dahlen, T., Mobasher, B., Dickinson, M., Ferguson, H. C., Giavalisco, M., Kretchmer, C., and Ravindranath, S.: 2007, *ApJ* **654**, 172

Dahlen, T., Mobasher, B., Somerville, R. S., Moustakas, L. A., Dickinson, M., Ferguson, H. C., and Giavalisco, M.: 2005, *ApJ* **631**, 126

Dahlen, T., Strolger, L., and Riess, A. G.: 2008, *ApJ* **681**, 462

Dai, Z. G. and Cheng, K. S.: 2001, *ApJ* **558**, L109

Damjanov, I., McCarthy, P. J., Abraham, R. G., Glazebrook, K., Yan, H., Mentuch, E., LeBorgne, D., Savaglio, S., Crampton, D., Murowinski, R., Juneau, S., Carlberg, R. G., Jørgensen, I., Roth, K., Chen, H.-W., and Marzke, R. O.: 2009, *ApJ* **695**, 101

D'Avanzo, P., Perri, M., Fugazza, D., Salvaterra, R., Chincarini, G., Margutti, R., Wu, X. F., Thöne, C. C., Fernández-Soto, A., Ukwatta, T. N., Burrows, D. N., Gehrels, N., Meszaros, P., Toma, K., Zhang, B., Covino, S., Campana, S., D'Elia, V., Della Valle, M., and Piranomonte, S.: 2010, *A&A* **522**, A20+

Davies, M. B., Benz, W., Piran, T., and Thielemann, F. K.: 1994, *ApJ* **431**, 742

Davies, M. B., Levan, A. J., Larsson, J., King, A. R., and Fruchter, A. S.: 2007, in M. Axelsson and F. Ryde (eds.), *American Institute of Physics Conference Series*, Vol. 906 of *American Institute of Physics Conference Series*, pp 69–78

Della Valle, M., Chincarini, G., Panagia, N., Tagliaferri, G., Malesani, D., Testa, V., Fugazza, D., Campana, S., Covino, S., Mangano, V., Antonelli, L. A., D'Avanzo, P., Hurley, K., Mirabel, I. F., Pellizza, L. J., Piranomonte, S., and Stella, L.: 2006, *Nature* **444**, 1050

Dempsey, J. T., Friberg, P., Jenness, T., Bintley, D., and Holland, W. S.: 2010, in *Society of Photo-Optical Instrumentation Engineers (SPIE) Conference Series*, Vol. 7741 of *Society of Photo-Optical Instrumentation Engineers (SPIE) Conference Series*

Diehl, R., Halloin, H., Kretschmer, K., Lichti, G. G., Schönfelder, V., Strong, A. W., von Kienlin, A., Wang, W., Jean, P., Knödlseder, J., Roques, J., Weidenspointner, G., Schanne, S., Hartmann, D. H., Winkler, C., and Wunderer, C.: 2006, *Nature* **439**, 45

Djorgovski, S. G., Frail, D. A., Kulkarni, S. R., Bloom, J. S., Odewahn, S. C., and Diercks, A.: 2001, *ApJ* **562**, 654

Economou, F., Jenness, T., Chrysostomou, A., Cavanagh, B., Redman, R., and Berry, D. S.: 2008, in R. W. Argyle, P. S. Bunclark, & J. R. Lewis (ed.), *Astronomical Data Analysis Software and Systems XVII*, Vol. 394 of *Astronomical Society of the Pacific Conference Series*, pp 450–+

Elíasdóttir, Á., Fynbo, J. P. U., Hjorth, J., Ledoux, C., Watson, D. J., Andersen, A. C., Malesani, D., Vreeswijk, P. M., Prochaska, J. X., Sollerman, J., and Jaunsen, A. O.: 2009, *ApJ* **697**, 1725

Ellison, S. L., Patton, D. R., Simard, L., and McConnachie, A. W.: 2008a, *ApJ* **672**, L107

Ellison, S. L., Patton, D. R., Simard, L., and McConnachie, A. W.: 2008b, *AJ* **135**, 1877

Evans, P. A., Beardmore, A. P., Page, K. L., Osborne, J. P., O'Brien, P. T., Willingale, R., Starling, R. L. C., Burrows, D. N., Godet, O., Vetere, L.,

Racusin, J., Goad, M. R., Wiersema, K., Angelini, L., Capalbi, M., Chincarini, G., Gehrels, N., Kennea, J. A., Margutti, R., Morris, D. C., Mountford, C. J., Pagani, C., Perri, M., Romano, P., and Tanvir, N.: 2009, *MNRAS* **397**, 1177

Evans, P. A., Beardmore, A. P., Page, K. L., Tyler, L. G., Osborne, J. P., Goad, M. R., O'Brien, P. T., Vetere, L., Racusin, J., Morris, D., Burrows, D. N., Capalbi, M., Perri, M., Gehrels, N., and Romano, P.: 2007, *A&A* **469**, 379

Filippenko, A. V. and Riess, A. G.: 2000, in J. F. Nieves (ed.), *Particle Physics and Cosmology*, Vol. 540 of *American Institute of Physics Conference Series*, pp 227–246

Fishman, G. J., Meegan, C. A., Wilson, R. B., Brock, M. N., Horack, J. M., Kouveliotou, C., Howard, S., Paciesas, W. S., Briggs, M. S., Pendleton, G. N., Koshut, T. M., Mallozzi, R. S., Stollberg, M., and Lestrade, J. P.: 1994, *ApJS* **92**, 229

Fox, D. W. and Frail, D. A.: 2002, *GRB Coordinates Network* **1250**, 1

Frieman, J. A., Bassett, B., Becker, A., Choi, C., Cinabro, D., DeJongh, F., Depoy, D. L., Dilday, B., Doi, M., Garnavich, P. M., Hogan, C. J., Holtzman, J., Im, M., Jha, S., Kessler, R., Konishi, K., Lampeitl, H., Marriner, J., Marshall, J. L., McGinnis, D., Miknaitis, G., Nichol, R. C., Prieto, J. L., Riess, A. G., Richmond, M. W., Romani, R., Sako, M., Schneider, D. P., Smith, M., Takanashi, N., Tokita, K., van der Heyden, K., Yasuda, N., Zheng, C., Adelman-McCarthy, J., Annis, J., Assef, R. J., Barentine, J., Bender, R., Blandford, R. D., Boroski, W. N., Bremer, M., Brewington, H., Collins, C. A., Crotts, A., Dembicky, J., Eastman, J., Edge, A., Edmondson, E., Elson, E., Eyler, M. E., Filippenko, A. V., Foley, R. J., Frank, S., Goobar, A., Gueth, T., Gunn, J. E., Harvanek, M., Hopp, U., Ihara, Y., Ivezić, Ž., Kahn, S., Kaplan, J., Kent, S., Ketzeback, W., Kleinman, S. J., Kollatschny, W., Kron, R. G., Krzesiński, J., Lamenti, D., Leloudas, G., Lin, H., Long, D. C., Lucey, J., Lupton, R. H., Malanushenko, E., Malanushenko, V., McMillan, R. J., Mendez, J., Morgan, C. W., Morokuma, T., Nitta, A., Ostman, L., Pan, K., Rockosi, C. M., Romer, A. K., Ruiz-Lapuente, P., Saurage, G., Schlesinger, K., Snedden, S. A., Sollerman, J., Stoughton, C., Stritzinger, M., Subba Rao, M., Tucker, D., Vaisanen, P., Watson, L. C., Watters, S., Wheeler, J. C., Yanny, B., and York, D.: 2008, *AJ* **135**, 338

Fruchter, A., Krolik, J. H., and Rhoads, J. E.: 2001, *ApJ* **563**, 597

Fruchter, A. S., Levan, A. J., Strolger, L., Vreeswijk, P. M., Thorsett, S. E., Bersier, D., Burud, I., Castro Cerón, J. M., Castro-Tirado, A. J., Conselice, C., Dahlen, T., Ferguson, H. C., Fynbo, J. P. U., Garnavich, P. M., Gibbons,

R. A., Gorosabel, J., Gull, T. R., Hjorth, J., Holland, S. T., Kouveliotou, C., Levay, Z., Livio, M., Metzger, M. R., Nugent, P. E., Petro, L., Pian, E., Rhoads, J. E., Riess, A. G., Sahu, K. C., Smette, A., Tanvir, N. R., Wijers, R. A. M. J., and Woosley, S. E.: 2006, *Nature* **441**, 463

Fryer, C. L.: 1999, *ApJ* **522**, 413

Fryer, C. L.: 2006, *NewAR* **50**, 492

Fugazza, D., D'Elia, V., D'Avanzo, P., Covino, S., and Tagliaferri, G.: 2008, *GRB Coordinates Network* **7293**, 1

Fynbo, J. P. U., Jakobsson, P., Prochaska, J. X., Malesani, D., Ledoux, C., de Ugarte Postigo, A., Nardini, M., Vreeswijk, P. M., Wiersema, K., Hjorth, J., Sollerman, J., Chen, H., Thöne, C. C., Björnsson, G., Bloom, J. S., Castro-Tirado, A. J., Christensen, L., De Cia, A., Fruchter, A. S., Gorosabel, J., Graham, J. F., Jaunsen, A. O., Jensen, B. L., Kann, D. A., Kouveliotou, C., Levan, A. J., Maund, J., Masetti, N., Milvang-Jensen, B., Palazzi, E., Perley, D. A., Pian, E., Rol, E., Schady, P., Starling, R. L. C., Tanvir, N. R., Watson, D. J., Xu, D., Augusteijn, T., Grundahl, F., Telting, J., and Quirion, P.: 2009, *ApJS* **185**, 526

Fynbo, J. P. U., Watson, D., Thöne, C. C., Sollerman, J., Bloom, J. S., Davis, T. M., Hjorth, J., Jakobsson, P., Jørgensen, U. G., Graham, J. F., Fruchter, A. S., Bersier, D., Kewley, L., Cassan, A., Castro Cerón, J. M., Foley, S., Gorosabel, J., Hinse, T. C., Horne, K. D., Jensen, B. L., Klose, S., Kocevski, D., Marquette, J.-B., Perley, D., Ramirez-Ruiz, E., Stritzinger, M. D., Vreeswijk, P. M., Wijers, R. A. M., Woller, K. G., Xu, D., and Zub, M.: 2006, *Nature* **444**, 1047

Fynbo, J. U., Jensen, B. L., Gorosabel, J., Hjorth, J., Pedersen, H., Møller, P., Abbott, T., Castro-Tirado, A. J., Delgado, D., Greiner, J., Henden, A., Magazzù, A., Masetti, N., Merlino, S., Masegosa, J., Østensen, R., Palazzi, E., Pian, E., Schwarz, H. E., Cline, T., Guidorzi, C., Goldsten, J., Hurley, K., Mazets, E., McClanahan, T., Montanari, E., Starr, R., and Trombka, J.: 2001, *A&A* **369**, 373

Gal-Yam, A., Fox, D. B., Price, P. A., Ofek, E. O., Davis, M. R., Leonard, D. C., Soderberg, A. M., Schmidt, B. P., Lewis, K. M., Peterson, B. A., Kulkarni, S. R., Berger, E., Cenko, S. B., Sari, R., Sharon, K., Frail, D., Moon, D., Brown, P. J., Cucchiara, A., Harrison, F., Piran, T., Persson, S. E., McCarthy, P. J., Penprase, B. E., Chevalier, R. A., and MacFadyen, A. I.: 2006, *Nature* **444**, 1053

Galama, T. J., Vreeswijk, P. M., van Paradijs, J., Kouveliotou, C., Augusteijn, T., Böhnhardt, H., Brewer, J. P., Doublier, V., Gonzalez, J., Leibundgut, B., Lidman, C., Hainaut, O. R., Patat, F., Heise, J., in't Zand, J., Hurley,

K., Groot, P. J., Strom, R. G., Mazzali, P. A., Iwamoto, K., Nomoto, K., Umeda, H., Nakamura, T., Young, T. R., Suzuki, T., Shigeyama, T., Koshut, T., Kippen, M., Robinson, C., de Wildt, P., Wijers, R. A. M. J., Tanvir, N., Greiner, J., Pian, E., Palazzi, E., Frontera, F., Masetti, N., Nicastro, L., Feroci, M., Costa, E., Piro, L., Peterson, B. A., Tinney, C., Boyle, B., Cannon, R., Stathakis, R., Sadler, E., Begam, M. C., and Ianna, P.: 1998a, *Nature* **395**, 670

Galama, T. J., Wijers, R. A. M. J., Bremer, M., Groot, P. J., Strom, R. G., Kouveliotou, C., and van Paradijs, J.: 1998b, *ApJ* **500**, L97+

Garnett, D. R., Shields, G. A., Skillman, E. D., Sagan, S. P., and Dufour, R. J.: 1997, *ApJ* **489**, 63

Gehrels, N., Norris, J. P., Barthelmy, S. D., Granot, J., Kaneko, Y., Kouveliotou, C., Markwardt, C. B., Mészáros, P., Nakar, E., Nousek, J. A., O'Brien, P. T., Page, M., Palmer, D. M., Parsons, A. M., Roming, P. W. A., Sakamoto, T., Sarazin, C. L., Schady, P., Stamatikos, M., and Woosley, S. E.: 2006, *Nature* **444**, 1044

Georgy, C., Meynet, G., Walder, R., Folini, D., and Maeder, A.: 2009, *A&A* **502**, 611

Giacconi, R., Gursky, H., Paolini, F. R., and Rossi, B. B.: 1962, *Physical Review Letters* **9**, 439

Giavalisco, M., Ferguson, H. C., Koekemoer, A. M., Dickinson, M., Alexander, D. M., Bauer, F. E., Bergeron, J., Biagetti, C., Brandt, W. N., Casertano, S., Cesarsky, C., Chatzichristou, E., Conselice, C., Cristiani, S., Da Costa, L., Dahlen, T., de Mello, D., Eisenhardt, P., Erben, T., Fall, S. M., Fassnacht, C., Fosbury, R., Fruchter, A., Gardner, J. P., Grogin, N., Hook, R. N., Hornschemeier, A. E., Idzi, R., Jogee, S., Kretchmer, C., Laidler, V., Lee, K. S., Livio, M., Lucas, R., Madau, P., Mobasher, B., Moustakas, L. A., Nonino, M., Padovani, P., Papovich, C., Park, Y., Ravindranath, S., Renzini, A., Richardson, M., Riess, A., Rosati, P., Schirmer, M., Schreier, E., Somerville, R. S., Spinrad, H., Stern, D., Stiavelli, M., Strolger, L., Urry, C. M., Vandame, B., Williams, R., and Wolf, C.: 2004, *ApJ* **600**, L93

Glazebrook, K., Abraham, R. G., McCarthy, P. J., Savaglio, S., Chen, H., Crampton, D., Murowinski, R., Jørgensen, I., Roth, K., Hook, I., Marzke, R. O., and Carlberg, R. G.: 2004, *Nature* **430**, 181

Gorosabel, J., Christensen, L., Hjorth, J., Fynbo, J. U., Pedersen, H., Jensen, B. L., Andersen, M. I., Lund, N., Jaunsen, A. O., Castro Cerón, J. M., Castro-Tirado, A. J., Fruchter, A., Greiner, J., Pian, E., Vreeswijk, P. M., Burud, I., Frontera, F., Kaper, L., Klose, S., Kouveliotou, C., Masetti,

N., Palazzi, E., Rhoads, J., Rol, E., Salamanca, I., Tanvir, N., Wijers, R. A. M. J., and van den Heuvel, E.: 2003a, *A&A* **400**, 127

Gorosabel, J., Klose, S., Christensen, L., Fynbo, J. P. U., Hjorth, J., Greiner, J., Tanvir, N., Jensen, B. L., Pedersen, H., Holland, S. T., Lund, N., Jaunsen, A. O., Castro Cerón, J. M., Castro-Tirado, A. J., Fruchter, A., Pian, E., Vreeswijk, P. M., Burud, I., Frontera, F., Kaper, L., Kouveliotou, C., Masetti, N., Palazzi, E., Rhoads, J., Rol, E., Salamanca, I., Wijers, R. A. M. J., and van den Heuvel, E.: 2003b, *A&A* **409**, 123

Grazian, A., Fontana, A., de Santis, C., Nonino, M., Salimbeni, S., Giallongo, E., Cristiani, S., Gallozzi, S., and Vanzella, E.: 2006, *A&A* **449**, 951

Greiner, J., Krühler, T., Fynbo, J. P. U., Rossi, A., Schwarz, R., Klose, S., Savaglio, S., Tanvir, N. R., McBreen, S., Totani, T., Zhang, B. B., Wu, X. F., Watson, D., Barthelmy, S. D., Beardmore, A. P., Ferrero, P., Gehrels, N., Kann, D. A., Kawai, N., Yoldaş, A. K., Mészáros, P., Milvang-Jensen, B., Oates, S. R., Pierini, D., Schady, P., Toma, K., Vreeswijk, P. M., Yoldaş, A., Zhang, B., Afonso, P., Aoki, K., Burrows, D. N., Clemens, C., Filgas, R., Haiman, Z., Hartmann, D. H., Hasinger, G., Hjorth, J., Jehin, E., Levan, A. J., Liang, E. W., Malesani, D., Pyo, T., Schulze, S., Szokoly, G., Terada, K., and Wiersema, K.: 2009, *ApJ* **693**, 1610

Groot, P. J., Galama, T. J., van Paradijs, J., Kouveliotou, C., Wijers, R. A. M. J., Bloom, J., Tanvir, N., Vanderspek, R., Greiner, J., Castro-Tirado, A. J., Gorosabel, J., von Hippel, T., Lehnert, M., Kuijken, K., Hoekstra, H., Metcalfe, N., Howk, C., Conselice, C., Telting, J., Rutten, R. G. M., Rhoads, J., Cole, A., Pisano, D. J., Naber, R., and Schwarz, R.: 1998, *ApJ* **493**, L27+

Grupe, D., Nousek, J. A., vanden Berk, D. E., Roming, P. W. A., Burrows, D. N., Godet, O., Osborne, J., and Gehrels, N.: 2007, *AJ* **133**, 2216

Habergham, S. M., Anderson, J. P., and James, P. A.: 2010, *ArXiv e-prints (1005.0511)*

Haislip, J. B., Nysewander, M. C., Reichart, D. E., Levan, A., Tanvir, N., Cenko, S. B., Fox, D. B., Price, P. A., Castro-Tirado, A. J., Gorosabel, J., Evans, C. R., Figueredo, E., MacLeod, C. L., Kirschbrown, J. R., Jelinek, M., Guziy, S., Postigo, A. D. U., Cypriano, E. S., Lacluyze, A., Graham, J., Priddey, R., Chapman, R., Rhoads, J., Fruchter, A. S., Lamb, D. Q., Kouveliotou, C., Wijers, R. A. M. J., Bayliss, M. B., Schmidt, B. P., Soderberg, A. M., Kulkarni, S. R., Harrison, F. A., Moon, D. S., Gal-Yam, A., Kasliwal, M. M., Hudec, R., Vitek, S., Kubanek, P., Crain, J. A., Foster, A. C., Clemens, J. C., Bartelme, J. W., Canterna, R., Hartmann, D. H., Henden, A. A., Klose, S., Park, H., Williams, G. G., Rol, E., O'Brien, P.,

Bersier, D., Prada, F., Pizarro, S., Maturana, D., Ugarte, P., Alvarez, A., Fernandez, A. J. M., Jarvis, M. J., Moles, M., Alfaro, E., Ivarsen, K. M., Kumar, N. D., Mack, C. E., Zdarowicz, C. M., Gehrels, N., Barthelmy, S., and Burrows, D. N.: 2006, *Nature* **440**, 181

Han, X. H., Hammer, F., Liang, Y. C., Flores, H., Rodrigues, M., Hou, J. L., and Wei, J. Y.: 2010, *A&A* **514**, A24+

Hashimoto, T., Ohta, K., Aoki, K., Tanaka, I., Yabe, K., Kawai, N., Aoki, W., Furusawa, H., Hattori, T., Iye, M., Kawabata, K. S., Kobayashi, N., Komiyama, Y., Kosugi, G., Minowa, Y., Mizumoto, Y., Niino, Y., Nomoto, K., Noumaru, J., Ogasawara, R., Pyo, T., Sakamoto, T., Sekiguchi, K., Shirasaki, Y., Suzuki, M., Tajitsu, A., Takata, T., Tamagawa, T., Terada, H., Totani, T., Watanabe, J., Yamada, T., and Yoshida, A.: 2010, *ArXiv e-prints (1003.3717)*

Heger, A., Fryer, C. L., Woosley, S. E., Langer, N., and Hartmann, D. H.: 2003, *ApJ* **591**, 288

Heger, A., Langer, N., and Woosley, S. E.: 2000, *ApJ* **528**, 368

Hjorth, J., Møller, P., Gorosabel, J., Fynbo, J. P. U., Toft, S., Jaunsen, A. O., Kaas, A. A., Pursimo, T., Torii, K., Kato, T., Yamaoka, H., Yoshida, A., Thomsen, B., Andersen, M. I., Burud, I., Castro Cerón, J. M., Castro-Tirado, A. J., Fruchter, A. S., Kaper, L., Kouveliotou, C., Masetti, N., Palazzi, E., Pedersen, H., Pian, E., Rhoads, J., Rol, E., Tanvir, N. R., Vreeswijk, P. M., Wijers, R. A. M. J., and van den Heuvel, E. P. J.: 2003a, *ApJ* **597**, 699

Hjorth, J., Sollerman, J., Møller, P., Fynbo, J. P. U., Woosley, S. E., Kouveliotou, C., Tanvir, N. R., Greiner, J., Andersen, M. I., Castro-Tirado, A. J., Castro Cerón, J. M., Fruchter, A. S., Gorosabel, J., Jakobsson, P., Kaper, L., Klose, S., Masetti, N., Pedersen, H., Pedersen, K., Pian, E., Palazzi, E., Rhoads, J. E., Rol, E., van den Heuvel, E. P. J., Vreeswijk, P. M., Watson, D., and Wijers, R. A. M. J.: 2003b, *Nature* **423**, 847

Hogg, D. W. and Fruchter, A. S.: 1999, *ApJ* **520**, 54

Hogg, D. W., Pahre, M. A., McCarthy, J. K., Cohen, J. G., Blandford, R., Smail, I., and Soifer, B. T.: 1997, *MNRAS* **288**, 404

Holland, S. T., Sbarufatti, B., Shen, R., Schady, P., Cummings, J. R., Fonseca, E., Fynbo, J. P. U., Jakobsson, P., Leitet, E., Linné, S., Roming, P. W. A., Still, M., and Zhang, B.: 2010, *ApJ* **717**, 223

Holland, W., MacIntosh, M., Fairley, A., Kelly, D., Montgomery, D., Gostick, D., Atad-Ettedgui, E., Ellis, M., Robson, I., Hollister, M., Woodcraft, A., Ade, P., Walker, I., Irwin, K., Hilton, G., Duncan, W., Reintsema, C.,

Walton, A., Parkes, W., Dunare, C., Fich, M., Kycia, J., Halpern, M., Scott, D., Gibb, A., Molnar, J., Chapin, E., Bintley, D., Craig, S., Chylek, T., Jenness, T., Economou, F., and Davis, G.: 2006, in *Society of Photo-Optical Instrumentation Engineers (SPIE) Conference Series*, Vol. 6275 of *Society of Photo-Optical Instrumentation Engineers (SPIE) Conference Series*

Hoopes, C. G., Heckman, T. M., Salim, S., Seibert, M., Tremonti, C. A., Schiminovich, D., Rich, R. M., Martin, D. C., Charlot, S., Kauffmann, G., Forster, K., Friedman, P. G., Morrissey, P., Neff, S. G., Small, T., Wyder, T. K., Bianchi, L., Donas, J., Lee, Y.-W., Madore, B. F., Milliard, B., Szalay, A. S., Welsh, B. Y., and Yi, S. K.: 2007, *ApJS* **173**, 441

Hopkins, A. M.: 2004, *ApJ* **615**, 209

Hopkins, A. M. and Beacom, J. F.: 2006, *ApJ* **651**, 142

Hubble, E. and Humason, M. L.: 1931, *ApJ* **74**, 43

Hunter, I., Dufton, P. L., Smartt, S. J., Ryans, R. S. I., Evans, C. J., Lennon, D. J., Trundle, C., Hubeny, I., and Lanz, T.: 2007, *A&A* **466**, 277

Jabran Zahid, H., Kewley, L. J., and Bresolin, F.: 2010, *ArXiv e-prints*

Jakobsson, P., Björnsson, G., Fynbo, J. P. U., Jóhannesson, G., Hjorth, J., Thomsen, B., Møller, P., Watson, D., Jensen, B. L., Östlin, G., Gorosabel, J., and Gudmundsson, E. H.: 2005, *MNRAS* **362**, 245

Jakobsson, P., Hjorth, J., Fynbo, J. P. U., Watson, D., Pedersen, K., Björnsson, G., and Gorosabel, J.: 2004, *ApJ* **617**, L21

Jakobsson, P., Levan, A., Fynbo, J. P. U., Priddey, R., Hjorth, J., Tanvir, N., Watson, D., Jensen, B. L., Sollerman, J., Natarajan, P., Gorosabel, J., Castro Cerón, J. M., Pedersen, K., Pursimo, T., Árnadóttir, A. S., Castro-Tirado, A. J., Davis, C. J., Deeg, H. J., Fiuza, D. A., Mykolaitis, S., and Sousa, S. G.: 2006, *A&A* **447**, 897

James, P. A. and Anderson, J. P.: 2006, *A&A* **453**, 57

Janka, H.-T., Langanke, K., Marek, A., Martínez-Pinedo, G., and Müller, B.: 2007, *physrep* **442**, 38

Jaunsen, A. O., Rol, E., Watson, D. J., Malesani, D., Fynbo, J. P. U., Milvang-Jensen, B., Hjorth, J., Vreeswijk, P. M., Ovaldsen, J., Wiersema, K., Tanvir, N. R., Gorosabel, J., Levan, A. J., Schirmer, M., and Castro-Tirado, A. J.: 2008, *ApJ* **681**, 453

Jenness, T., Berry, D., Chapin, E., Economou, F., Gibb, A., and Scott, D.: 2010, *ArXiv e-prints*

Jóhannesson, G., Björnsson, G., and Gudmundsson, E. H.: 2006, *ApJ* **647**, 1238

Kaiser, N., Aussel, H., Burke, B. E., Boesgaard, H., Chambers, K., Chun, M. R., Heasley, J. N., Hodapp, K., Hunt, B., Jedicke, R., Jewitt, D., Kudritzki, R., Luppino, G. A., Maberry, M., Magnier, E., Monet, D. G., Onaka, P. M., Pickles, A. J., Rhoads, P. H. H., Simon, T., Szalay, A., Szapudi, I., Tholen, D. J., Tonry, J. L., Waterson, M., and Wick, J.: 2002, in J. A. Tyson & S. Wolff (ed.), *Society of Photo-Optical Instrumentation Engineers (SPIE) Conference Series*, Vol. 4836 of *Presented at the Society of Photo-Optical Instrumentation Engineers (SPIE) Conference*, pp 154–164

Kawai, N., Kosugi, G., Aoki, K., Yamada, T., Totani, T., Ohta, K., Iye, M., Hattori, T., Aoki, W., Furusawa, H., Hurley, K., Kawabata, K. S., Kobayashi, N., Komiyama, Y., Mizumoto, Y., Nomoto, K., Noumaru, J., Ogasawara, R., Sato, R., Sekiguchi, K., Shirasaki, Y., Suzuki, M., Takata, T., Tamagawa, T., Terada, H., Watanabe, J., Yatsu, Y., and Yoshida, A.: 2006, *Nature* **440**, 184

Kelly, P. L., Kirshner, R. P., and Pahre, M.: 2007, *ArXiv e-prints* 712

Kelly, P. L., Kirshner, R. P., and Pahre, M.: 2008, *ApJ* **687**, 1201

Kennicutt, Jr., R. C.: 1998, *Annual Rev.* **36**, 189

Kistler, M. D., Yüksel, H., Beacom, J. F., Hopkins, A. M., and Wyithe, J. S. B.: 2009, *ApJ* **705**, L104

Klebesadel, R. W., Strong, I. B., and Olson, R. A.: 1973, *ApJ* **182**, L85+

Kluźniak, W. and Ruderman, M.: 1998, *ApJ* **505**, L113

Kocevski, D. and West, A. A.: 2010, *ArXiv e-prints*

Kouveliotou, C., Meegan, C. A., Fishman, G. J., Bhat, N. P., Briggs, M. S., Koshut, T. M., Paciesas, W. S., and Pendleton, G. N.: 1993, *ApJ* **413**, L101

Kudritzki, R. and Puls, J.: 2000, *Annual Rev.* **38**, 613

Kuepcue Yoldas, A., Yoldas, A., Greiner, J., Kruehler, T., Klose, S., and Szokoly, G.: 2008, *GRB Coordinates Network* **7279**, 1

Küpcü Yoldaş, A., Greiner, J., Klose, S., Krühler, T., and Savaglio, S.: 2010, *ArXiv e-prints (1005.1257)*

Langer, N., El Eid, M. F., and Baraffe, I.: 1989, *A&A* **224**, L17

Larson, R. B.: 1974, *MNRAS* **169**, 229

Larsson, J., Levan, A. J., Davies, M. B., and Fruchter, A. S.: 2007, *MNRAS* **376**, 1285

Law, N. M., Kulkarni, S. R., Dekany, R. G., Ofek, E. O., Quimby, R. M., Nugent, P. E., Surace, J., Grillmair, C. C., Bloom, J. S., Kasliwal, M. M., Bildsten, L., Brown, T., Cenko, S. B., Ciardi, D., Croner, E., Djorgovski, S. G., van Eyken, J., Filippenko, A. V., Fox, D. B., Gal-Yam, A., Hale, D., Hamam, N., Helou, G., Henning, J., Howell, D. A., Jacobsen, J., Laher, R., Mattingly, S., McKenna, D., Pickles, A., Poznanski, D., Rahmer, G., Rau, A., Rosing, W., Shara, M., Smith, R., Starr, D., Sullivan, M., Velur, V., Walters, R., and Zolkower, J.: 2009, *PAS-pacific* **121**, 1395

Lazzati, D., Covino, S., and Ghisellini, G.: 2002, *MNRAS* **330**, 583

Le Floc'h, E., Charmandaris, V., Forrest, W. J., Mirabel, I. F., Armus, L., and Devost, D.: 2006, *ApJ* **642**, 636

Le Floc'h, E., Duc, P., Mirabel, I. F., Sanders, D. B., Bosch, G., Diaz, R. J., Donzelli, C. J., Rodrigues, I., Courvoisier, T., Greiner, J., Mereghetti, S., Melnick, J., Maza, J., and Minniti, D.: 2003, *A&A* **400**, 499

Leitherer, C. and Heckman, T. M.: 1995, *ApJS* **96**, 9

Lequeux, J., Peimbert, M., Rayo, J. F., Serrano, A., and Torres-Peimbert, S.: 1979, *A&A* **80**, 155

Levan, A., Fruchter, A., Rhoads, J., Mobasher, B., Tanvir, N., Gorosabel, J., Rol, E., Kouveliotou, C., Dell'Antonio, I., Merrill, M., Bergeron, E., Castro Cerón, J. M., Masetti, N., Vreeswijk, P., Antonelli, A., Bersier, D., Castro-Tirado, A., Fynbo, J., Garnavich, P., Holland, S., Hjorth, J., Nugent, P., Pian, E., Smette, A., Thomsen, B., Thorsett, S. E., and Wijers, R.: 2006a, *ApJ* **647**, 471

Levan, A. J., Davies, M. B., and King, A. R.: 2006b, *MNRAS* **372**, 1351

Levesque, E. M., Berger, E., Kewley, L. J., and Bagley, M. M.: 2009, *ArXiv e-prints*

Levesque, E. M., Kewley, L. J., Berger, E., and Jabran Zahid, H.: 2010a, *AJ* **140**, 1557

Levesque, E. M., Kewley, L. J., Berger, E., and Jabran Zahid, H.: 2010b, *ArXiv e-prints*

Levesque, E. M., Kewley, L. J., Graham, J. F., and Fruchter, A. S.: 2010c, *ApJ* **712**, L26

Levesque, E. M., Kewley, L. J., Larson, K., and Snijders, L.: 2008, in L. K. Hunt, S. Madden, & R. Schneider (ed.), *IAU Symposium*, Vol. 255 of *IAU Symposium*, pp 162–166

Li, W., Van Dyk, S. D., Filippenko, A. V., Cuillandre, J., Jha, S., Bloom, J. S., Riess, A. G., and Livio, M.: 2006, *ApJ* **641**, 1060

MacFadyen, A. I. and Woosley, S. E.: 1999, *ApJ* **524**, 262

Madau, P., della Valle, M., and Panagia, N.: 1998a, *MNRAS* **297**, L17+

Madau, P., Pozzetti, L., and Dickinson, M.: 1998b, *ApJ* **498**, 106

Maeder, A.: 1987, *A&A* **178**, 159

Maiolino, R., Nagao, T., Grazian, A., Cocchia, F., Marconi, A., Mannucci, F., Cimatti, A., Pipino, A., Ballero, S., Calura, F., Chiappini, C., Fontana, A., Granato, G. L., Matteucci, F., Pastorini, G., Pentericci, L., Risaliti, G., Salvati, M., and Silva, L.: 2008, *A&A* **488**, 463

Malesani, D., Tagliaferri, G., Chincarini, G., Covino, S., Della Valle, M., Fugazza, D., Mazzali, P. A., Zerbi, F. M., D'Avanzo, P., Kalogerakos, S., Simoncelli, A., Antonelli, L. A., Burderi, L., Campana, S., Cucchiara, A., Fiore, F., Ghirlanda, G., Goldoni, P., Götz, D., Mereghetti, S., Mirabel, I. F., Romano, P., Stella, L., Minezaki, T., Yoshii, Y., and Nomoto, K.: 2004, *ApJ* **609**, L5

Mannucci, F., Cresci, G., Maiolino, R., Marconi, A., and Gnerucci, A.: 2010a, *MNRAS* **408**, 2115

Mannucci, F., Maiolino, R., Cresci, G., Della Valle, M., Vanzi, L., Ghinassi, F., Ivanov, V. D., Nagar, N. M., and Alonso-Herrero, A.: 2003, *A&A* **401**, 519

Mannucci, F., Salvaterra, R., and Campisi, M. A.: 2010b, *ArXiv e-prints*

Markova, N., Puls, J., Repolust, T., and Markov, H.: 2004, *A&A* **413**, 693

Masetti, N., Palazzi, E., Pian, E., Hunt, L. K., Méndez, M., Frontera, F., Amati, L., Vreeswijk, P. M., Rol, E., Galama, T. J., van Paradijs, J., Antonelli, L. A., Nicastro, L., Feroci, M., Marconi, G., Piro, L., Costa, E., Kouveliotou, C., Castro-Tirado, A. J., Falomo, R., Augusteijn, T., Böhnhardt, H., Lidman, C., Vanzi, L., Merrill, K. M., Kaminsky, C. D., van der Klis, M., Heemskerk, M. H. M., van der Hooft, F., Kuulkers, E., Pedersen, H., and Benetti, S.: 2000, *A&A* **354**, 473

Mattila, S., Smartt, S. J., Eldridge, J. J., Maund, J. R., Crockett, R. M., and Danziger, I. J.: 2008, *ApJ* **688**, L91

Maund, J. R. and Smartt, S. J.: 2009, *Science* **324**, 486

Maund, J. R., Smartt, S. J., Kudritzki, R. P., Podsiadlowski, P., and Gilmore, G. F.: 2004, *Nature* **427**, 129

McBreen, S., Foley, S., Watson, D., Hanlon, L., Malesani, D., Fynbo, J. P. U., Kann, D. A., Gehrels, N., McGlynn, S., and Palmer, D.: 2008, *ApJ* **677**, L85

McQuinn, M., Lidz, A., Zaldarriaga, M., Hernquist, L., and Dutta, S.: 2008, *MNRAS* **388**, 1101

Meegan, C. A., Fishman, G. J., Wilson, R. B., Horack, J. M., Brock, M. N., Paciesas, W. S., Pendleton, G. N., and Kouveliotou, C.: 1992, *Nature* **355**, 143

Meegan, C. A., Paciesas, W. S., Pendleton, G. N., Briggs, M. S., Kouveliotou, C., Koshut, T. M., Lestrade, J. P., McCollough, M. L., Brainerd, J. J., Hakkila, J., Henze, W., Preece, R. D., Connaughton, V., Kippen, R. M., Mallozzi, R. S., and Fishman, G. J.: 1998, in C. A. Meegan, R. D. Preece, & T. M. Koshut (ed.), *Gamma-Ray Bursts, 4th Hunstville Symposium*, Vol. 428 of *American Institute of Physics Conference Series*, pp 3–9

Melandri, A., Mundell, C. G., Kobayashi, S., Guidorzi, C., Gomboc, A., Steele, I. A., Smith, R. J., Bersier, D., Mottram, C. J., Carter, D., Bode, M. F., O'Brien, P. T., Tanvir, N. R., Rol, E., and Chapman, R.: 2008, *ApJ* **686**, 1209

Michałowski, M., Hjorth, J., and Watson, D.: 2010a, *A&A* **514**, A67+

Michałowski, M. J., Hjorth, J., Castro Cerón, J. M., and Watson, D.: 2008, *ApJ* **672**, 817

Michałowski, M. J., Watson, D., and Hjorth, J.: 2010b, *ApJ* **712**, 942

Minkowski, R.: 1941, *PAS-pacific* **53**, 224

Modjaz, M., Kewley, L., Kirshner, R. P., Stanek, K. Z., Challis, P., Garnavich, P. M., Greene, J. E., Kelly, P. L., and Prieto, J. L.: 2008, *AJ* **135**, 1136

Morsony, B. J., Lazzati, D., and Begelman, M. C.: 2010, *ApJ* **723**, 267

Niino, Y., Choi, J., Kobayashi, M. A. R., Nagamine, K., Totani, T., and Zhang, B.: 2010, *ArXiv e-prints*

Nousek, J. A., Kouveliotou, C., Grupe, D., Page, K. L., Granot, J., Ramirez-Ruiz, E., Patel, S. K., Burrows, D. N., Mangano, V., Barthelmy, S., Beardmore, A. P., Campana, S., Capalbi, M., Chincarini, G., Cusumano, G., Falcone, A. D., Gehrels, N., Giommi, P., Goad, M. R., Godet, O., Hurkett, C. P., Kennea, J. A., Moretti, A., O'Brien, P. T., Osborne, J. P., Romano, P., Tagliaferri, G., and Wells, A. A.: 2006, *ApJ* **642**, 389

Östlin, G., Zackrisson, E., Sollerman, J., Mattila, S., and Hayes, M.: 2008, *MNRAS* **387**, 1227

Paczynski, B.: 1998, *ApJ* **494**, L45+

Pagel, B. E. J., Edmunds, M. G., Blackwell, D. E., Chun, M. S., and Smith, G.: 1979, *MNRAS* **189**, 95

Panaitescu, A. and Kumar, P.: 2002, *ApJ* **571**, 779

Paxton, B., Bildsten, L., Dotter, A., Herwig, F., Lesaffre, P., and Timmes, F.: 2010, *ArXiv e-prints*

Pei, Y. C. and Fall, S. M.: 1995, *ApJ* **454**, 69

Perley, D. A., Bloom, J. S., Klein, C. R., Covino, S., Minezaki, T., Woźniak, P., Vestrand, W. T., Williams, G. G., Milne, P., Butler, N. R., Updike, A. C., Krühler, T., Afonso, P., Antonelli, A., Cowie, L., Ferrero, P., Greiner, J., Hartmann, D. H., Kakazu, Y., Küpcü Yoldaş, A., Morgan, A. N., Price, P. A., Prochaska, J. X., and Yoshii, Y.: 2010a, *MNRAS* **406**, 2473

Perley, D. A., Cenko, S. B., Bloom, J. S., Chen, H. ., Butler, N. R., Kocevski, D., Prochaska, J. X., Brodwin, M., Glazebrook, K., Kasliwal, M. M., Kulkarni, S. R., Lopez, S., Ofek, E. O., Pettini, M., Soderberg, A. M., and Starr, D.: 2009a, *ArXiv e-prints*

Perley, D. A., Cenko, S. B., Bloom, J. S., Chen, H., Butler, N. R., Kocevski, D., Prochaska, J. X., Brodwin, M., Glazebrook, K., Kasliwal, M. M., Kulkarni, S. R., Lopez, S., Ofek, E. O., Pettini, M., Soderberg, A. M., and Starr, D.: 2009b, *AJ* **138**, 1690

Perley, D. A., Morgan, A. N., Updike, A., Yuan, F., Akerlof, C. W., Miller, A. A., Bloom, J. S., Cenko, S. B., Li, W., Filippenko, A. V., Prochaska, J. X., Kann, D. A., Butler, N. R., Christian, P., Hartmann, D. H., Milne, P., Rykoff, E. S., Rujopakarn, W., Wheeler, J. C., and Williams, G. G.: 2010b, *ArXiv e-prints*

Podsiadlowski, P., Mazzali, P. A., Nomoto, K., Lazzati, D., and Cappellaro, E.: 2004, *ApJ* **607**, L17

Prantzos, N. and Boissier, S.: 2003, *A&A* **406**, 259

Prevot, M. L., Lequeux, J., Prevot, L., Maurice, E., and Rocca-Volmerange, B.: 1984, *A&A* **132**, 389

Prialnik, D.: 2000, *An Introduction to the Theory of Stellar Structure and Evolution*

Price, P. A. and Schmidt, B. P.: 2004, in E. Fenimore & M. Galassi (ed.), *Gamma-Ray Bursts: 30 Years of Discovery*, Vol. 727 of *American Institute of Physics Conference Series*, pp 503–507

Prieto, J. L., Stanek, K. Z., and Beacom, J. F.: 2007, *ArXiv e-prints* 707

Prochaska, J. X., Bloom, J. S., Chen, H., Hurley, K. C., Melbourne, J., Dressler, A., Graham, J. R., Osip, D. J., and Vacca, W. D.: 2004, *ApJ* **611**, 200

Prochaska, J. X., Chen, H., Dessauges-Zavadsky, M., and Bloom, J. S.: 2007, *ApJ* **666**, 267

Racusin, J. L.: 2008, *GRB Coordinates Network* **7266**, 1

Racusin, J. L., Karpov, S. V., Sokolowski, M., Granot, J., Wu, X. F., Pal'Shin, V., Covino, S., van der Horst, A. J., Oates, S. R., Schady, P., Smith, R. J., Cummings, J., Starling, R. L. C., Piotrowski, L. W., Zhang, B., Evans, P. A., Holland, S. T., Malek, K., Page, M. T., Vetere, L., Margutti, R., Guidorzi, C., Kamble, A. P., Curran, P. A., Beardmore, A., Kouveliotou, C., Mankiewicz, L., Melandri, A., O'Brien, P. T., Page, K. L., Piran, T., Tanvir, N. R., Wrochna, G., Aptekar, R. L., Barthelmy, S., Bartolini, C., Beskin, G. M., Bondar, S., Bremer, M., Campana, S., Castro-Tirado, A., Cucchiara, A., Cwiok, M., D'Avanzo, P., D'Elia, V., Valle, M. D., de Ugarte Postigo, A., Dominik, W., Falcone, A., Fiore, F., Fox, D. B., Frederiks, D. D., Fruchter, A. S., Fugazza, D., Garrett, M. A., Gehrels, N., Golenetskii, S., Gomboc, A., Gorosabel, J., Greco, G., Guarnieri, A., Immler, S., Jelinek, M., Kasprowicz, G., La Parola, V., Levan, A. J., Mangano, V., Mazets, E. P., Molinari, E., Moretti, A., Nawrocki, K., Oleynik, P. P., Osborne, J. P., Pagani, C., Pandey, S. B., Paragi, Z., Perri, M., Piccioni, A., Ramirez-Ruiz, E., Roming, P. W. A., Steele, I. A., Strom, R. G., Testa, V., Tosti, G., Ulanov, M. V., Wiersema, K., Wijers, R. A. M. J., Winters, J. M., Zarnecki, A. F., Zerbi, F., Mészáros, P., Chincarini, G., and Burrows, D. N.: 2008, *Nature* **455**, 183

Racusin, J. L., Liang, E. W., Burrows, D. N., Falcone, A., Sakamoto, T., Zhang, B. B., Zhang, B., Evans, P., and Osborne, J.: 2009, *ApJ* **698**, 43

Raskin, C., Scannapieco, E., Rhoads, J., and Della Valle, M.: 2008, *ApJ* **689**, 358

Riess, A. G., Strolger, L.-G., Tonry, J., Tsvetanov, Z., Casertano, S., Ferguson, H. C., Mobasher, B., Challis, P., Panagia, N., Filippenko, A. V., Li, W., Chornock, R., Kirshner, R. P., Leibundgut, B., Dickinson, M., Koekemoer, A., Grogin, N. A., and Giavalisco, M.: 2004, *ApJ* **600**, L163

Robitaille, T. P. and Whitney, B. A.: 2010, *ApJ* **710**, L11

Rol, E., van der Horst, A., Wiersema, K., Patel, S. K., Levan, A., Nysewander, M., Kouveliotou, C., Wijers, R. A. M. J., Tanvir, N., Reichart, D., Fruchter, A. S., Graham, J., Ovaldsen, J., Jaunsen, A. O., Jonker, P., van Ham, W.,

Hjorth, J., Starling, R. L. C., O'Brien, P. T., Fynbo, J., Burrows, D. N., and Strom, R.: 2007, *ApJ* **669**, 1098

Rol, E., Wijers, R. A. M. J., Kouveliotou, C., Kaper, L., and Kaneko, Y.: 2005, *ApJ* **624**, 868

Rolleston, W. R. J., Smartt, S. J., Dufton, P. L., and Ryans, R. S. I.: 2000, *A&A* **363**, 537

Rosswog, S., Ramirez-Ruiz, E., and Davies, M. B.: 2003, *MNRAS* **345**, 1077

Ruffert, M. and Janka, H.: 1999, *A&A* **344**, 573

Ryder, S. D., Sadler, E. M., Subrahmanyan, R., Weiler, K. W., Panagia, N., and Stockdale, C.: 2004, *MNRAS* **349**, 1093

Rykoff, E. S., Aharonian, F., Akerlof, C. W., Ashley, M. C. B., Barthelmy, S. D., Flewelling, H. A., Gehrels, N., Göğüş, E., Güver, T., Kiziloğlu, Ü., Krimm, H. A., McKay, T. A., Özel, M., Phillips, A., Quimby, R. M., Rowell, G., Rujopakarn, W., Schaefer, B. E., Smith, D. A., Vestrand, W. T., Wheeler, J. C., Wren, J., Yuan, F., and Yost, S. A.: 2009, *ApJ* **702**, 489

Sako, M., Bassett, B., Becker, A., Cinabro, D., DeJongh, F., Depoy, D. L., Dilday, B., Doi, M., Frieman, J. A., Garnavich, P. M., Hogan, C. J., Holtzman, J., Jha, S., Kessler, R., Konishi, K., Lampeitl, H., Marriner, J., Miknaitis, G., Nichol, R. C., Prieto, J. L., Riess, A. G., Richmond, M. W., Romani, R., Schneider, D. P., Smith, M., Subba Rao, M., Takanashi, N., Tokita, K., van der Heyden, K., Yasuda, N., Zheng, C., Barentine, J., Brewington, H., Choi, C., Dembicky, J., Harnavek, M., Ihara, Y., Im, M., Ketzeback, W., Kleinman, S. J., Krzesiński, J., Long, D. C., Malanushenko, E., Malanushenko, V., McMillan, R. J., Morokuma, T., Nitta, A., Pan, K., Saurage, G., and Snedden, S. A.: 2008, *AJ* **135**, 348

Salpeter, E. E.: 1955, *ApJ* **121**, 161

Salvaterra, R., Della Valle, M., Campana, S., Chincarini, G., Covino, S., D'Avanzo, P., Fernández-Soto, A., Guidorzi, C., Mannucci, F., Margutti, R., Thöne, C. C., Antonelli, L. A., Barthelmy, S. D., de Pasquale, M., D'Elia, V., Fiore, F., Fugazza, D., Hunt, L. K., Maiorano, E., Marinoni, S., Marshall, F. E., Molinari, E., Nousek, J., Pian, E., Racusin, J. L., Stella, L., Amati, L., Andreuzzi, G., Cusumano, G., Fenimore, E. E., Ferrero, P., Giommi, P., Guetta, D., Holland, S. T., Hurley, K., Israel, G. L., Mao, J., Markwardt, C. B., Masetti, N., Pagani, C., Palazzi, E., Palmer, D. M., Piranomonte, S., Tagliaferri, G., and Testa, V.: 2009, *Nature* **461**, 1258

Sari, R., Piran, T., and Narayan, R.: 1998, *ApJ* **497**, L17+

Savaglio, S., Fall, S. M., and Fiore, F.: 2003, *ApJ* **585**, 638

Savaglio, S., Glazebrook, K., and Le Borgne, D.: 2006, in S. S. Holt, N. Gehrels, and J. A. Nousek (eds.), *Gamma-Ray Bursts in the Swift Era*, Vol. 836 of *American Institute of Physics Conference Series*, pp 540–545

Savaglio, S., Glazebrook, K., and Le Borgne, D.: 2008, *ArXiv e-prints* 803

Savaglio, S., Glazebrook, K., and Le Borgne, D.: 2009, *ApJ* **691**, 182

Savaglio, S., Glazebrook, K., Le Borgne, D., Juneau, S., Abraham, R. G., Chen, H.-W., Crampton, D., McCarthy, P. J., Carlberg, R. G., Marzke, R. O., Roth, K., Jørgensen, I., and Murowinski, R.: 2005, *ApJ* **635**, 260

Schady, P., Mason, K. O., Page, M. J., de Pasquale, M., Morris, D. C., Romano, P., Roming, P. W. A., Immler, S., and vanden Berk, D. E.: 2007, *MNRAS* **377**, 273

Schady, P., Page, M. J., Oates, S. R., Still, M., de Pasquale, M., Dwelly, T., Kuin, N. P. M., Holland, S. T., Marshall, F. E., and Roming, P. W. A.: 2010, *MNRAS* **401**, 2773

Schlegel, D. J., Finkbeiner, D. P., and Davis, M.: 1998, *ApJ* **500**, 525

Seaton, M. J.: 1979, *MNRAS* **187**, 73P

Shankar, F. and Bernardi, M.: 2009, *MNRAS* **396**, L76

Siebenmorgen, R. and Krügel, E.: 2007, *A&A* **461**, 445

Silva, L., Granato, G. L., Bressan, A., and Danese, L.: 1998, *ApJ* **509**, 103

Sivaram, C. and Arun, K.: 2010, *ArXiv e-prints*

Smail, I., Chapman, S. C., Blain, A. W., and Ivison, R. J.: 2004, *ApJ* **616**, 71

Smartt, S. J., Eldridge, J. J., Crockett, R. M., and Maund, J. R.: 2009, *MNRAS* **395**, 1409

Smartt, S. J., Maund, J. R., Hendry, M. A., Tout, C. A., Gilmore, G. F., Mattila, S., and Benn, C. R.: 2004, *Science* **303**, 499

Smith, I. A., Tilanus, R. P. J., Tanvir, N., Barnard, V. E., Moriarty-Schieven, G. H., Frail, D. A., Wijers, R. A. M. J., Vreeswijk, P., Rol, E., and Kouveliotou, C.: 2005, *A&A* **439**, 987

Sollerman, J., Fynbo, J. P. U., Gorosabel, J., Halpern, J. P., Hjorth, J., Jakobsson, P., Mirabal, N., Watson, D., Xu, D., Castro-Tirado, A. J., Féron, C., Jaunsen, A. O., Jelínek, M., Jensen, B. L., Kann, D. A., Ovaldsen, J. E., Pozanenko, A., Stritzinger, M., Thöne, C. C., de Ugarte Postigo, A., Guziy, S., Ibrahimov, M., Järvinen, S. P., Levan, A., Rumyantsev, V., and Tanvir, N.: 2007, *A&A* **466**, 839

Sollerman, J., Östlin, G., Fynbo, J. P. U., Hjorth, J., Fruchter, A., and Pedersen, K.: 2005, *New Astronomy* **11**, 103

Sonneborn, G., Altner, B., and Kirshner, R. P.: 1987, *ApJ* **323**, L35

Stamatikos, M., Barthelmy, S. D., Cummings, J., Fenimore, E., Gehrels, N., Krimm, H., Markwardt, C., Palmer, D., Racusin, J. L., Sakamoto, T., Sato, G., Tueller, J., and Ukwatta, T.: 2008, *GRB Coordinates Network* **7272**, 1

Stanek, K. Z., Gnedin, O. Y., Beacom, J. F., Gould, A. P., Johnson, J. A., Kollmeier, J. A., Modjaz, M., Pinsonneault, M. H., Pogge, R., and Weinberg, D. H.: 2006, *Acta Astronomica* **56**, 333

Stanek, K. Z., Matheson, T., Garnavich, P. M., Martini, P., Berlind, P., Caldwell, N., Challis, P., Brown, W. R., Schild, R., Krisciunas, K., Calkins, M. L., Lee, J. C., Hathi, N., Jansen, R. A., Windhorst, R., Echevarria, L., Eisenstein, D. J., Pindor, B., Olszewski, E. W., Harding, P., Holland, S. T., and Bersier, D.: 2003, *ApJ* **591**, L17

Starling, R. L. C., Vreeswijk, P. M., Ellison, S. L., Rol, E., Wiersema, K., Levan, A. J., Tanvir, N. R., Wijers, R. A. M. J., Tadhunter, C., Zaurin, J. R., Gonzalez Delgado, R. M., and Kouveliotou, C.: 2005, *A&A* **442**, L21

Starling, R. L. C., Wiersema, K., Levan, A. J., Sakamoto, T., Bersier, D., Goldoni, P., Oates, S. R., Rowlinson, A., Campana, S., Sollerman, J., Tanvir, N. R., Malesani, D., Fynbo, J. P. U., Covino, S., D'Avanzo, P., O'Brien, P. T., Page, K. L., Osborne, J. P., Vergani, S. D., Barthelmy, S., Burrows, D. N., Cano, Z., Curran, P. A., De Pasquale, M., D'Elia, V., Evans, P. A., Flores, H., Fruchter, A. S., Garnavich, P., Gehrels, N., Gorosabel, J., Hjorth, J., Holland, S. T., van der Horst, A. J., Jakobsson, P., Kamble, A. P., Kuin, N. P. M., Kaper, L., Mazzali, P. A., Nugent, P. E., Pian, E., Thoene, C. C., and Woosley, S. E.: 2010, *ArXiv e-prints*

Strolger, L.-G., Riess, A. G., Dahlen, T., Livio, M., Panagia, N., Challis, P., Tonry, J. L., Filippenko, A. V., Chornock, R., Ferguson, H., Koekemoer, A., Mobasher, B., Dickinson, M., Giavalisco, M., Casertano, S., Hook, R., Blondin, S., Leibundgut, B., Nonino, M., Rosati, P., Spinrad, H., Steidel, C. C., Stern, D., Garnavich, P. M., Matheson, T., Grogin, N., Hornschemeier, A., Kretchmer, C., Laidler, V. G., Lee, K., Lucas, R., de Mello, D., Moustakas, L. A., Ravindranath, S., Richardson, M., and Taylor, E.: 2004, *ApJ* **613**, 200

Svensson, K. M., Levan, A. J., Tanvir, N. R., Fruchter, A. S., and Strolger, L.: 2010, *MNRAS* **405**, 57

Swinbank, A. M., Smail, I., Chapman, S. C., Blain, A. W., Ivison, R. J., and Keel, W. C.: 2004, *ApJ* **617**, 64

Tanvir, N. R., Barnard, V. E., Blain, A. W., Fruchter, A. S., Kouveliotou, C., Natarajan, P., Ramirez-Ruiz, E., Rol, E., Smith, I. A., Tilanus, R. P. J., and Wijers, R. A. M. J.: 2004, *MNRAS* **352**, 1073

Tanvir, N. R., Fox, D. B., Levan, A. J., Berger, E., Wiersema, K., Fynbo, J. P. U., Cucchiara, A., Krühler, T., Gehrels, N., Bloom, J. S., Greiner, J., Evans, P. A., Rol, E., Olivares, F., Hjorth, J., Jakobsson, P., Farihi, J., Willingale, R., Starling, R. L. C., Cenko, S. B., Perley, D., Maund, J. R., Duke, J., Wijers, R. A. M. J., Adamson, A. J., Allan, A., Bremer, M. N., Burrows, D. N., Castro-Tirado, A. J., Cavanagh, B., de Ugarte Postigo, A., Dopita, M. A., Fatkhullin, T. A., Fruchter, A. S., Foley, R. J., Gorosabel, J., Kennea, J., Kerr, T., Klose, S., Krimm, H. A., Komarova, V. N., Kulkarni, S. R., Moskvitin, A. S., Mundell, C. G., Naylor, T., Page, K., Penprase, B. E., Perri, M., Podsiadlowski, P., Roth, K., Rutledge, R. E., Sakamoto, T., Schady, P., Schmidt, B. P., Soderberg, A. M., Sollerman, J., Stephens, A. W., Stratta, G., Ukwatta, T. N., Watson, D., Westra, E., Wold, T., and Wolf, C.: 2009, *Nature* **461**, 1254

Tanvir, N. R., Levan, A. J., Rol, E., Starling, R. L. C., Gorosabel, J., Priddey, R. S., Malesani, D., Jakobsson, P., O'Brien, P. T., Jaunsen, A. O., Hjorth, J., Fynbo, J. P. U., Melandri, A., Gomboc, A., Milvang-Jensen, B., Fruchter, A. S., Jarvis, M., Fernandes, C. A. C., and Wold, T.: 2008, *MNRAS* **388**, 1743

Tanvir, N. R., Rol, E., Levan, A., Fruchter, A., Granot, J., Svensson, K. M., O'Brien, P. T., Wiersema, K., Starling, R. L. C., Jakobsson, P., Fynbo, J., Hjorth, J., Curran, P., van der Horst, A. J., Kouveliotou, C., Racusin, J. L., Burrows, D. N., and Genet, F.: 2010, *ArXiv e-prints 0812.1217*

Thöne, C. C., Fynbo, J. P. U., Östlin, G., Milvang-Jensen, B., Wiersema, K., Malesani, D., Della Monica Ferreira, D., Gorosabel, J., Kann, D. A., Watson, D., Michałowski, M. J., Fruchter, A. S., Levan, A. J., Hjorth, J., and Sollerman, J.: 2008a, *ApJ* **676**, 1151

Thöne, C. C., Kann, D. A., Jóhannesson, G., Selj, J. H., Jaunsen, A. O., Fynbo, J. P. U., Akerlof, C. W., Baliyan, K. S., Bartolini, C., Bikmaev, I. F., Bloom, J. S., Burenin, R. A., Cobb, B. E., Covino, S., Curran, P. A., Dahle, H., Ferrero, A., Foley, S., French, J., Fruchter, A. S., Ganesh, S., Graham, J. F., Greco, G., Guarnieri, A., Hanlon, L., Hjorth, J., Ibrahimov, M., Israel, G. L., Jakobsson, P., Jelínek, M., Jensen, B. L., J\o rgensen, U. G., Khamitov, I. M., Koch, T. S., Levan, A. J., Malesani, D., Masetti, N., Meehan, S., Melady, G., Nanni, D., Näränen, J., Pakstiene, E., Pavlinsky, M. N., Perley, D. A., Piccioni, A., Pizzichini, G., Pozanenko, A., Roming, P. W. A., Rujopakarn, W., Rumyantsev, V., Rykoff, E. S., Sharapov, D., Starr, D., Sunyaev, R. A., Swan, H., Tanvir, N. R., Terra, F., Vreeswijk, P. M., Wilson, A. C., Yost, S. A., and Yuan, F.: 2008b, *ArXiv e-prints*

Tremonti, C. A., Heckman, T. M., Kauffmann, G., Brinchmann, J., Charlot, S., White, S. D. M., Seibert, M., Peng, E. W., Schlegel, D. J., Uomoto, A., Fukugita, M., and Brinkmann, J.: 2004, *ApJ* **613**, 898

Trundle, C., Dufton, P. L., Hunter, I., Evans, C. J., Lennon, D. J., Smartt, S. J., and Ryans, R. S. I.: 2007, *A&A* **471**, 625

van den Heuvel, E. P. J. and Yoon, S.-C.: 2007, *ApSS* **311**, 177

van der Horst, A. J., Kouveliotou, C., Gehrels, N., Rol, E., Wijers, R. A. M. J., Cannizzo, J. K., Racusin, J., and Burrows, D. N.: 2009, *ApJ* **699**, 1087

van Paradijs, J., Groot, P. J., Galama, T., Kouveliotou, C., Strom, R. G., Telting, J., Rutten, R. G. M., Fishman, G. J., Meegan, C. A., Pettini, M., Tanvir, N., Bloom, J., Pedersen, H., Nørdgaard-Nielsen, H. U., Linden-Vørnle, M., Melnick, J., van der Steene, G., Bremer, M., Naber, R., Heise, J., in't Zand, J., Costa, E., Feroci, M., Piro, L., Frontera, F., Zavattini, G., Nicastro, L., Palazzi, E., Bennett, K., Hanlon, L., and Parmar, A.: 1997, *Nature* **386**, 686

Vanzella, E., Cristiani, S., Dickinson, M., Giavalisco, M., Kuntschner, H., Haase, J., Nonino, M., Rosati, P., Cesarsky, C., Ferguson, H. C., Fosbury, R. A. E., Grazian, A., Moustakas, L. A., Rettura, A., Popesso, P., Renzini, A., Stern, D., and The Goods Team: 2008, *A&A* **478**, 83

Vanzella, E., Cristiani, S., Dickinson, M., Kuntschner, H., Moustakas, L. A., Nonino, M., Rosati, P., Stern, D., Cesarsky, C., Ettori, S., Ferguson, H. C., Fosbury, R. A. E., Giavalisco, M., Haase, J., Renzini, A., Rettura, A., Serra, P., and The Goods Team: 2005, *A&A* **434**, 53

Vanzella, E., Cristiani, S., Dickinson, M., Kuntschner, H., Nonino, M., Rettura, A., Rosati, P., Vernet, J., Cesarsky, C., Ferguson, H. C., Fosbury, R. A. E., Giavalisco, M., Grazian, A., Haase, J., Moustakas, L. A., Popesso, P., Renzini, A., Stern, D., and The Goods Team: 2006, *A&A* **454**, 423

Venn, K. A., Lennon, D. J., Kaufer, A., McCarthy, J. K., Przybilla, N., Kudritzki, R. P., Lemke, M., Skillman, E. D., and Smartt, S. J.: 2001, *ApJ* **547**, 765

Venn, K. A., Tolstoy, E., Kaufer, A., Skillman, E. D., Clarkson, S. M., Smartt, S. J., Lennon, D. J., and Kudritzki, R. P.: 2003, *AJ* **126**, 1326

Verma, A., Lehnert, M. D., Förster Schreiber, N. M., Bremer, M. N., and Douglas, L.: 2007, *MNRAS* **377**, 1024

von Weizscker, C. F.: 1938, *Physikalische Zeitschrift* **39**, 633

Vreeswijk, P. M., Ellison, S. L., Ledoux, C., Wijers, R. A. M. J., Fynbo, J. P. U., Møller, P., Henden, A., Hjorth, J., Masi, G., Rol, E., Jensen, B. L., Tanvir, N., Levan, A., Castro Cerón, J. M., Gorosabel, J., Castro-Tirado, A. J., Fruchter, A. S., Kouveliotou, C., Burud, I., Rhoads, J., Masetti, N., Palazzi, E., Pian, E., Pedersen, H., Kaper, L., Gilmore, A., Kilmartin, P., Buckle, J. V., Seigar, M. S., Hartmann, D. H., Lindsay, K., and van den Heuvel, E. P. J.: 2004, *A&A* **419**, 927

Vreeswijk, P. M., Fruchter, A., Kaper, L., Rol, E., Galama, T. J., van Paradijs, J., Kouveliotou, C., Wijers, R. A. M. J., Pian, E., Palazzi, E., Masetti, N., Frontera, F., Savaglio, S., Reinsch, K., Hessman, F. V., Beuermann, K., Nicklas, H., and van den Heuvel, E. P. J.: 2001, *ApJ* **546**, 672

Watson, D., Hjorth, J., Jakobsson, P., Pedersen, K., Patel, S., and Kouveliotou, C.: 2004, *A&A* **425**, L33

Webbink, R. F.: 1984, *ApJ* **277**, 355

Wiersema, K., Savaglio, S., Vreeswijk, P. M., Ellison, S. L., Ledoux, C., Yoon, S., Møller, P., Sollerman, J., Fynbo, J. P. U., Pian, E., Starling, R. L. C., and Wijers, R. A. M. J.: 2007, *A&A* **464**, 529

Wiersema, K., van der Horst, A. J., Kann, D. A., Rol, E., Starling, R. L. C., Curran, P. A., Gorosabel, J., Levan, A. J., Fynbo, J. P. U., de Ugarte Postigo, A., Wijers, R. A. M. J., Castro-Tirado, A. J., Guziy, S. S., Hornstrup, A., Hjorth, J., Jelínek, M., Jensen, B. L., Kidger, M., Martín-Luis, F., Tanvir, N. R., Tristram, P., and Vreeswijk, P. M.: 2008, *A&A* **481**, 319

Wijers, R. A. M. J., Rees, M. J., and Meszaros, P.: 1997, *MNRAS* **288**, L51

Willingale, R., O'Brien, P. T., Osborne, J. P., Godet, O., Page, K. L., Goad, M. R., Burrows, D. N., Zhang, B., Rol, E., Gehrels, N., and Chincarini, G.: 2007, *ApJ* **662**, 1093

Wirth, G. D., Willmer, C. N. A., Amico, P., Chaffee, F. H., Goodrich, R. W., Kwok, S., Lyke, J. E., Mader, J. A., Tran, H. D., Barger, A. J., Cowie, L. L., Capak, P., Coil, A. L., Cooper, M. C., Conrad, A., Davis, M., Faber, S. M., Hu, E. M., Koo, D. C., Le Mignant, D., Newman, J. A., and Songaila, A.: 2004, *AJ* **127**, 3121

Wolf, C. and Podsiadlowski, P.: 2007, *MNRAS* **375**, 1049

Woosley, S. E.: 1993, *ApJ* **405**, 273

Woosley, S. E. and Heger, A.: 2006, *ApJ* **637**, 914

Woosley, S. E. and MacFadyen, A. I.: 1999, *A&A Supp.* **138**, 499

Xu, D., Starling, R. L. C., Fynbo, J. P. U., Sollerman, J., Yost, S., Watson, D., Foley, S., O'Brien, P. T., and Hjorth, J.: 2009, *ApJ* **696**, 971

Yoon, S., Langer, N., and Norman, C.: 2006, *A&A* **460**, 199

Yoon, S.-C. and Langer, N.: 2005, *A&A* **443**, 643

Yüksel, H., Kistler, M. D., Beacom, J. F., and Hopkins, A. M.: 2008, *ApJ* **683**, L5

Zhang, B., Fan, Y. Z., Dyks, J., Kobayashi, S., Mészáros, P., Burrows, D. N., Nousek, J. A., and Gehrels, N.: 2006a, *ApJ* **642**, 354

Zhang, Z., Xie, G. Z., Deng, J. G., and Jin, W.: 2006b, *MNRAS* **373**, 729